THE COMPUTATION OF THE AXISYMMETRIC SQUEEZE FILM PROBLEM IN ELASTOHYDRODYNAMIC LUBRICATION

by

Neil William James

A Thesis submitted for the degree of

DOCTOR OF PHILDSOPHY

of the University of London and also for the

DIPLOMA OF IMPERIAL COLLEGE

July 1978

Lubrication Laboratory
Department of Mechanical Engineering
Imperial College of Science and Technology
London S.W.7

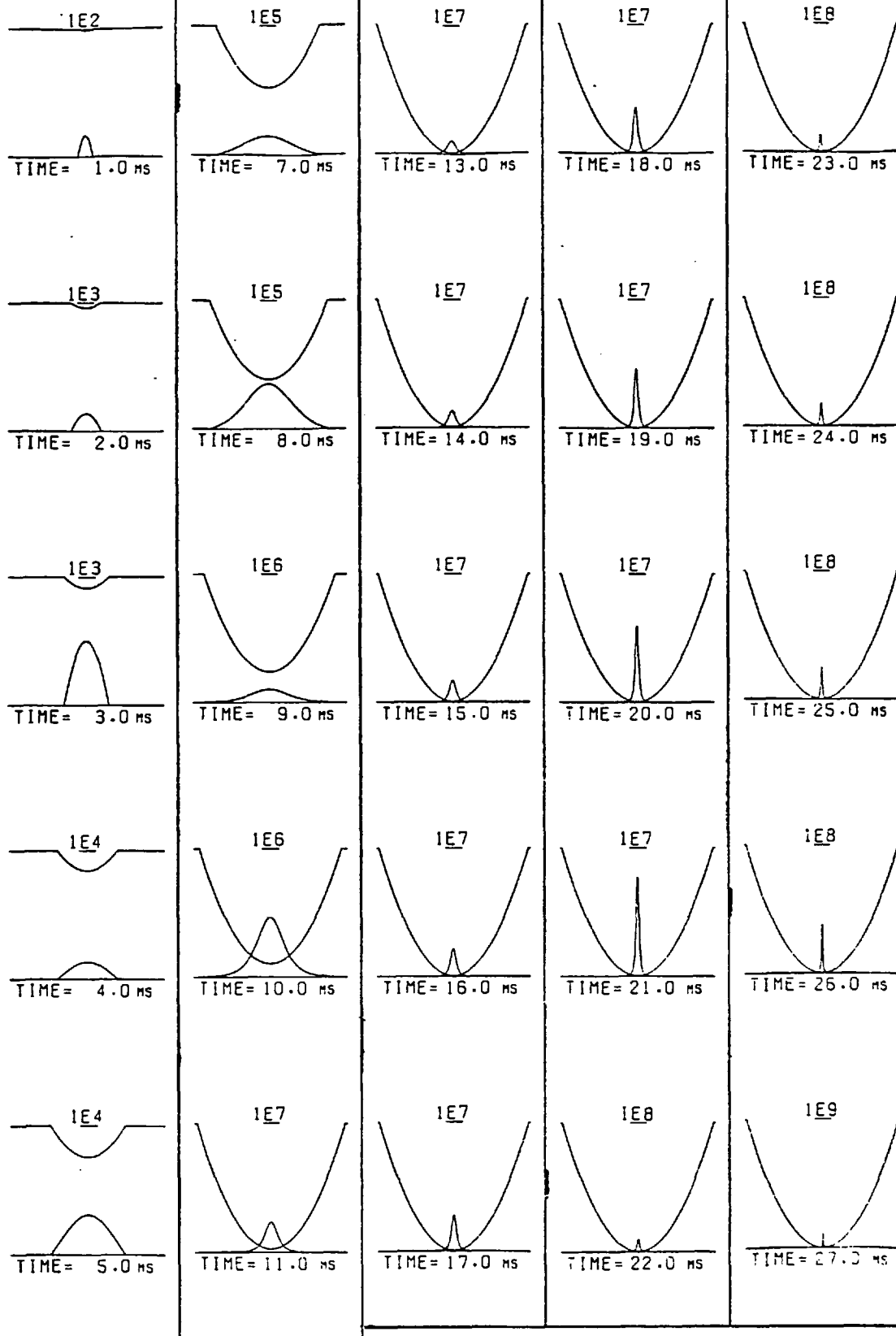

The Spatial Distribution of Pressure (Pa) for a rigid Parabola Impacting onto an Incompressible Exponential Piezoviscous Layer of Oil (see Section 3.5.5).

ABSTRACT

A numerical study has been made of an elastic ball normally impacting onto an elastic half-space covered by a thin layer of oil. The oil is compressible and has a pressure dependent viscosity.

The solution of the Reynolds, Elasticity and State equations are found simultaneously using Newton-Raphson techniques and with quintic spline elements. The pressure field is integrated to give the load which determines the trajectory. The effect of coupling the ball dynamics to the instantaneous solution gives rise to a stiff set of equations, thus adding greatly to the numerical problems.

An extended analysis of the rigid ball incompressible fluid system has been undertaken so that the effects of various parameters may be determined.

The effect of temperature generation is shown to be small under the conditions that hold if the ball is to lose its momentum by viscous action alone.

By integration of the Boussinesq formulae for the axisymmetric deformation, a general formula for the vertical deformation has been found, and if the applied pressure distribution is continuous up to the nth derivative, then by means of a simple recurrence relation the first n spatial derivatives of the deformation may be calculated. The formula for the horizontal distortion is obtained and is of a particularly simple form. The formulae are of general application.

In the region of significant elastic distortion, the ball is dropping effectively at zero acceleration (constant film force), thus results obtained here are not directly comparable with those of previous workers who have assumed the unlikely configuration of the ball dropping under constant central pressure.

Entrapments are obtained and the effect of the local elastic distortion velocity found to be significant.

ACKNOWLEDGEMENTS

I am indebted to Professor A. Cameron for the opportunity to undertake this work, to Dr. C. Ettles for supervision of the project and to the SRC for a research studentship.

I am grateful to members of the Lubrication Laboratory, especially Dr. A. Holmes and S. Carlson, for many helpful discussions.

I would like to thank my ex-colleagues in the College Computer Centre for helping me to understand the vagaries of the College computers, and in particular, John Greenaway and Robert Smythe for the photographic processing and Susan N. Coussens for the typing of this thesis.

Finally, my thanks go to my wife Helen who has encouraged and supported me throughout the production of this thesis.

CONTENTS

LIST OF FIGURES

For ease of reference, page 162 is of fold-out form and gives an expanded list of figures for Chapter Six.

NOMENCLATURE

a	Horizontal radius
$C_{lj}(r)$	Cardinal Interpolating Polynomial of Degree 1 with $C_{lj}(r_i) = \delta_{ij}$
$\underline{\underline{D}}_1, \underline{\underline{D}}_2$	Matrices such that $(\underline{\underline{D}}_k)_{ij} = \left(\frac{\partial}{\partial p_j}\left(\frac{\partial^k p}{\partial r^k}\right)\right)_{r_i}$
E_1, E_2	Elastic moduli of Impacting Surfaces
E'	Equivalent Vertical Elastic Constant $\left(\frac{1}{E'} = \frac{1-\nu_1^2}{E_1} + \frac{1-\nu_2^2}{E_2}\right)$
E^*	Equivalent Horizontal Elastic Constant $\left(\frac{1}{E^*} = \frac{(1+\nu_1)(1-2\nu_1)}{E_1}\right.$
F_0, F_1	Integrals used with the Full Reynolds Equation
$F(r,\xi)$	Kernel of Deformation Integral
$\underline{\underline{F}}$	Vertical Deformation Matrix
$g_1(r)$	Interpolating Polynomial of Degree 1
$\underline{\underline{G}}$	Vertical Deformation Derivative Matrix
h	Local film thickness
h_c	Minimum clearance between Rigid Ball and Plane. Also used in Elastic Case to represent Height of Centre of Gravity above datum point
h_s	Initial Film Thickness
I_{ik}^m	Deformation at R_i due to annulus of pressure R^m extending over $[R_k, R_{k+1}]$
J_{ik}^m	Deformation at R_i due to disc pressure R^m extending over $[0, R_k]$
$K(\ )$	Complete Elliptic Integral of the First Kind
k_1, k_2	Order of Truncation Error associated with $\underline{\underline{D}}_1, \underline{\underline{D}}_2$
K_1	Dimensional Group $\frac{mg}{\eta_0 R^2}$
K_2	Dimensional Group $\eta_0 R$
l	Degree of Interpolating Polynomial
m	Mass of Ball
M_1, M_2	Further integrals used with the Full Reynolds Equation
$p, p(r)$	Pressure

p_c	Pressure at r=0
p_L	Cutoff value for viscosity increase
$\underline{p}$	Set of pressures that determine p(r)
r	Radial co-ordinate
r_s	Radial Extent of Film
$\underline{r}$	Grid points at which Reynolds Equation is solved
R	Radius of Ball
$\underline{R}$	Linear multiple of $\underline{r}$ such that $R_1=0$, $R_2=1$
t	Time
u	Horizontal Deformation
$\underline{\underline{U}}$	Horizontal Deformation Matrix
v_c	Velocity of Centre of Gravity of Ball
v_s	Initial value of v_c
w	Vertical deformation
W	Weight of the Ball
Y	Dimensional Group - $\rho h^3/\eta$
z	Co-ordinate normal to r
Z	$\frac{2}{h_0}\frac{dh_0}{dr}$
α	Exponential Viscosity Coefficient
Δr	Number defined such that $\underline{r}=\underline{R}\,\Delta r$
Δt	Local time step
δ	Film thickness such that $p_c \rightarrow \infty$
η	Viscosity of Oil
η_0	Initial Viscosity
ν_1,ν_2	Poisson's Ratios for Impacting Surfaces
ξ	Dummy variable representing r
Ξ	Dummy variable representing R(=rΔr)
ρ	Density of Oil ($=\rho^*\rho_0$)
ρ_0	Initial Density
ρ_a,ρ_b	Density-Pressure Coefficients

$*$	Operator defined in Appendix V
x_i or $\underline{x}_i$	ith component of $\underline{x}$
$(X)_{r_i}$	x evaluated at $r_i (=X_i)$
$(\underline{p})_s$	sth iteration for $\underline{p}$

CHAPTER ONE

IMPACT SQUEEZE FILMS

1.1 Introduction.

Until comparatively recently squeeze film effects in lubrication have been overlooked as a factor for providing separation between lubricated surfaces. They arise whenever any two bodies approach each other along their common normal, and will occur due to vibration in almost all components of running machinery. In counterformed elements, such as gear teeth, cams and rolling bearings, the thinness of the oil film under normal running conditions causes very high localized pressures to be generated, which give rise to elastic distortions of the bounding solids. These distortions, though small in absolute measure, are large compared to the film thickness. This effect will be further heightened by any starvation condition of the system. It has been found that this pressure generation can seriously reduce the scuffing load in rolling contacts.

In this thesis, the various equations of Newtonian flow, continuity, acceleration, and elasticity for a ball dropping on to a lubricated half-space will be obtained and solved. In the isothermal case the pressure gradient varies approximately inversely as the cube of the film thickness; the viscosity-pressure model used changes approximately exponentially with the pressure; and the deformation is a linear function of the entire pressure field. They thus give a system of equations which are time-dependent as well as being inter-related in a highly non-linear way.

This thesis will extend previous work in the following ways:

1) By considering the dynamics of one ball dropping under the action of gravity so that the velocity, film thickness, and film force are coupled.

2) By allowing the viscosity to be an arbitary, continuous, differentiable function of pressure. An approximation to the second derivative needs to be defined numerically. Time-dependent viscosities will not be considered.

3) Previous workers (CHRISTENSEN, 1967, 1970; CHENG and LEE, 1971) have assumed that the ball or cylinder drops with a pre-determined constant central pressure. Methods used here allow for a varying central pressure.

4) The local approach velocity of the ball will be incorporated by an appropriate backward difference formula. This effects a space-time coupling, which together with the mass acceleration, presents a complicated system.

5) A novel way of calculating the elastic distortion will be presented, enabling the distortion derivatives to be accurately calculated. This is later shown to be necessary to the method.

6) A first order approximation to the horizontal distortion will be made, and its effects will be shown to be negligible.

This more realistic approach to the behaviour of the dropping ball makes it difficult to compare results with previous investigations.

1.2. Previous Investigations.

STEFAN, 1874, was probably the first to set up the equation relating the time of sinkage of a flat round plate on to a smooth plane from a given height, for an isoviscous fluid. In 1886, the classical work of REYNOLDS was produced, laying the basis for hydrodynamic lubrication theory. He combined the stress equations of STOKES, 1845, with the Lagrangian equation of motion for the fluid. Neglecting inertia terms and applying suitable boundary conditions he obtained the well-known Reynolds Equation. This is directly integrable for axisymmetric or elliptical plates, and also when the plate is rectangular but infinite in extent. The conditions that he assumed were:-

1) Effects due to gravity and inertia forces within the fluid were neglected (i.e. no body forces).

2) The fluid was Newtonian, incompressible and isoviscous.

3) The thickness of squeeze film was small compared to the plate dimensions.

4) There was no slip at the boundaries of fluid and bounding solids.

5) Surface tension effects were negligible.

6) The fluid was Stokesian.

7) The pressure was transmitted normally across the film without change.

8) Fluid velocity derivatives in the normal direction were large compared to those in the direction of the flow.

In 1940, NEEDS experimentally detected the influence of boundary surfaces on the viscosity of thin films between two optically plane parallel discs. He was able to verify the Stefan equation for both mineral oils and vegetable oils, but found that at large time values the experimental film thicknesses were much greater than the theoretical values. He attributed the increase to molecular effects, however it was subsequently determined (MOORE, 1965), that the molecular effects were of an order of magnitude too small to account for the observed behaviour. The theoretical models assumed an isoviscous oil to be present.

In 1947, EIRICH and TABOR investigated the dynamic behaviour of a flat squeeze film under impact loading. The pressure distribution, flow velocity, shear rate and temperature rise within the film were calculated. For heavy impacts the pressures generated are sufficient to plastically deform the surface, while the temperature rise may be attributed to both viscous flow and a rapid adiabatic compression of gas bubbles trapped in the liquid film. They equated the loss of kinetic energy to the work done against the pressure generated, and assumed that the effect of pressure on viscosity was negligible. For a bubble free fluid and a mass of 0.040 kg and impact velocity of 1.5 ms^{-1}, the maximum temperature generated by viscous flow was about 2^0C. The impact velocity was shown to have the major effect on producing this rise and was about 15 times greater than any considered here. BUTLER, 1960, extended the work of EIRICH and TABOR on surface deformation due to lubricant impaction to the case of a highly polished flat-ended cylindrical specimen compressed between polished dies. He showed that after impact the appearance of the impact faces is markedly changed according to the viscosity of the lubricant. In the general case of a pressure-sensitive viscosity it could

occur that the initially plane surfaces would take on a dished profile.

1.3 Experimental Work on Entrapment Formation.

RABINOWICZ, 1952, noted that when an impact occurred between metal surfaces, metal was transferred from one surface to the other in both lubricated and dry conditions. When a lubricant of low viscosity was used, metal transfer occured in the same form as the dry case but when a high viscosity oil was used a small portion of the centre did not have transferred metal. He concluded that the oil had not been completely squeezed from the contact zone. This work was further reported in the earlier paper by TABOR, 1949, where it was noted that a large initial viscosity is needed to form conical dents. Interferometric results were obtained by DOWSON and JONES, 1967, who show that as the film is squeezed out, the depth of the pocket remains nearly constant.

FOORD, 1968, obtained an interferogram which showed an entrapment with a minimum thickness of less than 200Å which remained unchanged over a period of nine hours. WESTLAKE, 1970, using white light, studied this in greater detail, and noted that in the last part of the descent there was very little leakage of fluid. That is, a body of liquid is trapped in the contact while the elastic ball deforms around it. This effect is confirmed in the present work.

PAUL, 1971, extended the interferometric work further by using monochromatic light at two differing angles and was able to determine the absolute film thickness. From elastic considerations he obtained the pressure distribution and hence, by numerical substitution into Reynolds equation, was able to obtain pressure-viscosity curves, as well as pressure-density curves. This system has not been directly modelled in the present

work due to the numerical indeterminacy of the highly non-linear damping mechanisms, i.e. dashpot and magnet assemblies, as well as the squeeze film process, and also a desire not to increase the number of independent parameters.

In 1974, GAMAN, HIGGINSON and NORMAN, looked at entrapments formed by the action of a rigid sphere falling through oil on to a silicone rubber surface layer resting on a rigid base. They noted that the time of descent to a specified centre film thickness was far shorter when the soft film was present.

1.4 Theoretical Elastohydrodynamic Work.

When the squeeze film occurring between elastic bodies is considered, a complex system results. The pressure generated gives rise to an elastic displacement which tends to reduce the squeezing pressure. In 1960, CHRISTENSEN established the equations governing the normal approach of two elastic cylinders separated by a lubricant with exponential viscosity-pressure characteristics, and presented numerical solutions for a number of cases, assuming isothermal conditions. CHRISTENSEN assumed that the rate of normal approach was constant across the surface of the film and took the central pressure to be fixed. The solution proceeded by decreasing the central deformed film thickness and solving the pressure field by iteration.

In 1962, CHRISTENSEN published a theory of the elastrohydrodynamics of the normal approach of two elastic cylinders and predicted that the pressures in the film could considerably exceed the Hertzian stress at a finite film thickness under certain conditions.

In 1967, he extended the work to consider the impact of spherical

elastic bodies in normal approach. As before, the system of equations was solved assuming the central pressure value to be a fixed constant and then, from the rigid solution, iterating to the elastic by using the elasticity equation to obtain the new film thickness. He made an approximation to the local velocity by using $\frac{\partial}{\partial t} = H_0 \frac{\partial}{\partial H_0}$ (H_0 is the normalized centre film thickness) and iterated for the actual distribution. He assumed that the differences calculated between solutions including this effect and those ignoring it were only a few percent of the solution values. From the results shown it is not apparent whether this is indeed true. He used a different integral transform for the calculation for elastic distortion from the one used here. The equations obtained are in fact identical.

In 1971, CHENG and LEE extended the earlier work of CHRISTENSEN for elastic cylinders by allowing for a compressible fluid,and also to account for the spatial variation in local velocity. They further considered two types of viscosity-pressure relations for the lubricant; first an exponential, and then a composite exponential type as developed by ALLEN, TOWNSEND and ZARETSKY, 1970. They showed that the effect of compressibility is small and that the exponential type oil gives rise to a sharp spike in the pressure field at the centre. However, for the composite exponential the width of the spike is greater and for all cases studied a pocket is formed elastically in the early stages and remains without much change during the rest of the contacting process, until at the end a pocket of lubricant is entrapped. They also modelled the cylinder to have constant central pressure during the squeeze process.

Meanwhile, HERREBRUGH, 1970, had produced an integral equation approach to the problem of approaching cylinders. This assumed that the local surface velocities were constant across the film and the equations were set up for either an isoviscous or an exponentially varying viscosity. Only the isoviscous case was solved; by means of successive approximations.

He then obtained an estimate of the variation of the local approach velocity.

CONWAY, 1973, by analysing the case of a soft layer squeezed between two rollers, noted that for large values of absolute velocity, or for thin films, or even for soft bounding surfaces, the assumption of CHRISTENSEN 1962, HERREBURGH, and GOULD, 1971, that the local approach velocity does not change radially, is invalid. He noted that this effect was exacerbated if an exponentially-varying viscosity oil was present.

In 1975, CONWAY and LEE, published work on impact films in which they considered a rigid parobola squeezing on to a rigid flat through an incompressible exponential viscosity oil. As the model that they used is the same as one that is in this thesis, the results of this paper will be commented on in a later chapter. It should be noted that they discard the boundary condition that the pressure reaches zero at an infinite distance from the contact. This has also been done in this work.

1.5 The Development of this Thesis.

In Chapter Two, the equations in their basic form are set up, together with appropriate boundary conditions. Some of the assumptions used are explained and justified here.

In Chapter Three, the impact of a rigid parabola on to a rigid semi-infinite solid with an incompressible liquid resting on the plate is discussed in some detail. The advantage of this is that a semi-analytical solution exists for this case and so it is much less expensive in computer time to analyse the behaviour of the system using this model, than to attempt the extensions to the (elastic ball, compressible liquid) case

immediately. It will be seen that, in the early stages of impact, there is no visible difference in the trajectories of the semi-analytical case and the fully varying case. This is because the pressures generated are low and the film thickness is large compared to the elastic distortions, and is partially a consequence of modelling only relatively hard materials.

The effects of changing initial values and parameters of the system are presented and discussed as well as the various methods of time integration used. It will be found that the system exhibits stiffness, (see for example, GEAR, 1971).

In Chapter Four, methods used for solving the Reynolds Equation taking into account elasticity and compressiblity effects are formulated and discussed. Several possible methods were rejected for various reasons, and the eventual method used is described and justified. It is important to note that space integration (i.e. solving for the instantaneous load) and time integration (i.e. obtaining the trajectories) may be considered separately since a partial decoupling of the equations may be made.

In Chapter Five, the calculations necessary to obtain the vertical compliance matrix are made. The elements of this matrix are in general given as an integral, but for the case of piecewise polynomial interpolating functions these have been calculated explicitly. The spatial derivative of vertical deformation is required and so a transformation is made and the elements of the matrix shown to be reducible to the same form as required for the compliance matrix. The horizontal compliance matrix is also calculated.

Chapter Six contains results for the fully varying case. The effect of the elastic and piezoviscous parameters are presented and discussed.

Chapter Seven contains a summary of results, a summary on the methods used and recommendations on further work.

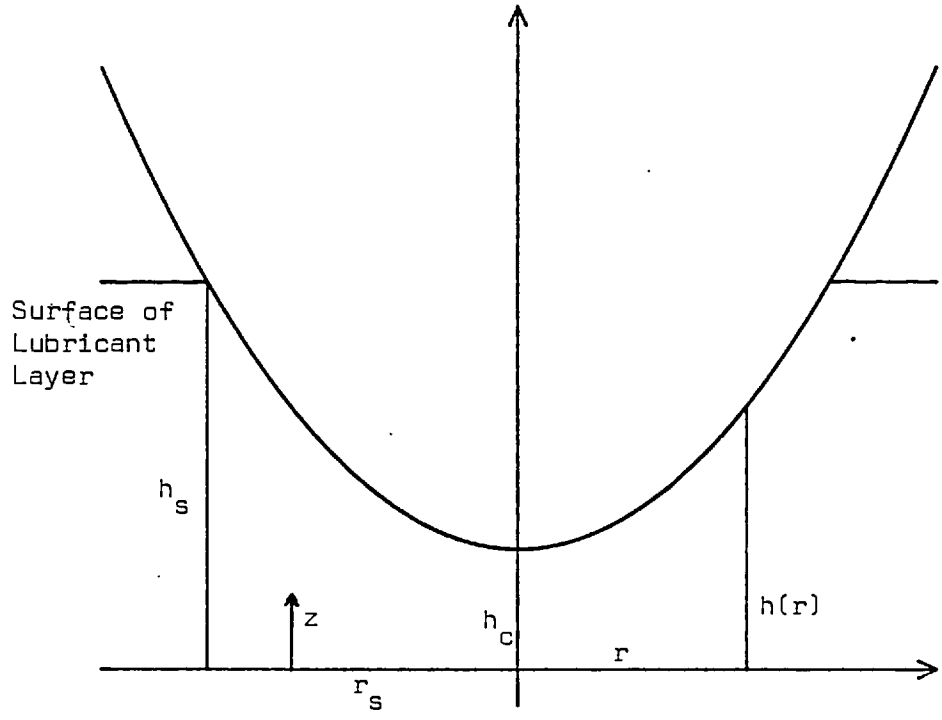

Figure 2.1. The Rigid Body Co-ordinate System

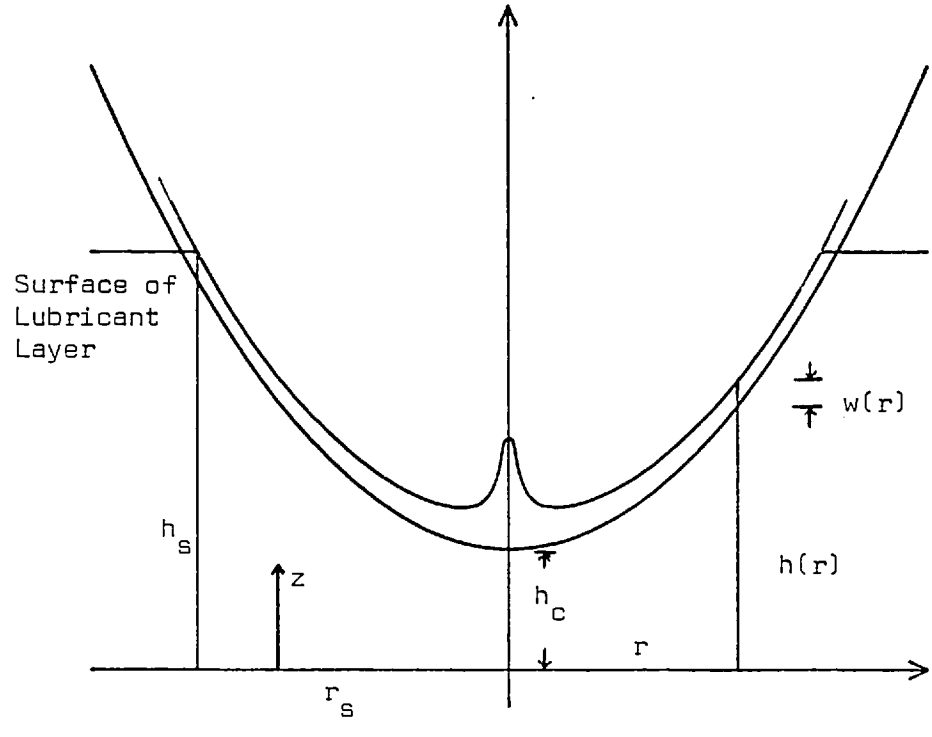

Figure 2.2. The Elastic Body Co-ordinate System.

CHAPTER TWO

THE EQUATIONS TO BE SOLVED

In this chapter the equations needed will be set up in their general form; during the remainder of the thesis particular cases considered will be obtained by substituting into these general equations.

Before they are presented, the physical system, together with relevant nomenclature, will be shown.

2.1 Physical System and Coordinates.

Consider a rigid ball of mass m approaching a rigid plane at velocity v_c (note that for approach $v_c < 0$), and h_c is the minimum clearance between the ball and the plane. (See Figure 2.1.)

By definition

$$v_c = \dot{h}_c \qquad (2.1)$$

At time t = 0, there is a layer of liquid of depth h_s and the ball is just touching the surface of the liquid. Its initial velocity is $v_c(0)=v_s$ and $h_c(0)=h_s$. $h(r)$, the local film thickness, is a function of h_c and the film shape. i.e.

$$h(r)=h_c+s(r) \qquad (2.2)$$

where $s(r)$ is the shape function.

r_s is defined such that $h(r_s)=h_s$.

When the ball and plane are both considered to be elastic, the co-ordinate system needs to be modified. To ease the representation of the system, the plane is assumed to be perfectly rigid and only the ball is elastic (as shown in Figure 2.2). This means that the ball is assumed to have elastic moduli that account for the elasticity of the plane as well as its own. This is reasonable as long as the radius of curvature is large compared to the local distortion, which is a requirement for the Reynolds equation to apply.

The local film thickness, h(r), may now be written as

$$h(r)=h_c+s(r)+w(r) \qquad (2.3)$$

where s(r) is the shape function

w(r) is the local vertical deformation.

The vertical velocity at any point on the surface is given by

$$\frac{dh(r)}{dt} = v_c + \frac{dw(r)}{dt} \qquad (2.4)$$

and h_c is the clearance that the ball would have had if it were rigid.

Cylinderical polar coordinates were used for this problem and, due to the axisymmetry, $\frac{dX}{d\theta} = 0$ for every function X. z gives the local co-ordinate across the film thickness.

2.2 The Dynamics Equation.

Consider a ball dropping under gravity into an oil film. There are two forces acting on the ball: gravity, which serves to accelerate it;

and the film force, which acts to retard it. If the ball in considered to be of point mass, then

$$m\ddot{h}_c = \int_0^{r_s} 2\pi pr.dr - mg \qquad (2.5)$$

where p(r) is the pressure field resulting from viscous action. The upper limit of integration is discussed in section 2.3.3.

Reference will be made to both net force and to film force. These represent $m\ddot{h}_c$ and $\int_0^{r_s} 2\pi pr.dr$ respectively. The film force may also be referred to as the fluid force.

The ball will be assumed to have its mass concentrated at its centroid and its surface to be instantly deformable. The assumption of point mass has no effect for the rigid case, and, for an elastic ball, although the distortions are large compared with film thickness, they are still very small relative to the radius of the ball. Comparing relative volume movements, the change in centroid position is seen to be negligible.

The effects of shock waves into the ball are neglected. They would travel over a diameter of a 1 cm radius steel ball and back in 8 μs and due to the curvature of the ball would have time to decay into random motion within one time step, typically 100 μs.

The effect of buoyancy is neglected, as only impacts into thin layers of oil are considered.

2.3 The Axisymmetric Reynolds Equation.

2.3.1 General Form.

DOWSON, 1962 (extended by FOWLES, 1970) has shown that if the following

assumptions hold for a fluid film in pure squeeze:-

1. The radius of curvature of the bearing components is large compared with the film thickness.

2. The lubricant is a Newtonian fluid.

3. Inertia and body force terms are small compared with the viscous and pressure terms in the equations of motion.

4. Owing to the geometry of the fluid film the fluid velocity derivative across the film is large compared with the other velocity gradients.

5. There is no slip between the fluid and bounding solids at common interfaces.

6. There are no surface tension effects.

7. The fluid is Stokesian.

8. Pressure is transmitted normally through the films without change.

then, using axisymmetric polar co-ordinates, and if

$$F_0 = \int_0^h \frac{dz'}{\eta}$$

$$F_1 = \int_0^h \frac{z'dz'}{\eta}$$

$$M_1 = \int_0^h \rho \int_0^z \frac{dz'}{\eta} \, dz$$

$$M_2 = \frac{F_1 M_1}{F_0} - \int_0^h \rho \int_0^z \frac{z'dz'}{\eta} \, dz$$

then

$$\frac{1}{r} \frac{\partial}{\partial r} \left(rM_2 \frac{\partial p}{\partial r}\right) = \int_0^h \left(\frac{\partial \rho}{\partial t}\right) dz + (\rho v)_h - (\rho v)_0 \qquad (2.6)$$

This equation has been obtained by using the continuity equation, together with the Navier-Stokes equation for the forces on an element, and then using an order of magnitude analysis to eliminate small order terms.

2.3.2. The Isothermal Reynolds Equation.

If it is further assumed that the fluid has constant properties over the thickness of the film, which will be true for a fluid with a time and temperature independent viscosity and density, then

$$F_0 = \frac{h}{\eta}$$

$$F_1 = \frac{h^2}{2\eta}$$

$$M_1 = \frac{\rho h^2}{2\eta} \qquad (2.7)$$

$$M_2 = \frac{1}{12} \frac{\rho h^3}{\eta}$$

$$\int_0^h \frac{\partial \rho}{\partial t} dz = h \frac{\partial \rho}{\partial t}$$

This gives, on writing $Y = \frac{\rho h^3}{\eta}$, the isothermal Reynolds equation

$$\frac{1}{r}\frac{\partial}{\partial r}\left(rY\frac{\partial p}{\partial r}\right) = 12\frac{\partial}{\partial t}(\rho h) \qquad (2.8)$$

which may be written, on expanding the derivative and dividing throughout by $Y (Y \neq 0)$

$$\frac{\partial^2 p}{\partial r^2} + \left(\frac{1}{r} + \frac{1}{Y}\frac{\partial Y}{\partial r}\right)\frac{\partial p}{\partial r} = 12\frac{\partial}{\partial t}(\rho h)/Y \qquad (2.9)$$

This is the most general form of the Reynolds Equation that is to be considered in the major part of this work.

2.3.3 Boundary Conditions on Reynolds Equation.

As the system is axisymmetric, from a consideration the continuity equation,

$$\frac{1}{r}\frac{\partial}{\partial r}(\rho u_r) + \frac{\partial}{\partial z}(\rho u_z) = \frac{\partial \rho}{\partial t}$$

then

$$\frac{\partial u_r}{\partial r} = 0 \text{ at } r=0$$

Consequently the first boundary condition is that

$$\frac{\partial p}{\partial r} = 0 \text{ at } r=0 \qquad (2.10)$$

The second boundary condition is one on the pressure value. Other workers CHRISTENSEN, 1970; CHENG and LEE, 1971, have used the condition that $\lim_{r \to \infty} p(r)=0$. This is normally interpreted as $p(x)=0$, where x is some "sufficiently" large value of radius.

In this work a more limited finite boundary condition was used, as the ball only only extends to r=R. The one chosen here was that $p(r_s)=0$.

A further assumption for the radial extent of the film, is that there is no wave making effect that alters the load by having any pressure (positive or negative) in the region outside $r=r_s$.

2.3.4 The Equation at the Origin.

If the spatial derivative term in Reynolds Equation is expanded, then

$$M_2 \frac{\partial^2 p}{\partial r^2} + \left\{\frac{M_2}{r} + \frac{\partial M_2}{\partial r}\right\} \frac{\partial p}{\partial r} = \int_0^h \frac{\partial \rho}{\partial t} \, dz + (\rho v)_h$$

At the origin both r=0 and $\frac{\partial p}{\partial r}=0$ so, using L'Hopital's rule, the above equation reduces to, as $M_2(0) \neq 0$,

$$2M_2 \frac{\partial^2 p}{\partial r^2} = \int_0^h \frac{\partial \rho}{\partial t} \, dz + (\rho v)_h \qquad (2.11)$$

which, on assuming constant properties across the film, gives

$$2Y \frac{\partial^2 p}{\partial r^2} - 12 \frac{\partial}{\partial t} (\rho v)_h = 0 \qquad (2.12)$$

2.3.5 The Validity of Using the Reynolds Equation.

In the initial stages of the impact, $r_s \ll h_c$, which reduces the validity of using the Reynolds Equation (2.6), as assumption (3) of DOWSON (in section 2.3.1) requires $r_s \gg h_c$.

However, in the initial stages of impact and at the velocities used here, there is negligible load in the first few milliseconds of impact

and consequently the ball is basically under free fall until such a time that $r_s \gg h_c$, when the pressure becomes significant and the conditions for the Reynolds Equation hold.

2.4 Ball Shape.

For a rigid ball of radius R having a minimum clearance h_c above a plane, the clearance normal to the surface at any other point within the ball radius is given by

$$h(r) = h_c + R\left(1 - \sqrt{1-(\frac{r}{R})^2}\right) \qquad (2.13)$$

For thin films, since the width of the contact region is small compared to the radius, $\frac{r}{R} \ll 1$. Also as h^3 is the important term for pressure generation when considering the shape of the ball, this effect is the dominant term near the origin. The expression for the film thickness may be expanded to give (on neglecting terms in $(\frac{r}{R})^4$ and higher)

$$h(r) = h_c + \frac{r^2}{2R} \qquad (2.14)$$

The effect of making this approximation is twofold: one is to reduce the curvature of the film in the outer regions; and the other is to move the radial extremity of the film further out from the centre.

In terms of the film force and pressure distribution obtained, these two effects tend to cancel each other out. Computer runs have been made to check this approximation and the results obtained are in section 3.9.

The results obtained in this work are referred to as either "ball"

or "parabola" depending on whether the exact shape is used or the parabolic approximation has been made. Almost all results are for the parabolic approximation.

2.5 Equations of State for the Fluids.

This work does not touch upon the problem of time dependent state equations. This is for two reasons:-

1) The computation using models of this form would be prohibitively expensive. The method used would be an extension of the temperature generation algorithm (see Appendix 3).
2) At this time there are no satisfactory models that have been obtained from experimental work. Consequently to include such effects is necessarily arbitrary.

2.5.1 Density/Pressure. $\rho=\rho(p)$

The relation used is that first given by DOWSON and WHITAKER (1965) that,

$$\rho=\rho_0\left(1+\frac{\rho_a p}{1+\rho_b p}\right) \qquad (2.15)$$

where $\rho_a = 5.828 \times 10^{-10}\ Pa^{-1}$, $\rho_b = 16.84 \times 10^{-10}\ Pa^{-1}$, p is the local pressure.

2.5.2 Viscosity/Pressure. $\eta=\eta(p)$

In this work three models are considered:

a) Exponential Model.

This is the standard model used in elastohydrodynamic lubrication.

$$\eta=\eta_0 e^{\alpha p} \qquad (2.16)$$

b) "Mark I" Model.

As the simple exponential model is known to give problems in numerical solution, it was decided to use a model with a limited viscosity. This was obtained by imposing a cut-off on the curve:

$$\eta = \eta_0 e^{\alpha p} \quad , \quad p<p_L$$
$$\eta_0 e^{\alpha p_L} \quad , \quad p \geq p_L \qquad (2.17)$$

There is evidence for a limiting viscosity from both the work of ALLEN, ZARETSKY and TOWNSEND, 1970, and from PAUL, 1971. Note that if $p_L=0$, the isoviscous case results.

c) "Mark II" Model.

The Mark I viscosity model was found to give rise to numerical problems when the peak pressure moved through the value p_L. Slight instabilities occured. It was felt that a physical property such as viscosity would not have a sharp cut-off and so a Mark II model was developed. It is basically a hyperbola with asymptotes $\log_e \eta/\eta_0=\alpha p$ $\log_e \eta/\eta_0=\alpha p_L$.

This model has the equation

$$\log_e \left(\frac{\eta}{\eta_0}\right) = X(\alpha p+\alpha p_L) - \sqrt{X^2(\alpha p+\alpha p_L)^2 - 2X\alpha p.\alpha p_L} \qquad (2.18)$$

where $X = 0.5\ (1+c)$.

Note that c and p are both free parameters. The value

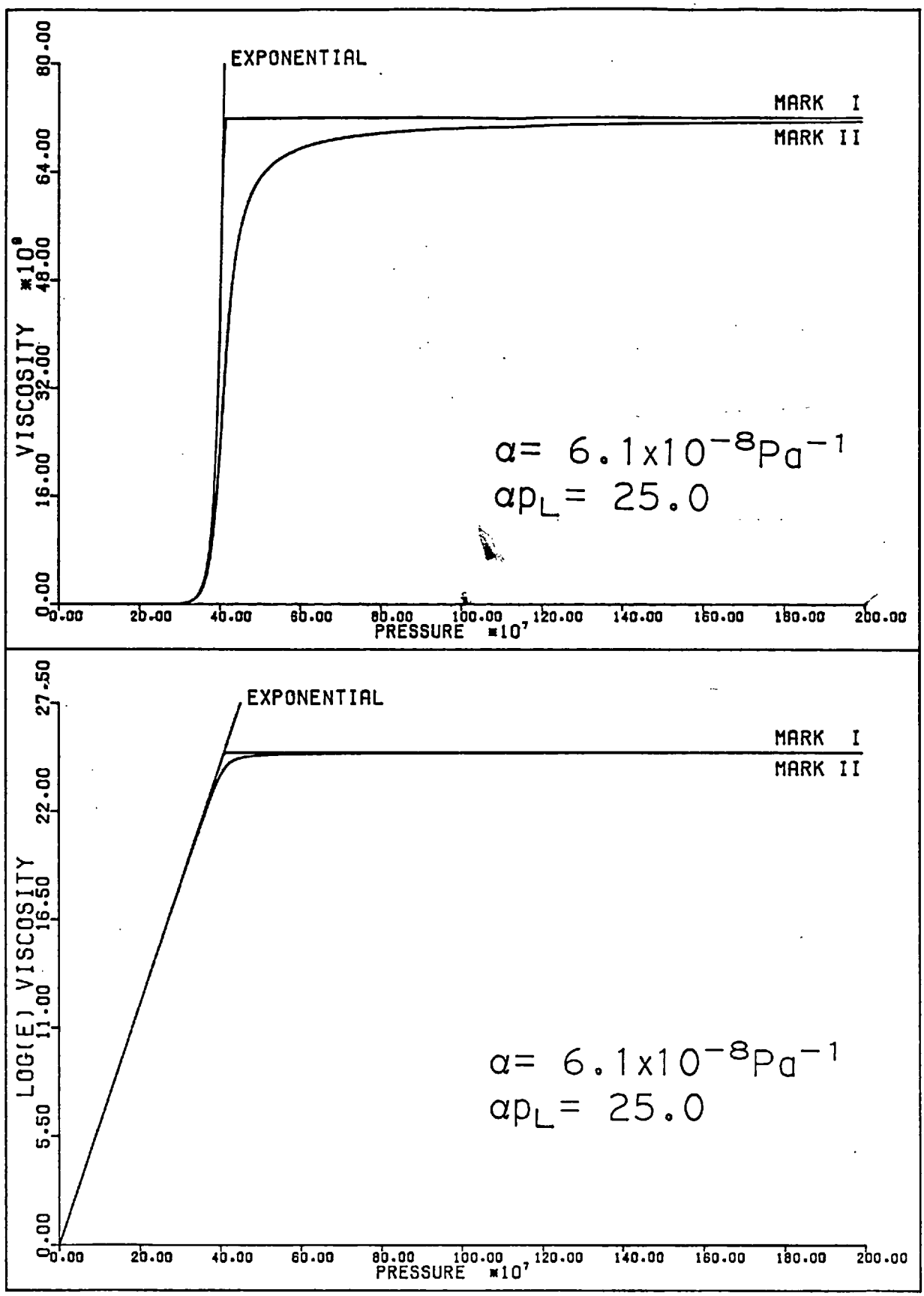

Figure 2.3. Viscosity-Pressure Graphs

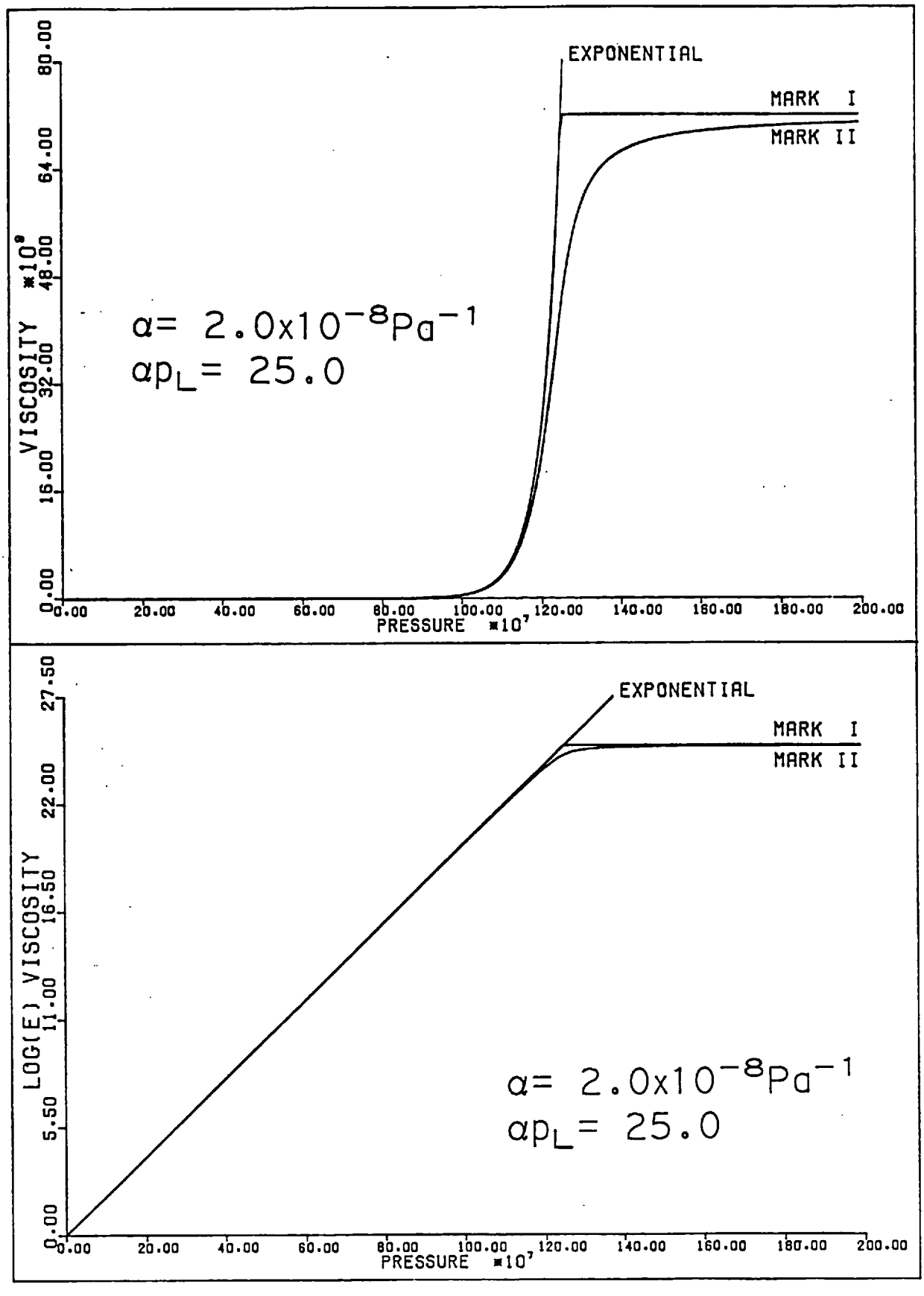

Figure 2.4. Viscosity-Pressure Graphs

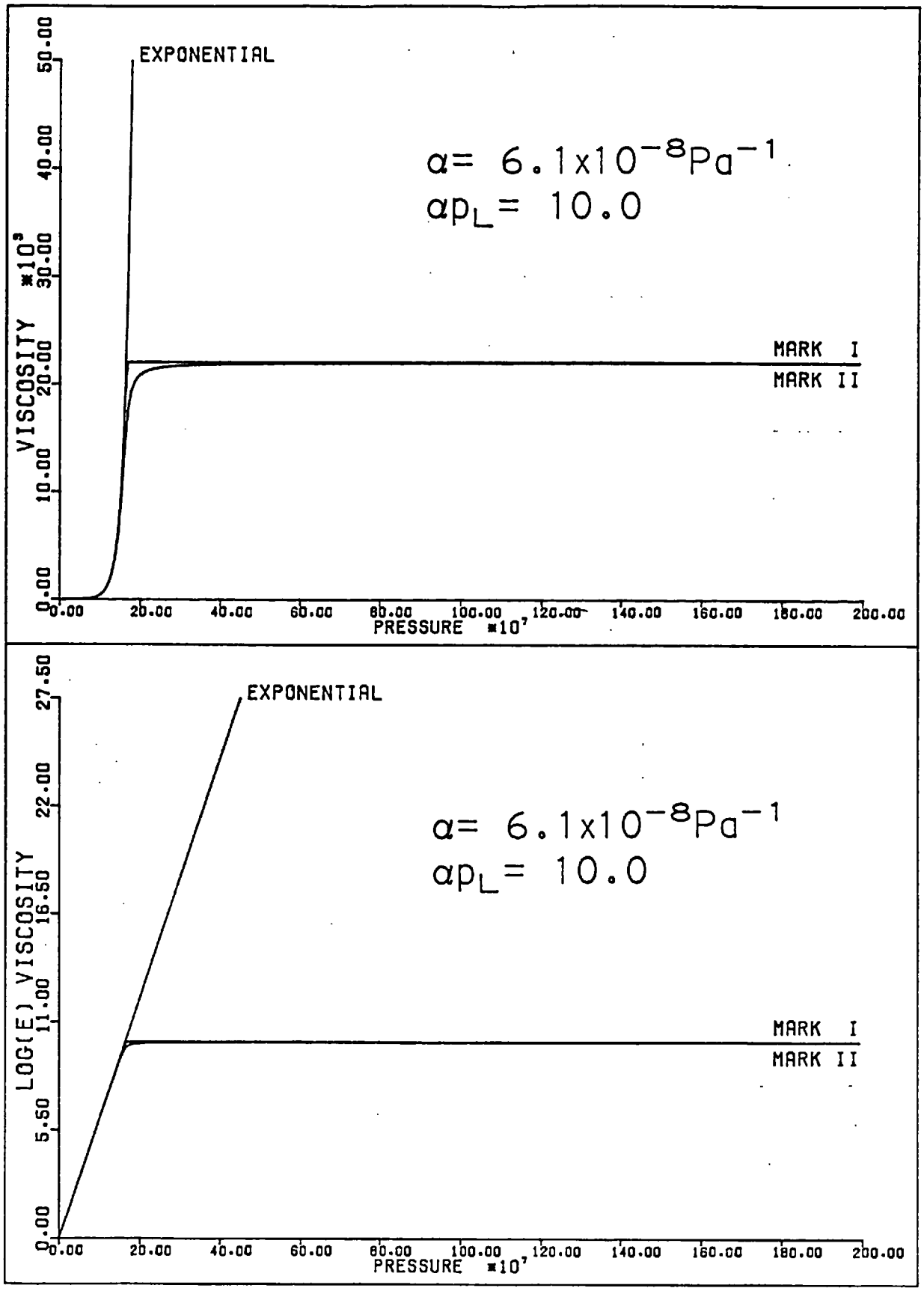

Figure 2.5. Viscosity-Pressure Graphs.

of c was chosen to be $\alpha \times 2\times10^4$ which gave a closely fitting curve. The value of αp_L was chosen to be 25, so that the base viscosity could change by at most 10 orders of magnitude. This is greater than has been observed experimentally in dynamic contacts. It must be emphasied that the general program developed here is capable of accepting any time-independent piezoviscous function as long as it is:-

1) well-defined;
2) has a well-defined first derivative with respect to p; and
3) an approximation to the second pressure derivative is given.

This may sound quite restrictive, but a consideration of the most probable physical systems will show that it is not so.

A viscosity-pressure function should be continuous and smooth, hence it will have a first derivative. The requirement on the second derivative is not so important, and may be obtained by a coarse difference method. However having an exact second derivative is likely to speed the solution process.

Figures 2.3, 2.4 and 2.5 show various distributions for differing values of α and αp_L. The values for α are the two used in the numerical calculation for the elastic case.

2.6 Elasticity of the Bounding Solids.

In this work the vertical distortion, w and horizontal distortion u are given by:

$$w = L_1 p \ , \qquad u = L_2 p \qquad (2.19)$$

where the L are linear operators acting on the distributed pressure and are calculated from the Boussinesq formulae (TIMONSHENKO and GOODIER, 1970).

They imply an assumption that the ball may be approximated by an infinite half space. It is reasonable to make this approximation for balls whose radii are large compared to the distortions. Further both the ball and plane are assumed to be homogenous and isotropic.

The Winkler foundation, one in which the distortion at a point is proportional only to the pressure applied at that point, was not considered. This model is often used when very soft materials are modelled. (NORMAN, 1971; CONWAY, 1973; NAKANO and HORI, 1975).

The effect of horizontal distortion was found to be small. When included in the calculation in one computer run, it gave no discernable difference in the results, the peak pressure being altered by at most 0.1%.

The effect was included by assuming that the film shape is given by:

$$h(r) = h_c + \frac{(r-u(r))^2}{2R} + w(r) \qquad (2.20)$$

Note that there is a small error in this due to the fact that u(r) is the distortion of a point originally at r when the pressure field was applied, whereas the accurate solution requires the deflection obtained for a point that moves to r after the pressure has been applied, that is, ideally

$$h(r) = h_c + \frac{s^2}{2R} + w(r) \qquad (2.21)$$

where $r = s + u(s)$.

The Boussinesq formulae state that for a point load W acting on the surface of a semi-infinite plane with elastic coefficients ν,E, then at

a distance r away, the vertical deformation w and the horizontal deformation u are given by

$$w = \frac{(1-\nu^2)}{\pi E} \frac{W}{r} , \qquad u = - \frac{(1+\nu)(1-2\nu)}{2\pi E} \frac{W}{r} \quad (2.22)$$

If the ball has elastic constants ν_1, E_1, and the plane has constants ν_2, E_2, and if E' and E* are defined by

$$\frac{1}{\pi E'} = \frac{1-\nu_1^2}{\pi E_1} + \frac{1-\nu_2^2}{\pi E_2} \quad (2.23)$$

$$\frac{1}{\pi E^*} = \frac{(1-2\nu_1)(1+\nu_1)}{\pi E_1} \quad (2.24)$$

then

$$w = \frac{1}{\pi E'} \frac{W}{r} , \qquad u = - \frac{1}{2\pi E^*} \frac{W}{r} \quad (2.25)$$

Note that E' is defined so that it is the sum of the effective elastic constants, whereas CHENG and LEE have defined E' to be the average effective elastic constant, and consequently it has a value twice that of this work.

E* includes only the elasticity of the ball and not of the plane. This is because the horizontal deformation is used in order to calculate the film thickness using equation 2.20. Any horizontal deformation of the flat plane will have no effect in this respect.

2.7 On the Note of GOULD, 1971.

It is appropriate to discuss the note by GOULD. He was concerned to show that the effect of temperature on the viscosity cannot be ignored if the pressure generated is such that it significantly alters the viscosity. He considered an isoviscous incompressible oil being squeezed

by a parabola and solved the isothermal Reynolds Equation using the boundary conditions $p(\infty)=0$ for a ball dropping at a constant velocity. Then, using the radial energy equation for incompressible fluids, he found the maximum temperature increase, assuming adiabatic conditions hold. He then concluded that

> "In squeeze films in which the variation of viscosity with temperature is important, the variation of viscosity with pressure will also be important."

It was felt that for the system discussed in this thesis, in regions where the elastic effects would become important, it was a serious error to assume that the velocity of approach to be constant. Instead it should be considered to be exponentially decaying, i.e.

$$h_c = h_0 e^{\lambda t}, \quad \lambda < 0 \tag{2.26}$$

$$v_c = \lambda h_c = \lambda h_0 e^{\lambda t} \tag{2.27}$$

(See section 3.7 for the solution of the isoviscous incompressible rigid system).

The equations of GOULD were reworked using these equations for film thickness and ball velocity, giving

$$p = -\frac{3\eta_0 \lambda h_c R}{(h_c + \frac{r^2}{2R})^2} \tag{2.28}$$

$$p_c = -\frac{3\eta_0 \lambda R}{h_c} \tag{2.29}$$

The adiabatic energy equation in which conductivity is ignored may

be written at the bounding surface z=0 (where $u_r=u_z=0$) and if T_w is the temperature at the wall (with initial value T_0) then

$$\frac{\partial T_w}{\partial t} = 9\,\frac{\eta_0}{\rho c}\;\;\frac{r^2\lambda^2 h_c^{\,2}}{(h_c+\frac{r^2}{2R})^4} \qquad (2.30)$$

This may be integrated with respect to time to obtain

$$T_w-T_0 = \int_0^t 9\,\frac{\eta_0}{\rho c}\;\;\frac{r^2\lambda^2 h_c^{\,2}}{(h_c+\frac{r^2}{2R})^4}\;\;dt$$

$$= \int_{h_0}^{h_c} 9\,\frac{\eta_0}{\rho c}\;\;\frac{r^2\lambda^2 h_c^{*}}{(h_c^{*}+\frac{r^2}{2R})^4}\;\;\frac{1}{\lambda h_c^{*}}\;dh_c^{*} \qquad \text{as } h_c=h_0e^{\lambda t}$$

$$= \int_{h_0}^{h_c} 9\,\frac{\eta_0}{\rho c}\;\;\frac{r^2\lambda h_c^{*}}{(h_c^{*}+\frac{r^2}{2R})^4}\;\;dh_c^{*}$$

$$= -\frac{3}{2}\;\;\frac{\eta_0}{\rho c}\;\;\left[r^2\lambda\;\;\frac{(3h_c^{*}+\frac{r^2}{2R})}{(h_c^{*}+\frac{r^2}{2R})^3}\right]_{h_0}^{h_c} \qquad (2.31)$$

The radial maximum of this function occurs where

$$\frac{12R^2h_c^{\,2}-8Rh_cr^2-r^4}{(2Rh_c+r^2)^4} - \frac{12R^2h_0^{\,2}-8Rh_0r^2-r^4}{(2Rh_0+r^2)^4} = 0 \qquad (2.32)$$

At this point

$$T_w-T_0 = -6\,\frac{\eta_0R^2\lambda}{\rho c}\;r^2\left(\frac{6Rh_c+r^2}{(2Rh_c+r^2)^3} - \frac{6Rh_0+r^2}{(2Rh_0+r^2)^3}\right) \qquad (2.33)$$

$$p = -\frac{3\eta_0\lambda h_c 4R^3}{(2Rh_c+r^2)^2} \qquad (2.34)$$

If it is assumed that the liquid has a viscosity-temperature pressure relation of the form

$$\eta=\eta_0 e^{\alpha p-\delta T} \qquad (2.35)$$

then, at any point the local viscosity will decrease or increase compared to η_0 as the ratio $\frac{\delta(T_w-T_0)}{\alpha p} \lesseqgtr 0$

GOULD used the ratio $\frac{\delta(T_w-T_0)}{\alpha p_c}$ which in general is less than the ratio given previously.

In this case

$$\frac{\delta(T_w-T_0)}{\alpha p} = D\,\frac{r^2(2Rh_c+r^2)^2}{2Rh_c}\left\{\frac{6Rh_c+r^2}{(2Rh_c+r^2)^3} - \frac{6Rh_0+r^2}{(2Rh_0+r^2)^3}\right\} \qquad (2.36)$$

This is significantly different from $\frac{8}{27}D$ - GOULD's result.

Writing $2Rh_0 = A$, $h_c = Ch_0$, $r^2 = kA$ (2.37)

The maximum wall temperature T_w^* occurs where

$$\frac{3C^2-4Ck-k^2}{(C+k)^4} - \frac{3-4k-k^2}{(1+k)^4} = 0 \qquad (2.38)$$

and

$$\frac{\delta(T_w^*-T_0)}{\alpha p} = D\,\frac{k(C+k)^2}{C}\left\{\frac{3C+k}{(C+k)^3} - \frac{3+k}{(1+k)^3}\right\} = D.F(C,k), \text{ say}$$

For any value of C, k may be calculated, hence the ratio, e.g.

C	k	F(C,k)
0.99	0.33166	0.011278
0.9	0.31586	0.11545

C	k	F(C,k) (cont...)
0.8	0.29664	0.23740
0.6	0.25126	0.50547
0.4	0.19313	0.81463
0.2	0.11385	1.16845
0.1	0.06176	1.33988
0.01	0.006453	1.42927
0.001	0.0006457	1.43049
0.0001	0.00006458	1.43050

As there is conduction from the fluid into the bounding solids, these temperatures give maximum values. Under appropriate conditions the temeperature rise is not significant during the phase where the elastic distortion is important. As C decreases, the ratio F(C,k) increases rapidly initially then increases only slowly. However, the trajectory is exponentially decaying and so the time taken for C to decrease by a fixed amount is increasing exponentially. Hence, time is available for conduction effects to be a significant factor in dissipating the energy from within the contact zone.

Allowing for conduction would tend to suggest that the effect of temperature rise is small initially, becoming relatively larger, but in the region of very thin films the effect of temperature decreases again.

When the effect of exponential viscosity is taken into account, this must be further amended, for the temperature rise is very small at the centre. The load concentrates towards the centre, thus as the pressure drops in the outer region (see frontispiece) the effect of the temperature rise will merely accelerate this concentration.

HIRST and LEWIS, 1973, come to the conclusion that the temperature

rise is negligible by considering the Peclet number under the conditions that should hold for this system.

CHAPTER THREE

THE SOLUTION FOR A PARABOLA SQUEEZING AN INCOMPRESSIBLE EXPONENTIAL PIEZOSCOUS FLUID.

3.1 The Mathematical Model.

In this chapter a solution will be presented for the case of a rigid parabola squeezing through an incompressible exponential fluid film. These conditions imply that the following equations need to be solved simultaneously:

1) Dynamic

$$m\ddot{h}_c = \int_0^{r_s} 2\pi p r dr - mg \qquad (3.1)$$

2) Reynolds

$$\frac{1}{r}\frac{\partial}{\partial r}\left(rY\frac{\partial p}{\partial r}\right) = 12\frac{\partial}{\partial t}(\rho h) \qquad (3.2)$$

3) Shape

$$h = h_c + \frac{r^2}{2R} \qquad (3.3)$$

4) Equations of State

$$\rho = \rho_0 \qquad (3.4.1)$$

$$\eta = \eta_0 e^{\alpha p} \qquad (3.4.2)$$

5) Elasticity

$$w = 0 \qquad (3.5)$$

Substituting (3.4.1) and (3.5) into (3.2), a reduced Reynolds Equation results:

$$\frac{1}{r}\frac{d}{dr}\left(r\frac{h^3}{\eta}\frac{dp}{dr}\right) = 12V_c \qquad (3.6)$$

This may be integrated with respect to r to obtain

$$r\frac{h^3}{\eta}\frac{dp}{dr} = 6r^2v_c + C$$

Using the boundary condition $\frac{dp}{dr} = 0$ at r=0, gives C=0, hence

$$\frac{h^3}{\eta}\frac{dp}{dr} = 6rv_c$$

Now, as $h^3 \neq 0$, dividing by h^3, integration w.r.t. r may again be performed and using $p(r_s) = 0$ as the second boundary condition

$$\int_0^p \frac{dp}{\eta} = 6v_c \int_{r_s}^r \frac{rdr}{h^3} \qquad (3.7)$$

The body is rigid and the viscosity is a function only of pressure. Thus the left hand side of the equation is a function of pressure and depends only on the viscosity model chosen; the right hand side is a function of the geometry and depends only on the impactor shape. Consequently they may be considered separately.

If equality cannot be achieved, then the model breaks down. This is discussed further in section 3.5.3.

If the left hand side of equation 3.7 is first considered, then, using equation 3.4.2

$$\int_0^p \frac{dp}{\eta} = \frac{1-e^{-\alpha p}}{\eta_0 \alpha} \qquad (3.8)$$

This expression has maximum value $\frac{1}{\eta_0 \alpha}$

For the right hand side, as equation 3.3 holds, then

$$Rdh = rdr \qquad (3.9)$$

so

$$6v_c \int_{r_s}^{r} \frac{rdr}{h^3} = 6v_c R \int_{h_s}^{h} \frac{dh}{h^3} = 3v_c R\left(\frac{1}{h_s^2} - \frac{1}{h^2}\right) \qquad (3.10)$$

Hence, combining (3.8) and (3.10)

$$p = -\frac{1}{\alpha} \log_e\left(1-3\eta_0\alpha v_c R\left(\frac{1}{h_s^2} - \frac{1}{h^2}\right)\right) \qquad (3.11)$$

In order to map the trajectory, equation (3.1) for the ball dynamics needs to be incorporated. Now

$$2\pi \int_0^{r_s} p(r)rdr = 2\pi R \int_{h_c}^{h_s} p(h)dh$$

$$= -\frac{2\pi R}{\alpha} \int_{h_c}^{h_s} \log_e\left(1-3\eta_0\alpha v_c R\left(\frac{1}{h_s^2} - \frac{1}{h^2}\right)\right) dh \qquad (3.12)$$

By writing

$$\beta^2 = 3\eta_0\alpha v_c R, \quad \gamma^2 = 1+\beta^2/h_s^2, \quad \delta = \beta / \gamma$$

after manipulation this integration yields

$$2\pi \int_0^{r_s} p(r)rdr = \frac{2\pi R}{\alpha} \left\{ h_c \log_e(\gamma^2-\beta^2/h_c^2)+\delta \log_e\left(\frac{h_s-\delta}{h_s+\delta} \cdot \frac{h_c+\delta}{h_c-\delta}\right) \right\}$$

$$= \frac{2\pi R}{\alpha} \left\{2h_c \log_e\left(\frac{\gamma}{h_c}\right) + (h_c+\delta) \log_e(h_c+\delta) \right.$$

$$\left. + (h_c-\delta) \log_e(h_c-\delta) + \delta \log_e \frac{h_s-\delta}{h_s+\delta} \right\} \qquad (3.13)$$

Now p_c may be written in the form

$$p_c = -\frac{1}{\alpha} \left\{2\log_e\left(\frac{\gamma}{h_c}\right)+\log_e(h_c+\delta)+\log(h_c-\delta) \right\} \qquad (3.14)$$

so $p_c \to \infty$ as $h_c \to \delta$, thus δ gives the minimum height at which flow can occur in this system for a given velocity. δ is a function of v_c only, for a given run has η_0, α, h_s fixed.

It can be seen that the corresponding term in the film force (3.13), is $(h_c-\delta)\log_e(h_c-\delta)$ which remains finite as $h_c \to \delta$. This has effects that will be discussed later in section 3.5.3.

3.2 Integration with Time.

The instantaneous force defined in (3.13) may be substituted into (3.1) to obtain an equation of the form

$$\ddot{h}_c = f(h_c, \dot{h}_c) \qquad (3.15)$$

subject to initial conditions $\dot{h}_c(0)=v_s$, $h_c(0)=h_s$

This formulation is recognizable as an initial value problem.

Even for this simplified physical system, there is no known analytical solution with time, so numerical approximation must be used. There are many methods available, but for this type of system the equation (3.15) is first written as two simultaneous first order differential equations

$$\dot{v}_c = f(v_c, h_c) \qquad (3.15.1)$$

$$\dot{h}_c = v_c \qquad (3.15.2)$$

where

$$f(v_c, h_c) = \frac{2\pi}{m}\int_0^{r_s} p(r)\,r\,dr - g$$

$f(v_c,h_c)$ is wholly defined by (v_c,h_c) and for a given run all other parameters remain fixed, hence there are no elastic effects to give rise to higher time derivatives. This problem is independent of time, except indirectly in that time derivatives of various functions are needed, so that altering the time base by a constant, T, will have no effect on the solution except a time axis displacememt.

The method used initially to integrate these equations was Runge-Kutta-Merson. This gives an approximation to the local truncation error committed per time step taken. It may be summarised as follows. For a step of length Δt in the independent variable from t_n to t_{n+1}, if $\dot{y} = f(t,y)$ and if

$$k_1=\Delta t.f(t_n,y_n)$$
$$k_2=\Delta t.f(t_n+\Delta t/3,\ y_n+k_1/3)$$
$$k_3=\Delta t.f(t_n+\Delta t/3,y_n+k_1/6+k_2/6)$$
$$k_4=\Delta t.f(t_n+\Delta t/2,y_n+k_1/8+3k_3/8)$$
$$k_5=\Delta t.f(t_n+\Delta t,\ y_n+k_1/2-3k_3/2+2k_4)$$

are calculated, then (3.17)

$$y_{n+1}=y_n+\frac{1}{6}(k_1+4k_4+k_5)$$

with local error estimate

$$E\doteq\frac{1}{30}[2k_1-9k_3+8k_4-k_5]$$

(and E is exact if $f(t,y)=At+By+C$)

This formula is obtained by expanding the Taylor series at several points and then eliminating the higher derivates up to order Δt^4. Thus

it has an error of $O(\Delta t^5)$. It is generally regarded as advantageous to have a method that has a high order of convergence. This may not always be so for the region of convergence may be smaller and only small steps may be made. The great advantage of using Runge-Kutta methods is that they are self starting, but there is a price to be paid, as five derivative evaluations are needed for each step, no matter how well-behaved the function is.

3.3 Eigenvalues of the Problem and Stability of the Integration Method.

3.3.1 Motivation for Investigating this Effect.

It was found by experience that the problem was unstable when using fixed length time step integration methods. This instability occured when the ball was at a stage where the net force on it was small, and was steadily decaying approximately exponentially, towards zero net force. Prior to instability, the ball velocity and minimum film thickness, as first and second integrals were similarly well behaved, and the central pressure was increasing approximately exponentially with time. All factors of the analysis appeared well-behaved, then suddenly the value of the net force started to oscillate, gradually increasing in amplitude until the numerical integration required a solution in which $h_c \leq \delta$ and the calculation would stop.

If the time step was reduced, the same trajectory was followed (to within truncation error), but at the time where the previous run had given oscillatory results, this run gave smoothly monotonic curves. However, this gave only temporary respite, for it just delayed the onset of the instability until a later time.

Figure 3.1 shows an illustration of these effects. (For an explanation

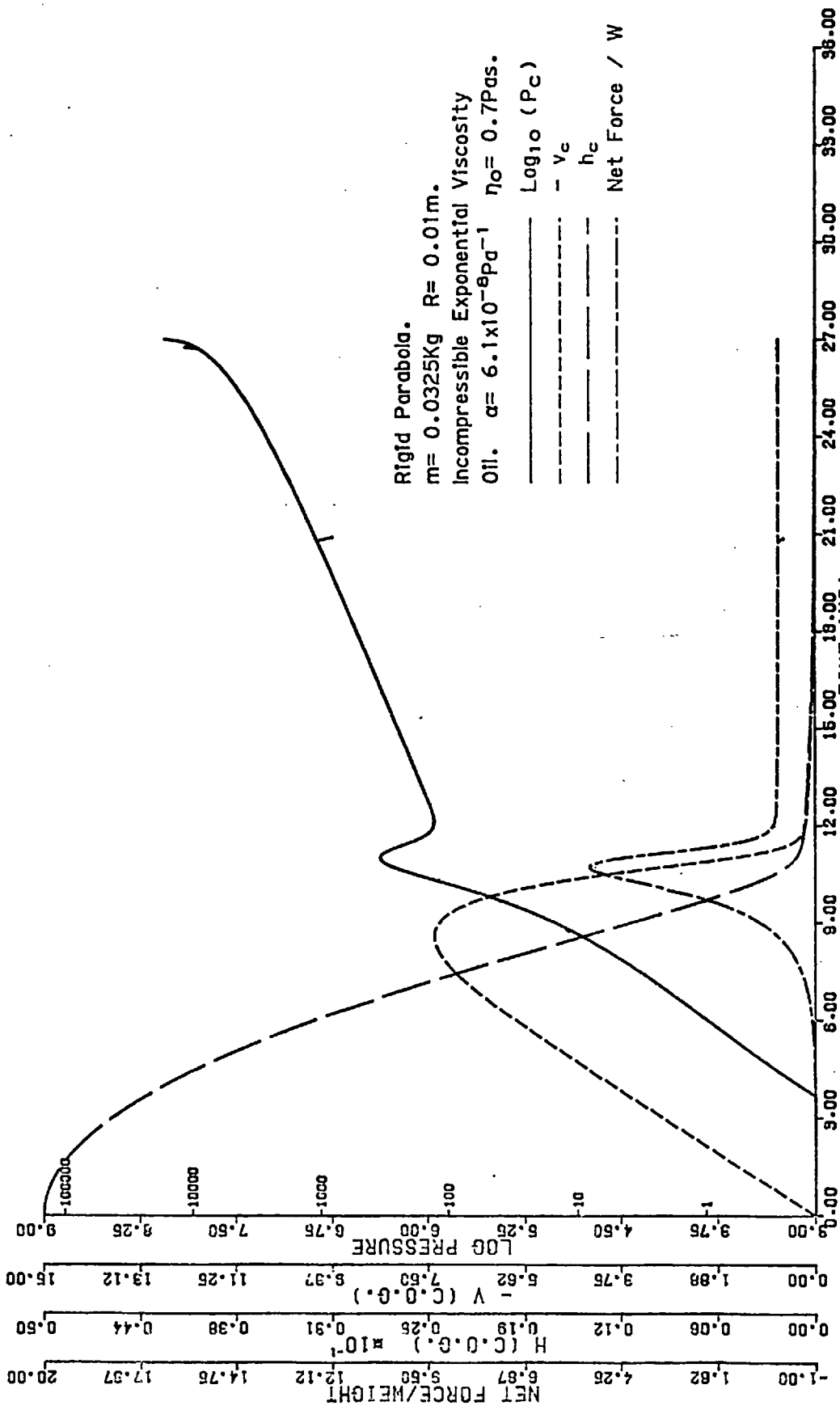

Figure 3.1. Base Run Solution With Fixed Step Integration.

of the graph coordinates see section 3.5.2).

There appear to be four curves drawn, but with slight branches at 21 ms and 27 ms. In fact there are three sets of four curves drawn, but most of the corresponding curves of each set are superimposed on each other.

The first set of curves were computed using a fixed time step of 10^{-4} second. At 21×10^{-3} s there is a branch from the main solution curve. This is where the instability occured for this time step.

The second set of curves use a time step of 10^{-5} second. This attains a time of 26.7×10^{-3} second before the fatal oscillations occur.

The third set of curves use a time step of 10^{-6} second. This solution does not exhibit the time step instability but gives $h_c \leq \delta$ on the solution curve and thus the problem cannot be integrated past this point, using the Runge-Kutta-Merson algorithm.

All curves were plotted at points a uniform 10^{-4} seconds apart. It may be seen, by inspection, that the sets of curves lie on one another, and so up to the time of instability the results are accurate to within truncation error for each value of time step.

This computational instability has been noted for incompressible isoviscous squeeze films by NORMAN, 1971. He states that "whatever finite difference method is used to calculate x and $\dot{x}$ (here h_c and $\dot{h}_c$), the trajectory finally goes unstable producing a spurious solution." This statement should be modified, but before this may be done, the eigenvalues of the system need to be considered.

3.3.2 The Solution of a first order ODE system with known eigenvalues.

In order to analyse this problem, consider initially the simplest non-trivial first order differential equation $\dot{y}=\lambda y+c$, with initial condition

$$y(0)=y_0 \tag{3.18.1}$$

This has the solution

$$y=y_0e^{\lambda t}+\frac{c}{\lambda}(e^{\lambda t}-1) \tag{3.18.2}$$

for whatever value λ locally takes. If $\lambda=\lambda(t)$ then by considering a small enough time interval Δt (One over which $\lambda(t)$ is sensibly constant)

$$y(t+\Delta t)=y(t)e^{\lambda(t)\Delta t}+\frac{c}{\lambda}(e^{\lambda(t)\Delta t}-1)$$

$\lambda(t)$ is known as the eigenvalue of the equation.

Now this may be extended to a second order system (such as is needed here)

$$\dot{v}_c=f(v_c,h_c)$$
$$\dot{h}_c=\cdot_c$$

This may be linearised into the form

$$\begin{pmatrix}\dot{v}_c\\ \dot{h}_c\end{pmatrix}=\begin{pmatrix}\frac{\partial\dot{v}_c}{\partial v_c} & \frac{\partial\dot{v}_c}{\partial h_c}\\ \frac{\partial h_c}{\partial v_c} & \frac{\partial h_c}{\partial h_c}\end{pmatrix}\begin{pmatrix}v_c\\ h_c\end{pmatrix}+\begin{pmatrix}C_v\\ C_h\end{pmatrix} \tag{3.19}$$

which may be written in matrix notation

$$\underline{\dot{x}}=\underline{\underline{J}}.\underline{x}+\underline{c} \tag{3.20}$$

This matrix $\underline{\underline{J}}$ may diagonalised by a transformation $\underline{\underline{T}}$ so that if $\underline{y}=\underline{\underline{T}}\underline{x}$ and $\underline{\underline{T}}\underline{\underline{J}}\underline{\underline{T}}^{-1}$ is a diagonal matrix

$$\dot{\underline{y}}=\underline{\underline{T}}\underline{\underline{J}}\underline{\underline{T}}^{-1}\underline{y} + \underline{\underline{T}}\,\underline{C} \qquad (3.21)$$

In this case the elements of $\underline{y}$ are independent of each other and thus they each have a solution of the type given in (3.18), hence there are two eigenvalues λ_1, λ_2. As $\underline{\underline{T}}^{-1}$ is non-diagonal and it is known (MINC and MARCUS, 1964), that under diagonalisation the eigenvalues are invariant, the solution contains a linear sum of both eigenvalue terms.

3.3.3 The Calculation of the Eigenvalues.

In order to find an explanation of the oscillatory behaviour, the linearised matrix $\underline{\underline{J}}$ was found and hence the eigenvalues of the system at any time were easy to calculate. Rather than differentiate (3.13) directly, it was decided to differentiate (3.12) and it was found that

$$\underline{\underline{J}} = \begin{pmatrix} -\frac{2\pi R}{m\alpha}\cdot\frac{1}{\gamma^2 v_c}\cdot\left[h(\gamma^2-1)+\frac{\delta}{2}\log\frac{h+\delta}{h-\delta}\right]_{h_c}^{h_s} & -\frac{2\pi R\alpha}{m\alpha}p_c \\ 1 & 0 \end{pmatrix} \qquad (3.22)$$

Hence the eigenvalues can be calculated for each point in time, and so as the problem is integrated in time, the values of $|\lambda\Delta t|$ were printed out. As there as two first order differential equations, there will be two eigenvalues. It was found that during the initial pressure rise the eigenvalues were a complex pair and were of a small enough magnitude such that the time steps normally taken were short enough to give $|\lambda\Delta t|=O(10^{-2})$. But, referring to Figure 3.1, just after the initial pressure peak, these changed into a real pair, both of negative sign, implying decaying terms. One was of fairly small magnitude and was basically the solution, however, the other was negative and increased

in magnitude as the solution proceeded. This second eigenvalue represented a transient part of the solution.

It was found that, when $\max|\lambda\Delta t| \doteq 3.0$, the oscillation began, resulting in spurious solutions.

3.4 Stiff Stability.

As was mentioned above, the oscillations began when $\max|\lambda\Delta t| \doteq 3.0$. Halving the time step just before this point gave only temporary respite, since this transient eigenvalue is continuously increasing in magnitude, and so after a short time $\max|\lambda\Delta t| > 3.0$ again.

In order to surmount this difficulty, another approach was needed. But first the type of problem will be defined. This configuration is called a stiff system (see GEAR, 1971). It occurs when there are large differences in the various rate processes of the system, the large negative eigenvalue(s) being transient compared to the main trend of the system.

An operational requirement of the Runge-Kutta methods (and most predictor-corrector methods in common use) is that $\max|\lambda\Delta t| < 2.7$, in order that they approximate $e^{\lambda t}$ accurately. If this condition is not satisfied, these methods produce a solution of the form $A(x)^m$, where $x < -1$ giving the oscillatory results found earlier.

There is a class of integration methods that are stiffly stable. (See, for example, GEAR, 1971). Methods of this type have solutions which are (using Figure 3.2):

1) absolutely stable in some region R_1 (Re $(\lambda\Delta t) \leq D$, for some $D<0$)

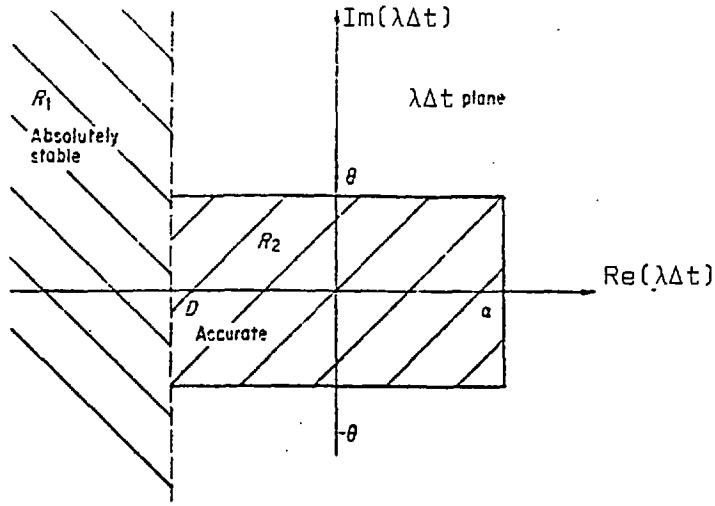

Fig. 11.5 Stiff stability. (GEAR)

Figure 3.2. Regions of Stability

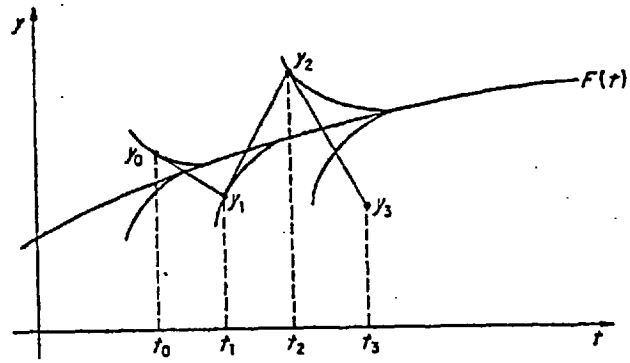

Fig. 11.2 Euler's method for stiff problems. (GEAR)

Figure 3.3. Stiff Forward Integration

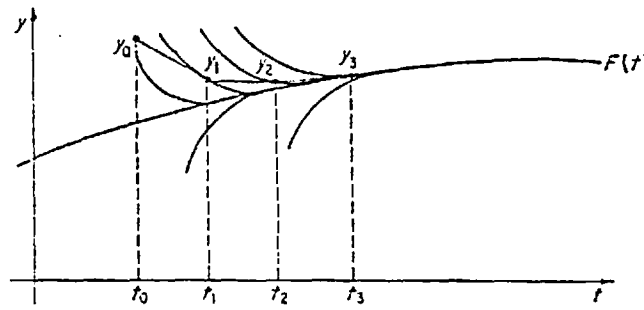

Fig. 11.3 The backward Euler method for stiff problems. (GEAR)

Figure 3.4. Stiff Backward Integration

of the $\lambda\Delta t$ plane (i.e. the solution is of the form $A(x)^m$, where $|x|<1$, so it decays to zero).

2) Accurate in the region of $R_2(0<Re(\lambda\Delta t)<\alpha, |Im(\lambda\Delta t)|<\beta)$ of the $\lambda\Delta t$ plane.

Thus if $\lambda\Delta t \epsilon R_1$ (i.e. the $\lambda\Delta t$ is in the region R_1) the solution has a rapidly decaying transient and some accuracy may be lost by neglecting the transient in order to obtain a solution at all. Δt should be chosen so that the non-transient part of the solution is integrated with $\lambda\Delta t \epsilon R_2$ (if there is more than one eigenvalue, a time step should be chosen to be compatible with the general trend of the solution).

A stiff system may be constructed by considering

$$y'=\lambda(y-F(t)) + F'(t) \qquad (3.23)$$

where $y_0 = F(t_0)$, $\lambda<<0$, and $F(t)$ is a smoooth, slowly varying function.

This has the solution

$$y=(y_0-F(t_0))e^{\lambda t}+F(t) \qquad (3.24)$$

Suppose $y_0-F(t_0)\neq 0$, due to numerical error (e.g. roundoff), then, soon λt is sufficiently negative for the first component to be insignificant compared to the second, but it is known (GEAR) that the local truncation error is determined by λt and a derivative of $F(t)$ by the time $\lambda t<<0$, whereas stability is dependent on $\lambda\Delta t$.

Consider the effect of integration using Euler's formula:

$$y_{n+1}=y_n+\Delta t.F'(t_n,y_n) \qquad (3.25)$$

in the stiff region, then if $y_0 \neq F(0)$, an oscillating solution of the form depicted in Figure 3.3 is obtained.

The solution starts at (t_0,y_0). At this point the derivative is calculated and, as $y_0 \neq F(t_0)$ and $\lambda \ll 0$, $y'(t_0,y_0)$ is quite large. This is used to integrate to the point (t_1,y_1) and this value has a greater error than at (t_0,y_0). This error increases in magnitude as each new step is taken.

If the same function is integrated using the Backward Euler Formula:

$$y_{n+1}=y_n-\Delta t.F'(t_{n+1},y_{n+1}) \qquad (3.26)$$

then a stable solution of the form shown in Figure 3.4 results.

Although this backward difference method is able to solve the stiff system, it gives an implicit equation for y_{n+1} to be solved. This is true for all stiffly stable methods.

Library subroutine packages which control the integration were used in this work. These were subroutines D02AEF, GEAR and EPISODE. NAG own the proprietry rights of D02AEF; and the latter two were obtained from the Argonne Code Center, Illinois, U.S.A. Further information may be found in NAG, 1971, HINDMARSH, 1974, BYRNE and HINDMARSH, 1975.

The packages required as input an estimate of the maximum truncation error that may be committed over any step. They then adjust the step length and order of integration to minimize the number of derivative evaluations. They also need a subroutine to give the derivative values

for an arbitrary (v_c, h_c) pair, corresponding to equation 3.1.

3.5 Observations on the Solution.

3.5.1 Roundoff and Truncation Errors - Their Effect on the Solution.

For this semi-analytical case, the eigenvalues of the system may be calculated, and the time step reduced just before the onset of the instability induced by the integration method, With a more generalised system, this process is not trivial, for the linearisation cannot be so easily performed, and hence the eigenvalues calculated.

The system is well-conditioned in the sense that small errors decay if a small enough time step is taken. Suppose that at any time an underestimate of the load is made: this means that the ball will tend to accelerate slightly more than it should over the next time step, and at the end of that step the ball will have dropped further and be moving faster than the real solution predicts. This gives rise to a greater load being predicted there than ought to be the case, for both a higher approach velocity and a thinner film predict higher pressure being generated. The behaviour is similar to that shown diagrammatically in Figure 3.3. This is the physical origin of the stiffness in the system. It becomes more stiff with time, for as the film thickness is decreased, the load becomes more and more sensitive to changes in the film thickness, i.e.

$$\frac{d\dot{v}_c}{dh_c} = \frac{2\pi R}{m\alpha}\alpha p_c$$

and p_c is an increasing function with time in the final stages of impact.

It is to be concluded that as long as the time step is sufficiently

small, the effect of either roundoff or truncation on the trajectory followed is not too serious as the well-conditioning will keep the numerical solution near to the actual solution.

Against this however, there is the problem of relative error. The problem consists of solving equation 3.1

$$m\ddot{h}_c = \int_0^{r_s} 2\pi r\, p(r)\,dr - W$$

In the second stage of solution the net force on the body is small and decaying approximately exponentially. It is here that the problem of relative error arises. If $m\ddot{h}_c = 0.01\ W$, then the film force is $1.01\ W$. Thus for a 1% accuracy in the net force, the film force needs to be accurate to 0.01%. This process continues indefinitely as the net force decreases requiring that the film force be ever more accurately determined, in order to give a preset relative error.

However, there is a limit to the ability of the computer to calculate the film force. Even if the film force may be calculated exactly for a given (v_c, h_c) pair at any instant of time (i.e. with no roundoff errors) there is an error in the (v_c, h_c) pair itself. This is because the values of v_c and h_c are known only to a finite number of significant digits - about 14 on the CDC machine.

From equation 3.22 it may be deduced that if $\varepsilon_{\dot{v}_c}$ is the error in $\dot{v}_c$ due to roundoff errors ε_{v_c} and ε_{h_c} in v_c, h_c respectively, then

$$\varepsilon_{\dot{v}_c} = -\frac{2\pi R}{m\alpha}\frac{1}{\gamma^2 v_c}\left[h^2(\gamma^2-1) + \frac{\delta}{2}\log_e\frac{h+\delta}{h-\delta}\right]_{h_c}^{h_s}\varepsilon_{v_c} - \frac{2\pi R}{m\alpha}\, p_c\, \varepsilon_{h_c}$$

For any particular values this may be calculated. As the impact continues

Figure 3.5. Base Run

and the system becomes stiffer this error increases in absolute as well as relative magnitude.

There is a further error obtained by not being able to calculate the load exactly even if an exact (v_c, h_c) pair could be found.

When these effects become important, it is perhaps appropriate to change the problem to be solved, and consider the system

$$\int_0^{r_s} 2\pi r p(r)\,dr = W$$

i.e. model the case of a ball dropping under constant load. This case is discussed in section 3.5.7.

3.5.2 The Graphical Behaviour of the Solution.

Figure 3.5 is a representative graph of this type of problem and has four curves plotted against time:-

1) Centre Pressure (p_c)

As the pressure at the centre ranges over many orders of magnitude it was decided to plot $\log_{10} p_c$ against time (using the solid line), rather than the pressure itself. Since 10^3 Pa is a very low pressure all pressures less than this are not shown and this value is used as origin. As an aid to comprehension the positions of 10^n psi, n=0,1,2,3,4,5 are marked by small numbers written on the right side of the pressure axis.

2) Parabola Velocity $(-v_c/R)$

The absolute value of the velocity is shown with the short dashed line and is measured non-dimensionalised with respect to the semi-

latus rectum (i.e. the local radius of curvature at r=0). Since R=0.01m, this scale is cm/sec.

3) Minimum Film Thickness (h_c/R)

This value is also given non-dimensionalised with respect to the semilatus rectum and thus similarly is measured in cm.

4) Net Force ($m\ddot{h}_c/W$)

This gives the resultant force on the parabola but non-dimensionalised with respect to its weight. Initially the fluid force is zero and consequently the scale starts at -1.

At the end of the contact the fluid force will just balance the gravitational force and so the net force tends to zero. This graph may be adapted to give a measure of the fluid force by adding one to all values, since

$$m\ddot{h}_c = \int_0^{r_s} 2\pi p(r)dr - W$$

$$\frac{m\ddot{h}_c}{mg} + 1 = \int_0^{r_s} \frac{2\pi r p(r)dr}{W}$$

This particular computer run, which has initial conditions $v_s=0$, $h_s = 0.0005$m, gives a solution that has characteristics that are common to all runs for this type of system. The results may be divided into two stages. The first stage lasts for about 15ms and is the initial build up of pressure and force due to the gravitational field. At about 10 ms there is a pressure peak with an associated force peak. These "velocity-induced" pressure peaks reduce the velocity of the parabola

to a very low value. It can be seen that the force is already reducing from its peak value when the pressure reaches its peak.

For the first 5ms the fluid force is negligible. This is confirmed by noting that the velocity increases in a virtually linear way during this time and that the film thickness curve is parabolic. The central pressure takes about 6ms to reach a value of 1psi. The ball has travelled about half of its total movement during this first interval.

The net force rises to a peak value of about 5mg, where mg is the weight of the parabola, and is due to a film force of about 6mg, with a peak pressure of $2.3X10^{6}$Pa at a time 11ms into the contact.

Subsequent to the pressure peak, the force and pressure values drop due to the large amount of momentum suddenly removed. The net force drops close to zero, and thereafter it decays slowly and approximately exponentially. However the pressure starts to rise again, and the parabola enters the second stage of the impact process.

This second stage has the net force, v_c and h_c all tending to zero. The pressure, however, starts rising as a power law in time(since $\log_{10}$ (pressure) is linear with time), and is due to h_c becoming extremely small and the highly non-linear film shape rather than the earlier peak associated with v_c. At 27ms, the net force remains small but the pressure continues to increase and goes towards infinity.

It is possible for an "infinite" pressure to occur without an "infinite" force. This is due to the particular model of viscosity chosen, and will always occur with this exponential piezoviscous system at some point in time, either in the first stage (before the velocity pressure peak) or

during the final stage of "settlement".

The first stage covers the impulse that virtually reduces the momentum of the ball to zero, and the second stage is the final part where the flim force is almost constant.

3.5.3 The "Infinite" Pressure, Why it can occur.

Equation 3.7 is rewritten below

$$\int_0^p \frac{dp}{\eta} = 6v_c \int_{r_s}^r \frac{rdr}{h^3}$$

In its derivation it was noted that each side is independent of the other in that the left hand side is a function of pressure only and the right hand side is a function the geometry only. For any (v_c, h_c) pair the right hand side may be calculated. This integral will be a well-defined function of r.

Consider the left hand side, with the viscosity pressure function

$$\eta = \eta_0 e^{\alpha p}$$

then

$$\int_0^p \frac{dp}{\eta} = \frac{1-e^{-\alpha p}}{\eta_0 \alpha} \leq \frac{1}{\eta_0 \alpha} \qquad (3.27)$$

Given the limitation (3.27), there is a restriction on the solution space for the pressure to be finite, using (3.10)

$$\frac{1}{\eta_0 \alpha} > 3 v_c R \left(\frac{1}{h_s^2} - \frac{1}{h_c^2} \right)$$

or

$$1 - 3\eta_0 \alpha v_c R \left(\frac{1}{h_s^2} - \frac{1}{h_c^2} \right) > 0 \qquad (3.28)$$

This condition is obvious by considering (3.11).

It was noted in section 3.1. that $p_{max} \to \infty$ as $h_c \to \delta$ and that the film force remains finite. This, together with the conditions which will be discussed in the next section (3.5.4), allows the solution to have an "infinite" pressure, yet the net force remains nearly constant.

There is a breakdown in the model if this situation occurs. A physical explanation for this behaviour may be found by considering the process which is actually occurring. The ball is dissipating its energy (both kinetic and potential) into the oil film. If a (v_c, h_c)pair is obtained by the integration method which does not satisfy condition (3.28) then it implies that the energy cannot be dissipated by viscous action alone. From the experience of PAUL, 1971, it appears that the ball would bounce unless viscous dampers are also used, reducing the velocity of approach.

This infinity occurs due to the particular viscosity pressure model chosen. If, for example, the Mark I viscosity-pressure model was used:-

$$\int_0^p \frac{dp}{\eta} = \frac{1-e^{-\alpha p}}{\eta_0 \alpha} \quad , \quad p<p_L$$

$$= \frac{1-e^{-\alpha p_L}}{\eta_0 \alpha} + \frac{p - p_L}{\eta_0 e^{\alpha p_L}} , \qquad p \geq p_L \qquad (3.29)$$

This has no upper bound, and so no restriction exists on solution space. this statement, though theoretically true, must be qualified as only finite length arithmetic may be performed. This is discussed further in the next section.

As a general rule, if

$$\int_0^{\infty} \frac{dp}{\eta} = L < \infty, \text{ for some } L$$

then a singular value of pressure can exist, as there are regions that cannot be reached with a finite pressure.

3.5.4 The "q-model" and Precision Limitations.

Other workers, CHRISTENSEN; CHENG and LEE; RANGER, 1974, in the field of elastio-hydrodynamic lubrication have used the q-model for solving Reynolds Equation. The basis of this that if $\eta=\eta_0 e^{\alpha p}$, on writing

$$q = \frac{1-e^{-\alpha p}}{\alpha} \qquad (3.30)$$

then

$$\frac{1}{\eta_0}\frac{dq}{dr} = \frac{1}{\eta}\frac{dp}{dr} \qquad (3.31)$$

In this way the explicit pressure dependent viscosity term in the Reynolds Equation is eliminated.

However, the actual pressure distribution is found from

$$p = -\frac{1}{\alpha}\log_e(1-\alpha q) \qquad (3.32)$$

Here arise problems that are not often discussed in the literature, though RANGER refers to it. First, the maximum value that q can attain is $\frac{1}{\alpha}$. This is a condition of the substitution made, not directly on the reduced Reynolds Equation, so solutions of that equation can exist in which $q>\frac{1}{\alpha}$. A second problem is one due to the fact that computation is done to a specified number of significant digits, e.g. about 14 places in CDC single precision (with which most of this work was undertaken) or approximately 15 places in IBM double precision.

If either the "q-model" or equation (3.11) is used, then a formula

of the type

$$p = \frac{1}{\alpha} \log_e(1-X)$$

is obtained.

The question arises as to what the maximum pressure that can be possibly calculated? The answer lies in the so-called unit round-off, which is the smallest positive number such that $1+u \neq 1$ when using finite length arithmetic.

u=7.11E-15 (CDC single precision)
=2.52E-29 (CDC double precision)
=2.22E-16 (IBM double precision)

Now

$\log_e(7.11E-15) = -32.58$

$\log_e(2.52E-29) = -65.85$

$\log_e(2.22E-16) = -36.04$

thus

$p_c < 1/\alpha.33$ (CDC single)

$p_c < 1/\alpha.66$ (CDC double)

$p_c < 1/\alpha.36.5$ (IBM) (3.33)

These are the maximum attainable central pressures (pressures larger than this cannot be calculated without using multiword precision). The values of (v_c, h_c) also have small errors in them due to round-off and it was found empirically that the maximum pressure that could be calculated in CDC single precision was about $12/\alpha$, using the Runge-Kutta-Merson method.

When the Mark I viscosity model was used, with the same integration method controlling it, it was found that p_L had to be less than $12/\alpha$. This is because up to that pressure the two models are identical, thus if one model breaks down so does the other, if $p_L > 12/\alpha$.

Using the variable order, variable step method contained in the EPISODE package, the value of p_L could be increased to $20/\alpha$, compared with the theoretical limit of $32/\alpha$.

Results obtained using this model will be presented and discussed in section 3.6.5.

Using the "q-model" substitution, equation 3.29, may lead one to believe that the problem of the large spatial change of the viscosity have been eliminated. However, the problem has merely changed and the question of precision limitation now arises. It would be necessary to calculate the reduced pressures with far greater accuracy than at first appeared.

The "q-model" was not used in this work. However, this semi-analytical model may be considered to be a degenerate case.

This pressure limitation gives a further justification for using the Runge-Kutta-Merson method and shortening the time step, to eliminate the stiffness oscillations because there is a limit to the solution, and thus on the amount of time step shortening. With an appropriate Mark I viscosity liquid, the is no such limitation, consequently this method is unsuitable.

3.5.5 The Spatial Distribution of Pressure and its Change with Time.

Considering the second stage of the solution, the load remains virtually constant, but the centre pressure is increasing. This can only mean that the pressure is decreasing elsewhere. From the frontispiece, this can be seen to be so. It was generated for the same conditions as given in Figure 3.5. A frame shows the following information:

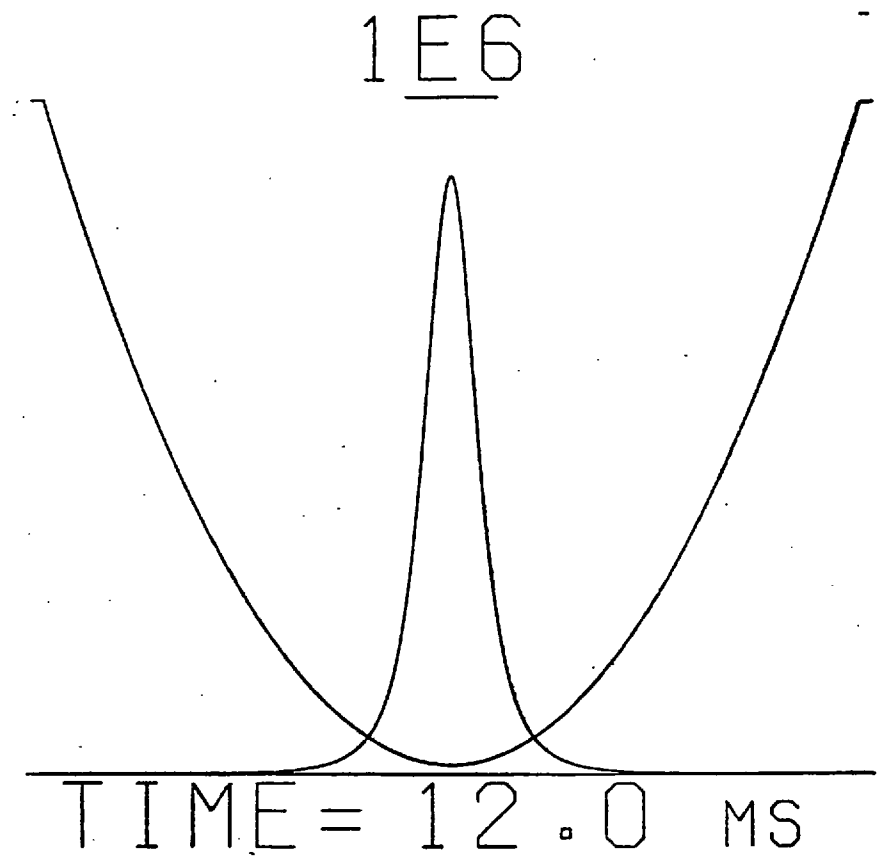

The parabola falling into the liquid is represented by the upper curve. The lower curve is the instantaneous pressure distribution at the clocktime (measured in ms.). The pressure varies over such a large range that there is a variable scale which is changed so as to give the maximum curve, except for the first few diagrams. The scale is shown by the symbols 1En, where n is an integer. The line represents a pressure of 10^nPa . Logarithms were not used in order not to distort the pressure distribution when showing the radical change of pressure with time. In the initial stage the solution is very similar to that for the isoviscous case, i.e.

$$p = 3\eta_0 v_c R\left(\frac{1}{h_s^2} - \frac{1}{h_c^2}\left(1 - \frac{r^2}{h_c R}\right)\right) = C_1 + C_2 r^2 \qquad (3.34)$$

When the film becomes thin the effect of the viscosity-pressure characteristic becomes more important, eventually dominating the solution. Its effect is to concentrate the load carrying capacity at the centre.

3.5.6 The Effect of Errors on the Solution.

The solution of a non-linear equation normally requires an iterative method of solution and because such methods would be used for solving the fully varying (elastic) case, it was though appropriate to find the effect of errors on the integrated solution. Instead of integrating $\dot{v}_c = f(v_c, h_c)$ as given in (3.15), this was performed by integrating

$$\dot{v}_c = (1.0 + ERMEAN + ERR.RANF(X)) * \frac{2\pi}{m} \int_0^{r_s} p(r) r dr - g \qquad (3.35)$$

where RANF(X) is a random number uniformly distributed on $[-1, 1]$ and $\dot{h}_c = v_c$ as defined.

It may be seen that a non-zero value for ERMEAN applies a bias to the film force obtained and a value for ERR gives the magnitude of errors obtained. These are relative values because they are multiplied by the film force.

With the substitution (3.35) and using constant time step integration with the Runge-Kutta-Merson method, it was found that with (ERMEAN=X, ERR=0.01) there was a relative error of about -4X in the peak pressure due to the relative error X in the film force. The error was found to be virtually independent of the step length taken (though in the cases considered these were small compared to the maximum possible for stability). This error tended to increase with time as the stiff phase was reached.

The effect of (ERMEAN=0, ERR= X) error was much more dependent on the time step, but tended to decrease on shortening the time step. At the peak pressure, its error was about 0.15X and remained at this level until $|\lambda \Delta t| > 2.0$ when stiffness became a problem and then the errors greatly increased.

By using combinations of these types of error it was found that the errors at any time were additive, in the sense that the errors obtained with (ERMEAN=X, ERR=Y) were virtually identical to those of (ERMEAN=X, ERR=0) added to those with (ERMEAN=0, ERR=Y). From the results is was concluded that if ERMEAN≠0 then the results are not those required but is a solution to a different problem and as long as ERR is small and stiffness is not a problem then the errors globally are not too large.

This procedure was run again using the GEAR package instead of the Runge-Kutta-Merson method. There are two points to be noted:-

Firstly, GEAR allows integration using either stiff or non-stiff methods. The non-stiff methods (Adams-Moulton with functional iteration) are more appropriate for the initial increase in force, and stiff methods (Backward difference with the Jacobian calculated numerically) are better for the remainder of the impact. This policy was adopted.

Secondly, the GEAR (and EPISODE) packages require a parameter EPS, used to control the maximum local truncation error over any step. The solution is integrated so that

$$\left(\sum_{i=1}^{2} (E_i/Y_i)^2 \right)^{\frac{1}{2}} < \text{EPS}$$

where E_i is the local truncation error and

$Y_i=\max(X_i(t))$ during the first part of the impact (non-stiff)

$Y_i=X_i(t)$ during the remainder (stiff)

with $X_1(t)=v_c(t)$, $X_2(t)=h_c(t)$

With this method it was found that the value of EPS had a strong effect on the ability of the system to be integrated within a reasonable time. The effect of mean error was the same as that obtained with the Runge-Kutta-Merson method, ie. the error accumulated in a non-trivial manner.

From results using a range of errors, it was found that if ERR>EPS with ERMEAN=0 the system integrated virtually exactly, but took a very long time to do so. It was only when ERR<EPS, that the system was able to be integrated with only a small increase of computational time over that with ERR=0. It should be remembered that the stiff methods need to use the Jacobian of the system (3.15) and although it is known analytically for this case (3.22), the object was to find the effect of errors to throw light on the behaviour of the general case, thus it was decided to calculate the Jacobian numerically, i.e.

$$\frac{\partial f_i}{\partial x_1} = \frac{f_i(x_1+\Delta x_1 , x_2) - f_i(x_1, x_2)}{\Delta x_1} \quad , i=1,2$$

$$\frac{\partial f_i}{\partial x_2} = \frac{f_i(x_1, x_2 + \Delta x_2) - f_i(x_1,x_2)}{\Delta x_2} \qquad (3.36)$$

Finding the Jacobian requires three function evaluations, each one gives a random error due to machine roundoff. Since the Jacobian is found by subtracting two similar numbers and dividing by a small number, this process magnified the errors, accounting for the relation

$$ERR<EPS \qquad (3.37)$$

To obtain an acceptable solution, EPS must be fairly small, for example, 10^{-6}, for in the second stage of impact the acceleration becomes small compared to the film force. This implies that

$$ERR<10^{-6} \qquad (3.38)$$

This is quite a tight convergence criterion and prospective solution methods need to take account of this.

3.5.7 Alternative Methods for Integration when $\ddot{h}_c \to 0$.

In the second stage, $\ddot{h}_c \to 0$ and the ball is dropping under virtually constant load. One way to eliminate the problem of stiffness is to solve another system,

$$2\pi \int_0^{r_s} p(r) r dr - mg = 0 \qquad (3.39)$$

This is obtained from equation 3.1 by neglecting $m\ddot{h}_c$ relative to the other two terms, and is equivalent to considering that the ball becomes inertialess.

To solve this system a step Δh in h_c was taken, the change Δv in v_c estimated by linear extrapolation, and a (v_c, h_c) pair obtained. This was used to find the load. If equation 3.39 was solved to within a convergence criterion, then the value of v_c was accepted. Otherwise v_c was corrected using a secant method (CONTE and DE BOOR, 1972) and the cycle repeated.

This gave a set of solutions of the form (v_c, h_c) and as it was found that locally v_c was nearly linear with h_c, it was decided to assume $v_c = a*h_c^2 + b*h_c + c$ and to calculate the time for the ball to drop from $(v_c, h_c)_2$ to $(v_c, h_c)_3$ by passing a parabola through $(v_c, h_c)_1$, $(v_c, h_c)_2$, and $(v_c, h_c)_3$ using $v_c = \dot{h}_c$.

It was subsequently found that NORMAN, 1971, had used a similar method but he had stepped the solution in units of Δv and estimated, then iterated for, the solution in h_c.

3.5.8 On the Paper by CONWAY and LEE, 1975.

After the inception of this project, the paper of CONWAY and LEE was

published. Their model is identical to the one used here and so it was repeated using the computer program developed for this work, but set with their initial conditions.

Using single precision arithmetic, at the last time interval before the singularity was reached:-

$t=1.1830\times10^{-5}s$ $(\Delta t=10^{-8}s)$

$h_c/R=1.16258\times10^{-3}$

$p_c = 3.52624 \times 10^{8}Pa$

giving

$\tau=v_s t/h_s=0.41878$	compared to their	$\tau=0.4159268$
$\bar{h}_0=h_c/h_s=0.58129$	compared to their	$\bar{h}_0=0.5841$
$\bar{p}=p/(3\eta_0 v_c/h_s^2)=13.2$	compared to their	$\bar{p}=34.2$

The whole program was repeated using double precision calculations; an effort was made to see how far the system could be integrated. With a minimum time step of $10^{-15}s$, it was possible to integrate to:-

$t=1.18362177\times10^{-5}s$	giving	$\tau=0.419001$
$h_c/R=1.16214\times10^{-3}$	giving	$\bar{h}_0=0.58107$
$p_c = 1.24382\times10^{9}Pa$	giving	$\bar{p}=46.8$

The results indicate close agreement, but the slight changes are attributable to using different machines, and hence word lengths, to obtain the results.

Even with extremely short time steps, the maximum value of αp_c attained is 25.13, significantly lower than the limiting machine precision value (see section 3.5.4). Using yet shorter time increments could increase this value.

They give the model of CAMERON, 1966 as an example of a viscosity-pressure function that also gives a pressure singularity. This model has $\eta=\eta_0(1+cp)^{16}$.

Now

$$\int_0^\infty \frac{dp}{\eta_0(1+cp)^{16}} = \frac{1}{15c\eta_0}$$

Hence this function does have a finite limit and so can have a singularity, (see section 3.5.3).

3.6 Varying the Problem Parameters.

3.6.1 Introduction.

In this section the effect of changing the various parameters are discussed. The available parameters are v_s, h_s, α, αp_L, η_0, m and R. Each will be considered in turn. The plots were mainly obtained by using an initial time step, $\Delta t=10^{-4}$ sec and integrating using the Runge-Kutta-Merson method with the time step being divided in two when $\max|\lambda\Delta t|>2.0$. For the cases in which p_L is finite this method is inappropriate as it resulted in extremely stiff equations and eigenvalue ratios of the order 10^{20} were obtained. The EPISODE package was then used to control the integration process.

The base system from which parameters were changed was

$$\begin{aligned} &v_s = 0\ ms^{-1}, \quad h_s=0.0005m, \quad R=0.01\ m \\ &\eta_0=0.7Pas \quad , \quad \alpha=6.1E\text{-}8\ Pa^{-1}, \quad m=0.0325\ kg \\ &\alpha p_L=0 \end{aligned} \tag{3.40}$$

and the changes with time are shown in Figure 3.5.

Figure 3.6. Low Mass V_s = - 0.1 ms^{-1}

This value of α is large compared to that expected for normal mineral oils. It will be seen that changing differeing physical parameters can bring about the same effect on the solution. Considering the isoviscous case (which give a simpler, more obvious, grouping of the parameters) will allow a greater insight into the behaviour of the piezo-viscous case. The isoviscous case is considered in section 3.8.

There are two groups each containing 3 parameters which give rise to the same set of curves, given an initial set of conditions (v_s, h_s). There exists a whole family of solutions obtainable from only one result by linear scaling..

3.6.2 On Changing v_s

Figure 3.6 shows the effect of increasing the initial velocity of impact to $v_s = -0.1\ ms^{-1}$. It may be seen that the peak force and pressure occur much earlier, at about 4.5 ms after contact with the oil first occurs. Further, both these peaks are higher and narrower than was the case for zero initial velocity. The increase in velocity under gravity is less than with $v_s = 0$ because there is less time for the ball to be accelerated.

It was found that in the second stage, the pressure field seemed to retrace the same profile, for both velocities, although displaced in time. It was therefore decided to see if this was indeed so. This was done by arbitrarily choosing a value of centre pressure, say $5 \times 10^7 Pa$, then for each run the time at which that pressure was attained was found by linear interpolation.

Let the time for the ith run be denoted by t_i. Then time displacements $T_i = t_i - t_1$ were found. The curves were then plotted assuming a displacement of T_i for curve $i (T_1 = 0)$.

Figure 3.7. Effect of Different V_s

Figure 3.7 shows the result obtained for $v_s=0$, $v_s= -0.05\ ms^{-1}$, $v_s= -0.1ms^{-1}$. To assist clarity, h_c has not been plotted.

The pressure curves displaced in time fall onto one line, but it was only required that the pressure values should agree at just one point.

It may be concluded that for rigid balls after the first stage of impact the intital velocity of the ball is no longer a factor determining its trajectory. It will be shown later that for cases presented here that this fact remains true for elastic impacts when only reasonably hard materials and low initial velocities are considered.

The velocity at which the fluid film could not withstand the impact so that the "infinite" pressure occured in the initial stage was approximately $-0.115\ ms^{-1}$, all other parameters being as before. This is equivalent to free fall from 0.0007 m above the liquid surface.

From Figure 3.7, it may be seen that although the initial velocities are equally spaced, the peak force and initial peak pressure are by no means changed by similiar amounts. It is clear that as the initital velocity is increased these values increase superlinearly.

3.6.3 On Changing h_s

There are two differing cases to be considered. One is to change h_s in the obvious way implying that the ball is to be dropped from a different height. The other, not really a change in h_s at all, is to change r_s, i.e. the radial extent of the film for r_s defined such that $h(r_s)=h_s$. This is physically equivalent to putting the ball at a height $h_c(0)$ above the plane but in a pool of liquid $h_s>h_c(0)$, and then releasing the ball. This value of h_s is then used in the calculation of the load (equation 3.13) and is similar to the assumption of CHRISTENSEN, 1967, 1970;

Figure 3.8. Base Run and Run with h_s=0.00025 m.

Figure 3.9. Base Run and Run With r_s=0.01 m

Figure 3.10. Changing α with v_s=0

CHENG and LEE, 1971, and NORMAN, 1971).

Considering the first case, Figure 3.8 shows the effect of the base run and also with h_s=0.00025 m. In the latter, the pressure and force both rise much more quickly though to lower peaks - the force is decreased more than the pressure. In the first stage all trajectory time derivatives are less than those of the base curve. In the second stage the results follow those of the base run (but again displaced in time).

Just as there is an initial velocity that is too great for the oil film to stop the ball by viscous flow alone, there is a film thickness that is too great. This is because there is virtually no film force generated in the initial moments of impact, which allows the ball to accelerate under gravity and to attain a sufficiently high velocity.

Figure 3.9 shows a run with h_s=0.01 m and $h_c(0)$=0.0005 m. There is an almost immediate rise in the pressure and force curves, giving a very low maximum force of about 1.5 W, compared to about 4.5W for the base run. Again, the solution curves merge into those of the base run.

Thus it may be concluded that at low film thicknesses, the rigid solution is effectively independent of the initial height from which the ball is dropped and of the extent of the oil film.

3.6.4 On Changing α.

Runs were made with α=6.1E-8Pa^{-1} and with α=2E-8Pa^{-1} (this second value is more representative of a normal mineral oil). From Figure 3.10 there is no difference due to the decrease in α over that of the base run during the initial stage. The second stage is drawn out longer and the (log) pressure curve remains on the straight line for a greater time.

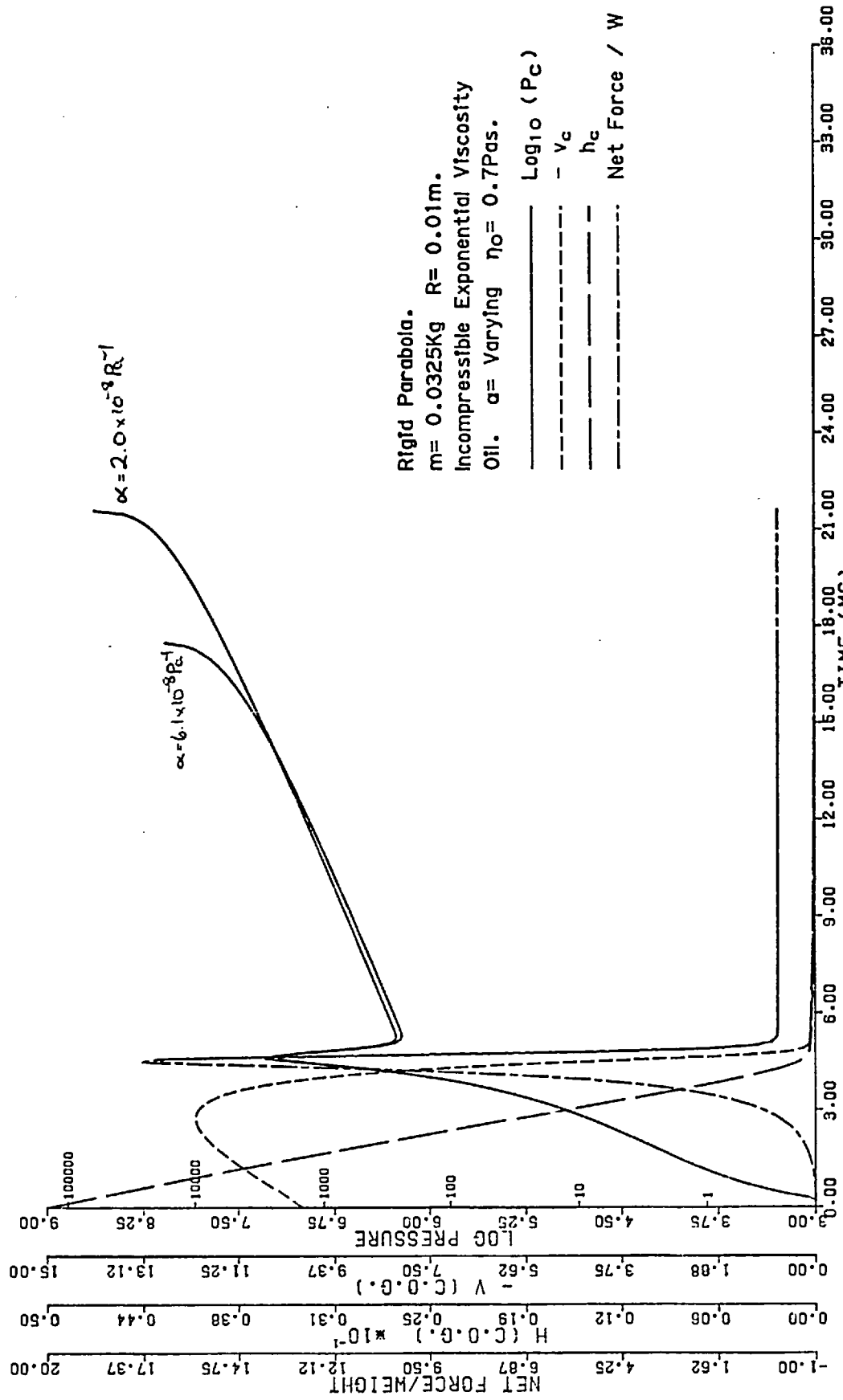

Figure 3.11 Changing α with v_s= -0.1 ms^{-1}

Figure 3.12. Varying Values of αp_L.

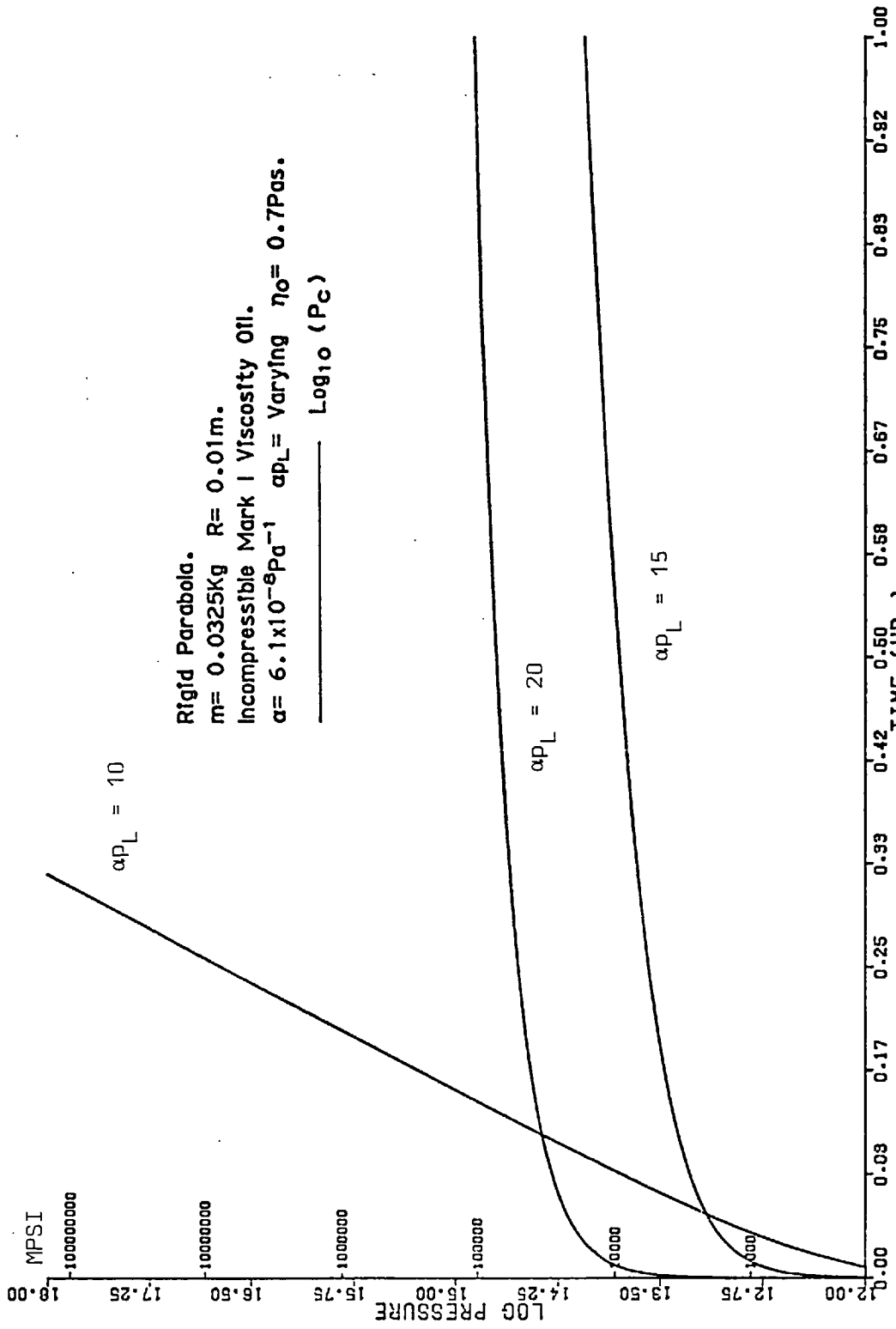

Figure 3.13. Extreme Values Obtained with Mark I Viscosity Model

The final pressure attained is approximately three times higher than that for α=6.1E-8Pa^{-1}, being a confirmation of the pressure limitation mentioned in section 3.5.4.

Before coming to the conclusion that the value of α has no effect in the inital stages of impact (which one might deduce from Figure 3.10) another run, in which v_s= -0.1 ms^{-1}, was completed. This is shown in Figure 3.11. It is seen here that the peak pressure is such that the value of α is significant, hence altering the impact trajectory. The pressure curves in the second stage of impact are no longer co-incident but, by altering the time base in such a manner similar to that of section 3.6.2, these could be made to give a similar pair of curves as Figure 3.7 in the second stage.

3.6.5 On Changing αp_L

These runs were performed using the EPISODE package as there was no longer a limit to the amount of time step halving needed due to the singularity. Indeed it was found that the value of max$|\lambda\Delta t|$ was doubling faster than once every step in places. The model used here is the Mark I viscosity model where the maximum viscosity is $\eta_0 e^{\alpha p_L}$. If αp_L=0, then the isoviscous case is obtained. Figure 3.12 shows the results for several runs with various values of αp_L. It may be seen that the solution is initially close to the isoviscous solution except at the initial peak pressure, but during the final stages as αp_L increases, the solutions diverge more and more from the isoviscous case and tend to the exponential model.

It was found that for $10<\alpha p_L<20$ approximately this system could be integrated out further in time compared to those obtainable with either the exponential or isoviscous models. Figure 3.13 shows the pressures

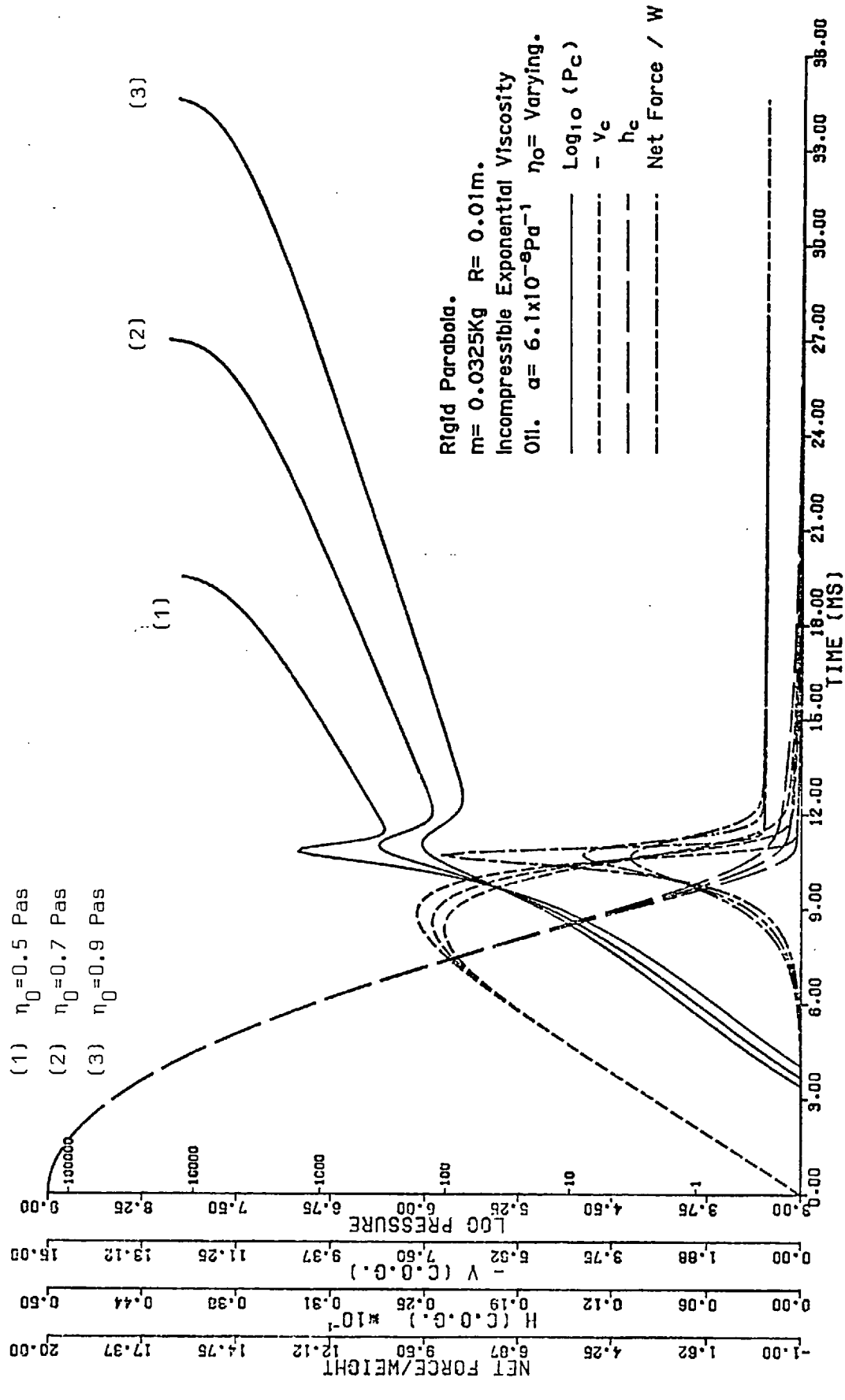

Figure 3.14. Changing η_0.

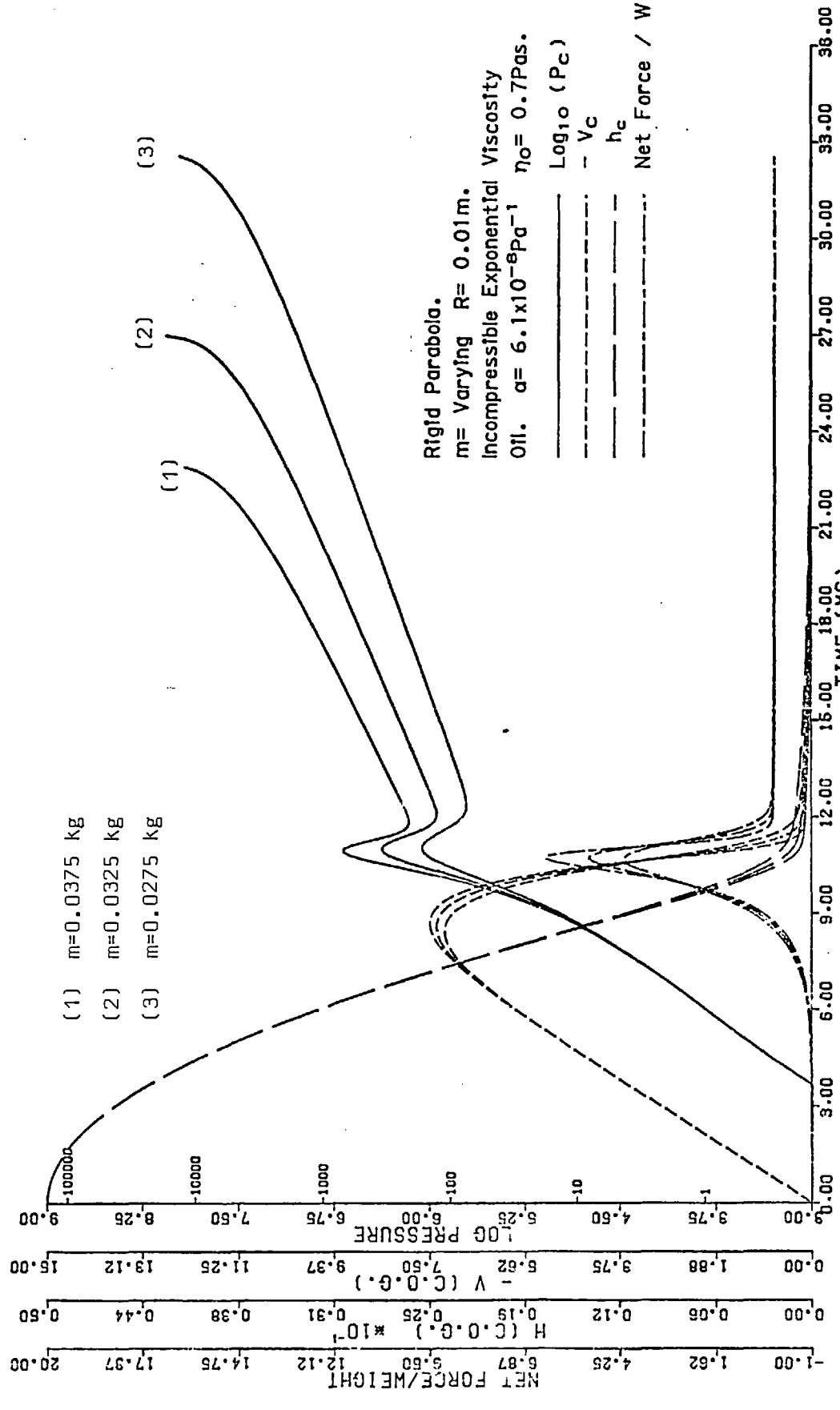

Figure 3.15. Changing m

obtained from this system with αp_L=10, 15 and 20. It must be stressed that these results only apply to a hypothetically absolutely rigid system, as the pressures shown are extremely high. Further, the film thickness predicted is of sub-atomic dimensions, but the results show that in extreme regions solutions may be obtained.

3.6.6 On Changing η_0

Figure 3.14 shows the effect of changing η_0. Three sets of curves are shown:- η_0=0.5, 0.7, 0.9 Pas. As the base viscosity is increased, the rise in force and pressure starts earlier, but rise to a decreased peak. The time gradients in all physical variables are reduced as η_0 is increased.

Because the initial peak values depend on η_0, the maximum velocity of impact that can be supported by viscous action in the initial phase is dependent on the base viscosity as well as the depth of the film. This is supported by the conclusions of RABINOWICZ, 1952: that a thick oil is needed in order to form the conical indentation, rather than a dent typical of dry contact.

The second stage shows an initially linear slope of ($\log_{10}$ pressure) against time, giving a power law relation, the slope depending on the base velocity. The dependence is presented in section 3.7.2.

3.6.7 On Changing m.

It may be seen by inspecting Figure 3.14 and Figure 3.15 that the effect of increasing the mass of the ball is similar to that of decreasing the base viscosity of the oil. This relationship holds very closely in the second stage of the impact, but not so closely as the first part.

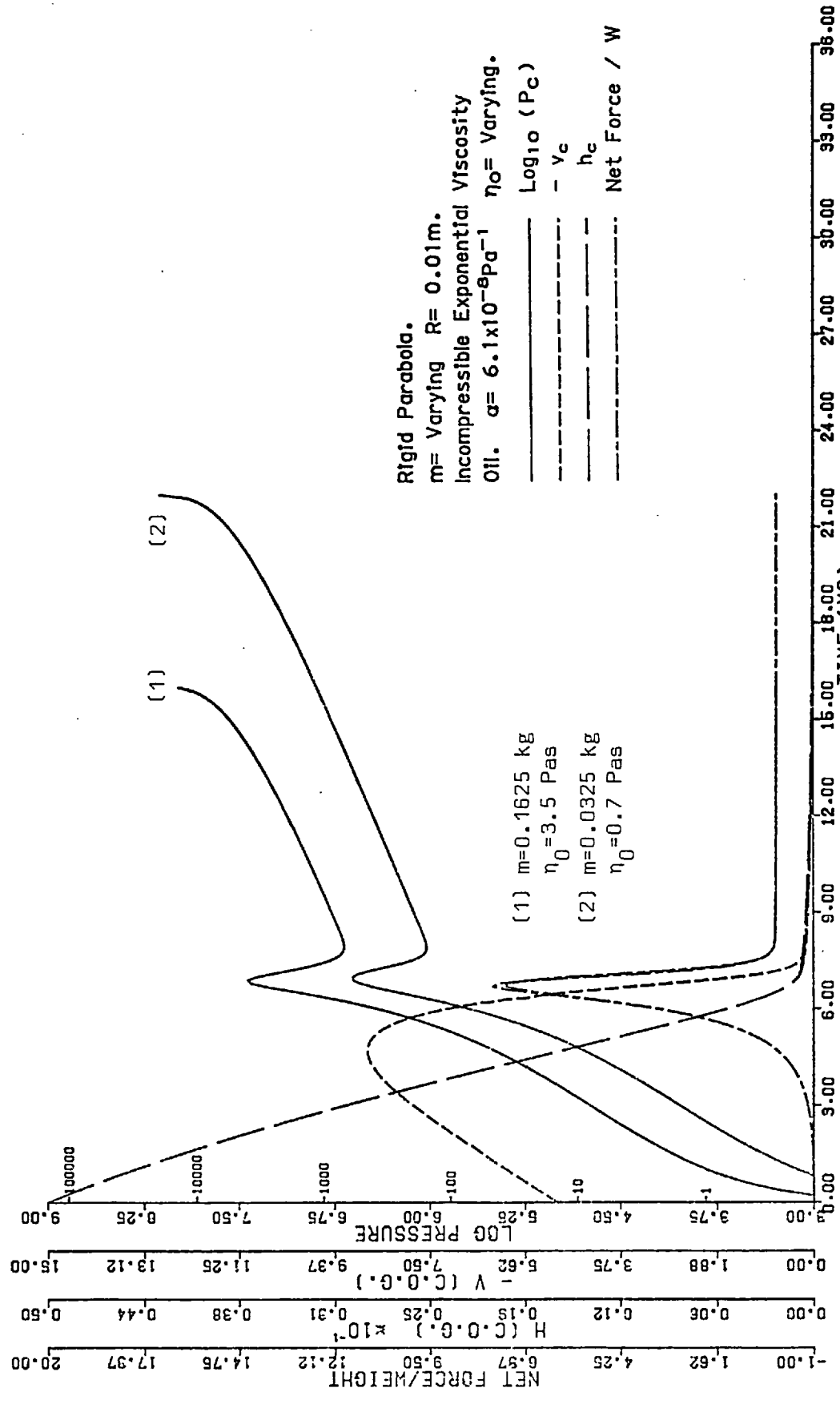

3.16. Runs Modelling Exponential Oil with Different η_0 and m

Keeping η_0/m constant.

The difference arises due to the very small film force generated in the initial stage, thus the trajectory initially followed is the same for differing masses, and as the other parameters remain fixed the same pressure curve results. The runs which have different initial viscosities allow changes in the generated pressure field which are quickly visible.

Having found the effects, it was decided to ascertain if the problems could be defined in terms of groups of parameters. For example, as increasing the mass gave the same effect as decreasing the base viscosity, there could be a group (η_0/m), that would characterise the problem. Consequently a run was made in which (η_0/m) was kept fixed, the results are shown in Figure 3.16. The curves of h_c, v_c and $\ddot{h}_c$ were nearly identical but the pressure curve was displaced.

The equations of motion do not give an immediately obvious grouping of terms. It was decided to investigate the isoviscous incompressible solution and it was there that the answer was found.

3.6.8 On Changing R.

This section is included for logical completeness. It will be shown in sections 3.7 and 3.8 that the problem may be characterised by two groups, each a function of (m, η_0, R), thus a change in R is equivalent to one in η_0 and m.

3.7 The Isoviscous Incompressible Fluid Solution.

3.7.1 Introduction.

To aid in the comprehension of the total system it was decided to solve for the rigid parabola squeezing onto an incompressible isoviscous fluid. Using this analysis, an understanding of the interaction of the

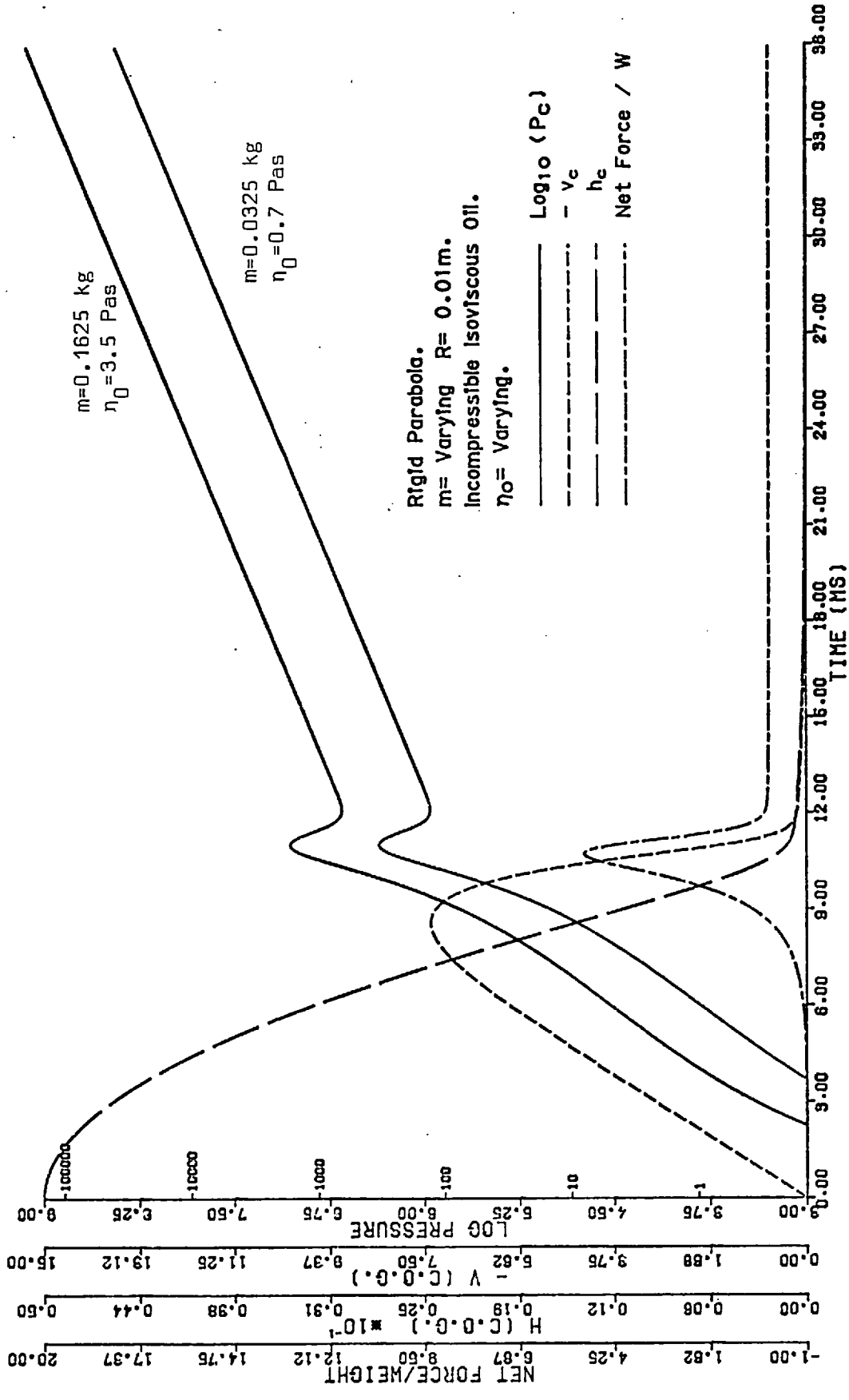

Figure 3.17. Runs Modelling Isoviscous Oil With Different η_0 and m keeping η_0/m constant.

various physical parameters was obtained. This is the base system used by NORMAN in his work on porous squeeze films.

3.7.2 The Differential Equation to be Solved and Dimensional Groups.

The solution of the Reynolds Equation is found by using the isoviscous equation of state in equation 3.7. Then

$$p(h) = -3\eta_0 R\, v_c\, (1/h^2 - 1/h_s^2) \qquad (3.41)$$

Integrating this in the same manner as given above over $[0, r_s]$, the equation of motion is obtained

$$m\dot{v}_c = 2\pi .\ 3\eta_0 R^2 v_c \left[\frac{2}{h_s} - \left(\frac{h_c}{h_s^2} + \frac{1}{h_c} \right) \right] - mg \qquad (3.42)$$

This may be rewritten to give

$$\frac{\dot{v}_c}{g} = 6\pi \frac{\eta_0 R^2}{mg} v_c \left[\frac{2}{h_s} - \left(\frac{h_c}{h_s^2} + \frac{1}{h_c} \right) \right] - 1 \qquad (3.43)$$

In this form it is immediately clear that for a given set of initial conditions (v_s, h_s), there is only one group $\frac{\eta_0 R^2}{mg}$ that determines the trajectory. Thus any set of results which have the same value for that group will give rise to the same trajectory, given the same initial conditions. This is shown in Figure 3.17 using the base values and then with $m^* = 5m$ and $\eta_0^* = 5\eta_0$. It is seen that the values of h_c, $\dot{h}_c$, $\ddot{h}_c$ are the same for both runs. (Remember that the force has been divided by the weight of the ball).

The pressure curve does not lie on the same curve as before and an explanation

of this is needed. If the equation for the centre pressure is substituted into the trajectory equation, then

$$\frac{\dot{V}_c}{g} = \frac{\eta_0 R^2}{mg} \left[\frac{h_c P_c}{\eta_0 R} - 6v_d \left(\frac{h_c - h_s}{h_s^2} \right) \right] - 1 \qquad (3.44)$$

This implies that to obtain a family of parameters that lie on only one curve then both $\frac{\eta_0 R^2}{mg}$ and $\eta_0 R$ need to remain constant for the entire family.

It was found empirically by plotting $\frac{p_c}{\eta_0}$ instead of p_c that for the parameters of Figure 3.17, the value of "pressure" did indeed lie on just one curve.

Thus if only $\frac{\eta_0 R^2}{mg}$ is constant, then the centre pressure is known to within a multiplication factor.

3.7.3 The Behaviour of the Solution.

With insight into the behaviour of the isoviscous solution, it is appropriate to discuss the solution and compare it to that of the exponential viscosity model.

It is seen from the results that the solutions for the exponential case follows very closely those for the corresponding isoviscous case during the first stage of impact. There are only small differences for the value of α typically encountered with mineral oils.

In the second stage of impact, when the pressure curve lies on a straight line, (log. pressure linear with time), the effect of the exponential viscosity becomes visibly apparent and the pressure curve diverges from the isoviscous solution, rising to the "infinite" value.

Let the two groups be denoted by

$$K_1 = \frac{\eta_0 R^2}{mg} \qquad K_2 = \eta_0 R \tag{3.45}$$

Using this isoviscous model the value of the power law may be ascertained from the formula

$$\text{Slope} = \frac{\log p_c(t_2) - \log p_c(t_1)}{t_2 - t_1}$$

and it is known that the slope is a function of K_1 alone. This is because it has been determined that by fixing only K_1, a change in K_2 will displace the pressure line vertically as can be seen by considering 3.41 and 3.43. Thus a series of runs altering η_0 were made and it was found that

$$p_c = C\, e^{5.30516E\text{-}2\ t/K_1}$$

Considering the dynamics equation and neglecting terms in h_s compared to h_c, if $\dot{v}_c$ is negligible compared to the magnitude of the other terms, then

$$6\pi K_1 v_c \left(\frac{-1}{h_c}\right) - 1 = 0$$

Now if $h_c = Ae^{\lambda t}$, then $\lambda = \frac{-1}{6\pi K_1} = -5.39516E\text{-}2/K_1$. Similarly the terms in p_c give $p_c = Ce^{\lambda t} = Ce^{t/6\pi K_1}$.

These results may be further confirmed by the ratios v_c/h_c; also the analytical calculation of the eigenvalues.

There does not appear to be a grouping that includes the intital conditions (v_s, h_s) to give a family of solutions, that allows an extra physical variable to be removed from the defining set. A consideration of possible substitutions or rearrangement of the force equation 3.42 will confirm this.

3.7.4 The Method Used to Integrate the Differential Equations.

It has been mentioned previously that to integrate the dynamical equation a Runge-Kutta method with step halving was used. When this was applied to the isoviscous case (or the Mark I viscosity model) it was found to use large amounts of computer time but with an extremely slow rate of advance. One reason for this is that the model has no obvious time limit for the integration process. The only method that was effective in integrating this equation was the EPISODE package. Even with this care was need, because of the sensitivity of the solution to small changes in v_c or h_c. This could be controlled to some extent by using a local error estimate of the order 10^{-10}, a criterion that would normally be considered excessively small. At the time where even this was giving rise to integration problems, the film thickness predicted is in fact far below sub-atomic dimensions, but the pressure had remained log-linear with time up to values of about 10^{25}Pa. The ratio between the eigenvalues of the solution became greater than 10^{20} - giving a very stiff problem indeed, whose solution is not feasible to obtain using conventional methods.

Thus, although it appears at first sight to be simpler to solve the isoviscous case than the exponential case, there are numerical problems that make it just as difficult.

3.8 Using the Groups with the Piezoviscous Liquid.

Given an understanding of the interrelationship of the groups for the isoviscous case, it is now appropriate to find the effect on the exponential viscosity oil system.

Two sets of runs were performed, one in which only the group K_1 was

Figure 3.18. Large Mass with Differing α.

kept constant and the other in which both K_1 and K_2 were fixed.

It was found that when just K_1 was kept constant, there were small changes between the runs, due to the changing viscosity. The run was made by altering m to km and η_0 to $k\eta_0$, thus varying K_2. The value of pressure obtained is approximately k times greater (see Figure 3.18) except near the end of the solution space. Using the time displacement method gave the same pressure curve for the second stage.

When K_1 and K_2 were kept constant (i.e. $m \rightarrow km$, $R \rightarrow kR$, $\eta_0 \rightarrow \frac{1}{k}.\eta_0$) and keeping h_s and v_s fixed, both sets of trajectories were coincident, as were pressure and force/weight curves, thus giving a whole family of curves from a single set. These computer runs were made using a very large value of $\alpha(=6E\text{-}7Pa^{-1})$, one that would quickly show up any difference and using k=50.

It may be concluded that for each set of initial conditions (v_s, h_s), together with an α value, as well as K_1 and K_2, there is a single infinity of parameter values giving rise to the same solution curves. This is because three independent parameters are required to define the two groups K_1 and K_2.

Similar tests were run using the Mark I viscosity model, it was found if both K_1 and K_2 are conserved over runs, then all four curves are coincidental between runs.

In general, the results are very similar for the ranges of α considered here. A knowledge of the groups may be used to give a rough idea of the behaviour for other sets of (m, η_0, R). For example, for the base system

$$K_1 = \frac{0.7.(0.01)^2}{0.0325.9.807} = 2.196E\text{-}4 \qquad s$$

$$K_2 = 0.007 \qquad Pasm$$

Now consider m = 0.65kg, R=0.02m, η_o=3.5Pas

then

$$K_1 = 2.196E\text{-}4 \qquad s$$

$$K_2 = 0.07 \qquad Pasm$$

As the group K_1 is equal for both sets, the behaviour of the solution should be very similar. However, the pressure generated at any time should be about 10 times greater than for the base system. The results for this run are shown in Figure 3.18.

This system will be integrated for the fully varying elastic case.

3.9. The Solution for a Rigid Sphere with an Exponential Viscosity Oil.

It is interesting to see the effect on not making the assumption that the ball isof parabolic cross-section, but to retain the assumption of sphericity. The equations (3.1 -3.5) are solved, but instead of using equation 3.3, use

$$h = h_c + R\sqrt{1-(\frac{r}{R})^2} \qquad (3.46)$$

This gives

$$dh = -R\frac{-\frac{r}{R^2}}{\sqrt{1-(\frac{r}{R})^2}} \quad dr$$

Or

$$((R + h_c) - h)\, dh = rdr \qquad (3.47)$$

Substituting into equation 3.7

Figure 3.19. Base Solution for a Sphere.

$$\int_0^p \frac{dp}{\eta} = 6v_c \int_{h_s}^{h} \frac{R + h_c - h}{h^3}\, dh \qquad (3.48)$$

Hence

$$p = -\frac{1}{\alpha} \log \left(1-3\eta_0\alpha v_c(R+h_c)\left(\frac{1}{h_s^2} - \frac{1}{h^2}\right) + 6\eta_0\alpha v_c\left(\frac{1}{h_s} - \frac{1}{h}\right)\right) \qquad (3.49)$$

The film force is, on writing,

$$C = 3\eta_0\alpha v_c(R+h_c)$$

$$B = -6\eta_0\alpha v_c$$

$$A = 1 - \frac{B}{h_s} - \frac{C}{h_s^2}$$

with

$$D = \sqrt{B^2-4AC}$$

given by

$$F = 2\pi \int_0^{r_s} pr\,dr = -\frac{2\pi}{\alpha} \int_{h_s}^{h_c} (R+h_c-h)\log(A+B/h+C/h^2)\,dh$$

Integrating by parts gives

$$F = -\frac{2\pi}{\alpha} \left\{h_c\left(R - \frac{h_c}{2}\right)(-\alpha p_c) - \frac{1}{4A^2}\left[-2ABh+\log(Ah^2+Bh+C) - \frac{D^3}{B}\log\frac{2Ah+B-D}{2Ah+B+D}\right]_{h_s}^{h_c}\right\} \qquad (3.50)$$

Figure 3.19 shows the results from a run using the base parameters and it is seen that there are only small differences in the curves plotted. There is a small increase in the peak pressure and force values. In the second stage of impact, the peak pressure is slightly greater than for the parabolic case, though it gives virtually the same curve when displaced in time. The similarity between the two sets of results is mainly due to the strong coupling effected by the dynamic equation.

3.10 Discussion on the Rigid Body Solutions.

Having run many tests using the rigid body model, insight has been obtained into the likely behaviour of the elastic solution. This is because the elastic effects are small for most of the impact up to the time that the rigid system becomes computationally unstable.

These effects may be summarised by considering the results as a whole.

1. The solution is stable as long as time steps are sufficiently short.
2. The equations have been shown to exhibit stiffness, thus time integration methods need to be stiffly stable in order to obtain a solution in a reasonable time, or need to use very short time steps with conventional methods.
3. When using exponential viscosity models, at pressures not considered to be high in the literature, machine precision limitations become apparent, which together with theoretical considerations of the applicability of this type of model, mean that results using these models should be used with caution.
4. It was found that, using random errors of known form, quite small errors gave results that were unacceptable. This is due to the solution being a difference of very nearly equal quantities at later solution times. This has ramifications on the acceptability of solution methods for the elastic case.
5. The alternative methods used when $\ddot{h}_c \to 0$, are stable and do not have the problems that beset the normal dynamic solution. However, in section 6.1, it will be shown that for the elastic solution this introduces its own errors due to an instability in the pressure obtained with time.

6. With regard to the various problem parameters, it may be seen that these fall into two classes:- (a) Physical Parameters (α, αp_L, η_0, m, R) which are intrinsic to a particular ball and oil combination, and (b) Initial Conditions (v_s,h_s) which are freely variable. It was found that the range of suitable initial conditions was quite small and when the ball reached the second stage, then the initial conditions no longer had any effect on the behaviour of the trajectory or the peak pressure generated. However, the physical parameters (m, η_0,R) did. The value of K_1 determined the basic gradient of pressure rise in the second stage. K_2 is not as important as it may be considered to move the time base along if only the elastohydrodynamic region is considered.
7. By solving for both the sphere and its parabolic approximation and showing that the results are virtually indentical confirms that the approximation is a good one in that the equations to be solved are simplified yet no significant error is introduced.
8. The statement of NORMAN, 1971, quoted in section 3.3.1 should be modified to read "whatever finite difference method is used to calculate x and $\dot{x}$, the ability to determine the trajectory is limited by either machine precision limitation or algorithmic deficiencies.

CHAPTER FOUR

SOLUTION METHODS FOR THE NON-ANALYTICAL ISOTHERMAL REYNOLDS EQUATION

4.1 General Considerations.

4.1.1 Introduction.

In this chapter several methods of solving the non-linear Reynolds Equation will be presented. They range from the so-called Direct methods to Newton-Raphson techniques, using a Vogelpohl type substitution and quintic spline elements, (see 4.6 and 4.8).

If the liquid is compressible, (using formula 2.15), or the bounding solids are elastic, there is no analytic solution to the Reynolds Equation. Consequently, all methods used for solving these non-linear equations are numerical.

The pressure distribution was assumed to be quasi-static, i.e. at each instant in time the Reynolds Equation holds, and if the ball centre velocity and height are given, together with any previous values that have been calculated, the pressure distribution at that instant may be found, i.e. Inertia and temperature effects are ignored.

The programs to solve these equations were built up with a main routine which set up the variables, and a time integrator, which controlled the impacting process, together with a subroutine. This subroutine, when given a (v_c, h_c) pair, would calculate the pressure distribution and film force. If the integration method gave values that lay outside some preassigned convergence criterion, the subroutine could be called

again using a slightly different (v_c, h_c) pair. Consequently, this pressure solution method may be discussed separately from any time integration aspects.

To check that a method was sufficiently accurate, it was tested with the parameters set to solve the rigid parabola, incompressible exponential viscosity fluid system. The integration of the dynamics equation using the Runge-Kutta-Merson method with time, and a comparison with that obtained from the analytical solution method, (also using Runge-Kutta-Merson), allowed a check to be made on the efficacy of any solution method. The fixed time step method was used in order to eliminate any uncertainties that could have arisen from the time integration rather than those of space integration. This is because a variable time step method uses local results to determine the time step to be used, so varying the space integration method would alter the integration process between the tests.

4.1.2 The General Method of Solving the Reynolds Equation.

The general method used to solve the non-linear Reynolds Equation was to replace the problem of solving a non-linear differential equation by that of solving a set of non-linear difference equations. To do this it is necessary to map a set of node, or grid, points onto the independent variable domain $[0, r_s]$.

$$\underline{r} = \{r_i,\ 1 \leq i \leq n \mid 0 = r_1 < r_2 < \ldots < r_n = r_s\} \qquad (4.1)$$

and define $\Delta r = r_2 - r_1$.

At each point r_i let there be defined a value p_i, so that

$\underline{p} = \{p_i, 1 \leq i \leq n\}$ with $p_n = 0$. (One of the boundary conditions on the Reynolds Equation.)

It is the aim to satisfy the Reynolds Equation at each node point by changing $\underline{p}$ appropriately.

Now Reynolds Equation is an equation in $\frac{dp}{dr}$ and $\frac{d^2p}{dr^2}$.

Thus "connectedness" relations are needed between $\frac{dp}{dr}$ and $\underline{p}$, and $\frac{d^2p}{dr^2}$ and $\underline{p}$. i.e.

$$\frac{dp}{dr} = \{\frac{dp}{dr}\}_i = \underline{\underline{D}}_1 \underline{p} \frac{1}{\Delta r} + O(\Delta r^k 1) \tag{4.2}$$

$$\frac{d^2p}{dr^2} = \{\frac{d^2p}{dr^2}\}_i = \underline{\underline{D}}_2 \underline{p} \frac{1}{\Delta r^2} + O(\Delta r^k 2) \tag{4.3}$$

where the last term in each equation is the local truncation error made by using the relation. The exact form of these relations depends on the particular method used, but will be of polynomial form in this thesis. By substituting them in the Reynolds Equation the difference equations are obtained.

The methods presented here fall into two classes. One class may be referred to as the Direct methods. They give directly the new pressure vector and assume that the equations are locally linear and thus do not take into account varying coefficients during an interation.

The second class is the Newton methods, which do not give the pressure directly, but give the changes that need to be made in the

pressure vector. This class of method estimates the effect on the coefficients of changing the pressure vector, and consequently tends to have a higher order of convergence than the linear methods.

4.1.3. The Relatively Fixed Grid and its Importance to the Solution Method.

The definition of the grid mesh $\underline{r}$ has been chosen so that there are n points covering the domain $[0,r_s]$. However, from its definition, r_s is a function of time, so it was decided to choose a grid such that

$$\underline{r}\,(t) = \underline{R}\,.\Delta r(t) \qquad (4.4)$$

Thus, $R_1=0$, $R_2=1$, $\ldots\ldots,R_n=r_s/\Delta_r$.

This implies that $\underline{R}$ is a fixed grid at all times for a given run, and r is a scaling factor, giving a relatively fixed grid for $\underline{r}$, i.e. $\dfrac{r_i(t)}{r_j(t)} = \dfrac{R_i}{R_j}$, a constant.

Now consider the set of pressures mapped onto the vector $\underline{R}$ rather than the space vector $\underline{r}$. Then, using the "connectedness" relations to find the gradients of the pressure curves,

$$\frac{d\underline{p}}{dR} = \underline{\underline{D}}_1\underline{p}\,, \qquad \frac{d^2\underline{p}}{dR^2} = \underline{\underline{D}}_2\underline{p}$$

As $\underline{R}$ is fixed for a given run, then $\underline{\underline{D}}_1$ and $\underline{\underline{D}}_2$ are similarly fixed and so need to be calculated once only.

Similarly, if the pressure is integrated over the domain, then

$$\int_0^{r_s} p(r)dr \quad = \quad \int_0^{R_n} p(R)dR.\ \Delta r$$

This will be used in chapter five to calculate the elastic distortions in order that they may be calculated during the intialisation of the problem and not be recalculated with each step.

4.2 Direct Difference Method.

If it assumed that the ball is rigid and that $\frac{d\rho}{dt}$ may be assumed negligible (4.5), the Reynolds Equation may be written as

$$\frac{d^2p}{dr^2} + \left(\frac{1}{r} + \frac{1}{Y}\frac{dY}{dr}\right)\frac{dp}{dr} = \frac{12\rho V}{Y} \qquad (4.5)$$

If the domain is divided into n-1 equal segments of length Δr, then if the values of $\underline{\underline{D}}_1$ and $\underline{\underline{D}}_2$ are obtained by assuming that the solution curve at r_i is locally a parabola passing through (r_{i-1}, p_{i-1}), (r_i, p_i), (r_{i+1}, p_{i+1}), then the "3-point formulae" are obtained.

$$\underline{\underline{D}}_1 = \begin{bmatrix} 0 & 0 & & & \\ -\frac{1}{2} & 0 & \frac{1}{2} & & \\ & \ddots & \ddots & \ddots & \\ & & -\frac{1}{2} & 0 & \frac{1}{2} \end{bmatrix} \frac{1}{\Delta r}$$

$$\underline{\underline{D}}_2 = \begin{bmatrix} -2 & 2 & & & \\ 1 & -2 & 1 & & \\ & \ddots & \ddots & \ddots & \\ & & 1 & -2 & 1 \end{bmatrix} \frac{1}{\Delta r^2}$$

Note that the first row of $\underline{\underline{D}}_1$ is zero as $(\frac{dp}{dr})_1 = 0$, also $(\underline{\underline{D}}_2)_{2}=2$ as the function is symmetric and $p(-\Delta r)=p(\Delta r)$. $\underline{\underline{D}}_1$ and $\underline{\underline{D}}_2$ are only of size $(n-1) \times (n-1)$ for there are only $n-1$ unknowns as $p_n=0$.

Thence the tridiagonal system.

$$A_i p_{i-1} + B_i p_i + C_i p_{i+1} = E_i \quad , 1 \leq i \leq n-1 \tag{4.6}$$

where $$A_i = \frac{1}{\Delta r^2} - \frac{1}{2\Delta r}\left(\frac{1}{r} + \frac{1}{Y}\frac{dY}{dr}\right)_i \quad , 2 \leq i \leq n-1$$

$$B_i = -\frac{2}{\Delta r^2} \quad , 2 \leq i \leq n-1$$

$$C_i = \frac{1}{\Delta r^2} + \frac{1}{2\Delta r}\left(\frac{1}{r} + \frac{1}{Y}\frac{dY}{dr}\right)_i \quad , 2 \leq i \leq n-1$$

$$E_i = \left(\frac{12\rho V}{Y}\right)_i \quad , 1 \leq i \leq n-1$$

and A_1 is not defined

$$B_1 = -\frac{4}{\Delta r^2}$$

$$C_1 = \frac{4}{\Delta r^2}$$

The value $(\frac{1}{Y}\frac{dY}{dr})_i$ is needed, this could be approximated by $\frac{Y_{i+1}-Y_{i-1}}{2\Delta r}$, however, at small film thicknesses, due to excessive curvature in h, a better approximation is

$$\frac{1}{Y}\frac{dY}{dr} = (\frac{1}{\rho}\frac{d\rho}{dp} - \frac{1}{\eta}\frac{d\eta}{dp})\frac{dp}{dr} + \frac{3}{h}\frac{dh}{dr} \qquad (4.7)$$

This is the one place where non-linearity arises, for this expression is a function of $\underline{p}$.

As the system is non-linear, an initial estimate of the pressure distribution is needed in order to calculate ρ,η,h and Y. It is normally obtained by extrapolating the values of the elements of previous solution vectors. Let this be denoted by $(\underline{p})_0$. Using this vector the values may be calculated and the tridiagional scheme quickly solved to give a new distribution $(\underline{p})_1$, which may be used as an initial pressure vector to calculate $(\underline{p})_2$. This process may be carried on ad infinitem, but the solution is attained when $(\underline{p})_{s+1} = (\underline{p})_s$. An approximation has already been made by converting the differential equation into a difference equation, thus when the difference between successive iterations becomes sufficiently small, it is assumed that the solution has been obtained.

This will be so when

$$\frac{\sum_{i=1}^{n-1} |(p_i)_s - (p_i)_{s-1}|}{\sum_{i=1}^{n-1} |(p_i)_s|} < \varepsilon \qquad (4.8)$$

for some predetermined ε.

At not very high pressures (i.e. about 10^7 Pa) this method becomes unstable due to the strong dependence of the viscosity on the pressure, coupled with the pressure distribution being strongly peaked at the centre. There are several ways to reduce this problem. One is to use more grid points, which involves more computational work, and is not really feasible remembering that a time integration is needed.

Another way is to use a damping, or relaxation factor, where, instead of using the new calculated pressure as the iterate, only a fraction of the change calculated is used. From work by RANGER, 1974, it appears that for the EHD rolling ball problem a relaxation factor in the range 0.02 to 0.05 must be used, making this a computationally expensive method, especially considering the number of pressure distributions required per run.

The third method is aimed at reducing the effect of the pressure peak by concentrating the node points in the centre zone and spreading them out in the outer regions where the pressure is less (and the pressure gradients smaller). This method improves the accuracy, however, the nodes in the outer regions cannot be placed too far apart, otherwise the film force becomes inaccurate due to the weighting given to the outer values.

Modifications to this method include using higher order elements, and instead of using 3-point formulae for the derivatives, 5-point ones could be used, obtaining a pentadiagonal matrix equation to solve. The Direct Difference method was rejected due to the low values after which solutions could not be obtained.

4.3 Direct Integral Method.

Taking as the initial equation to be solved

$$\frac{1}{r}\frac{d}{dr}\left(rY\frac{dp}{dr}\right) = 12\rho v_c \qquad (4.9)$$

Integrating this with respect to r

$$rY\frac{dp}{dr} = 12v_c\int_0^r \rho r dr + C_1$$

Using the boundary conditions $\frac{dp}{dr}$ at r=0 gives C_1=0.

Hence

$$p = \int_0^r \frac{12v_c}{rY}\int_0^r \rho r'dr'dr + C_2 \qquad (4.10)$$

Now p=0 at r_s, so

$$0 = \int_0^{r_s}\frac{12v_c}{rY}\int_0^r \rho r'dr'dr + C_2$$

Hence

$$p = \int_{r_s}^r \frac{12v_c}{rY}\int_0^r \rho r'dr'dr \qquad (4.11)$$

The functions ρ and Y are functions of pressure, so again an iterative process is obtained.

The second integration was carried out from the centre to the edge, starting with an arbitrary value of p_1 (normally the previously iterated value). When the pressure had been integrated to r_s, then, in general,

$p_n=\delta$, for some δ. Finally δ is subtracted from all node values, obtaining the second boundary condition $p_n=0$.

This cycle is repeated until the convergence criterion (4.8) is reached. In order to perform these integrations, different interpolating functions may be assumed. If these are assumed to be linear, the trapezium rule is obtained. Using this allows the grid spacing to be easily altered. If the function is to be quadratic then a form of Simpson's rule is used. Use is made of the fact that at the centre the pressure is symmetric and its gradient is antisymmetric.

With this method, derivatives of the density-pressure and of the viscosity-pressure relations are not required and if the local deformations are calculated between each iteration then the elastic case can be solved with no further work.

However, a Vogelpohl substitution (see section 4.6) cannot be used with this method. It is very useful as it can speed up convergence, so the Direct Integral Method was not pursued.

4.4 Newton-Raphson Method.

4.4.1 Algorithm.

Potentially, the Reynolds Equation gives a highly non-linear system of equations. Due to the strong effect of the pressure on the viscosity at high pressure, the direct methods become unstable as they do not account for the changes in the coefficients. This effect was also found by previous workers, for example, CHRISTENSEN, 1970. It is possible to reduce this effect by using a small relaxation factor, but

this only serves to delay the onset of the instability.

If the equations are written in the form

$$\underline{f}\,(\underline{p}\,)=\underline{0} \tag{4.12}$$

where, with * defined in Appendix IV

$$\underline{f}(\underline{p}\,) = (\frac{1}{\Delta r^2}\ \underline{\underline{D}}_2 + \frac{1}{\Delta r}\ \underline{H}^*\ \underline{\underline{D}}_1)\underline{p} - \underline{M}$$

$$(\underline{H})_i = (\frac{1}{r} + \frac{1}{Y}\frac{dY}{dr})_{r_i}$$

$$(\underline{m})_i = (12\ \frac{d}{dt}\ (\rho h)/Y)_{r_i}$$

then, given an initial approximation for the pressure $(\underline{p})_0$ (which is needed for every method), and if the jacobian $\underline{\underline{J}}(\underline{p}\,)_s$ can be calculated

$$\underline{\underline{J}}\ (\ (\underline{p}\,)_s)_{ij} = \frac{\partial f_i}{\partial p_j}\ \Big|_{(\underline{p}\,)_s} \tag{4.13}$$

We can form

$$(\underline{\Delta p}\,)_s = \underline{\underline{J}}^{-1}((\underline{p}\,)_s)\ .\ \underline{f}\ ((\underline{p}\,)_s) \tag{4.14}$$

then the next approximation for the pressure is given by

$$(\underline{p}\,)_{s+1} = (\underline{p}\,)_s - (\underline{\Delta p}\,)_s \tag{4.15}$$

This is the (n-1) dimensional version of the Newton-Raphson method. It will iterate to a solution for $\underline{p}$ if $(\underline{p})_0$ is sufficiently near that solution of the fuctional. It is known that this region will generally be larger than the region for solution of the direct iteration method. The method estimates the effect of changes in the pressure values on changing the values of the coefficients as well as the derivatives.

Consider again the rigid parabola squeezing onto a compressible exponential viscosity-pressure fluid. We obtain as a difference formula

$$f_i = \frac{p_{i+1}-2p_i+p_{i-1}}{\Delta r^2} + \left(\frac{1}{r} + \frac{1}{Y}\frac{dY}{dr}\right)_i \frac{p_{i+1}-p_{i-1}}{2\Delta r} - (12\rho V_c/Y)_i$$

If it is assumed that the 3-point formulae of section (4.3) for the derivatives hold, then $\underline{\underline{D}}_1$ and $\underline{\underline{D}}_2$ are those given above, and the problem is to solve for $\underline{p}$ in $\underline{f}(\underline{p})=\underline{0}$.

Now $$\left(\frac{1}{Y}\frac{dY}{dr}\right)_i = \left(\frac{1}{\rho}\frac{d\rho}{dp} - \frac{1}{\eta}\frac{d\eta}{dp}\right)_i \frac{p_{i+1}-p_{i-1}}{2\Delta r} + \frac{3r_i}{h_i}$$

so
$$\frac{df_i}{dp_j} = 0 \qquad ,j\neq i,i\pm1$$

$$= \frac{1}{\Delta r^2} \pm \left\{\left(\frac{1}{r} + \frac{1}{Y}\frac{dY}{dr}\right)_i + \left(\frac{1}{\rho}\frac{d\rho}{dp} - \frac{1}{\eta}\frac{d\eta}{dp}\right)_i \frac{p_{i+1}-p_{i-1}}{2\Delta r}\right\} \frac{1}{2\Delta r} \qquad ,j=i\pm1 \tag{4.16}$$

$$= -\frac{2}{\Delta r^2} + \frac{d}{dp_i}\left(\frac{1}{\rho}\frac{d\rho}{dp} - \frac{1}{\eta}\frac{d\eta}{dp}\right)_i \left(\frac{p_{i+1}-p_{i-1}}{2\Delta r}\right)^2 - 12\frac{d\rho}{dp}V_c/Y_i$$

$$+ 12\rho V/Y_i \cdot \left(\frac{1}{\rho}\frac{d\rho}{dp} - \frac{1}{\eta}\frac{d\eta}{dp}\right)_i \qquad ,j=i$$

Thus a tridiagonal matrix is again obtained, but instead of solving for the pressures, it is the changes in them that are calculated. This also gives the changes in the pressures needed to estimate the convergence directly.

4.4.2 The Advantage of Higher Order Convergence Methods.

The second major advantage is that if $(\underline{p})_s$ is sufficiently near the root, then the convergence to the root is quadratic, that is if the values of $(\underline{p})_s$ are accurate to five significant digits, then the next iteration $(\underline{p})_{s+1}$ will be accurate to ten places. So if the convergence criterion CRIT=10^{-5}, then the solution vector obtained is accurate to approximately ten places.

However, this shows how the pressures converge to the solution of the difference equation, not to the solution of the differential equation. There is a truncation error made in solving this different problem given by k_1 and k_2 in equations (4.2) and (4.3). Note that for the case considered here k_1 and k_2 are 2. If, instead of using a tridiagonal scheme, a pentadiagonal scheme is used, then k_1 and k_2 equal 4, and a more accurate solution may be obtained.

Using higher order approximations increases the bandwidth of the matrices $\underline{\underline{D}}_1$, $\underline{\underline{D}}_2$, thus more work is needed to solve for $(\underline{\Delta p})_s$. To compensate for this it is expected that the number of nodes may be reduced so that overall accuracy is maintained.

Consider now, the elastic case. The compliance matrix is full since pressure at a point gives rise to distortion at every other point and hence a full matrix for the partial derivatives is obtained. Thus if the Newton-Raphson method is used, it is worthwhile to find the highest possible order method and reduce the number of grid points. If there are n equations to solve, the work needed to find the solution of the matrix equation (4.12) is proportional to n^3.

Consider the curve to be represented by $\underline{p}$. So far it has only been defined at the node points. Given a set of points $(\underline{r}, \underline{p})$ there are infinitely many functions $g(r)$ that can be constructed such that $g(r_i)=p_i$. It is desirable that the function should pass through $(\underline{r},\underline{p})$.

For example, suppose the interpolating function is chosen to be

$$g(r) = p_i + \frac{r-r_i}{r_{i+1}-r_i}(p_{i+1}-p_i) \quad , \quad r\varepsilon[r_i,r_{i+1}]$$

The derivatives have not been defined at the node points, where the gradient is discontinuous. The 3-point formula for the first derivative is equivalent to requiring the derivative at r_i to be the linearly interpolated gradient over (r_{i-1}, r_{i+1}) calculated by weighting the gradient at each segment mid-point with respect to the length of that segment.

4.5 Interpolating Functions.

4.5.1 The Cardinal Interpolating Functions.

In the last section it was seen that in order to reduce the number of equations in the finite difference form of the Reynolds Equation, large values of k_1 and k_2 were needed. It is appropriate to discuss various interpolating functions and their relationship with the solution of the Reynolds Equation.

Assume that there is a set of grid points $\underline{r}$ and a calculated set of pressures $\underline{p}$, with $(\underline{p})_i$ defined at $(\underline{r})_i$. The problem is to construct the function $g(r)$ with the condition

$$g(r_j)=p_j \tag{4.17}$$

As elements of $\underline{p}$ are independent variables (excepting that as a set they must satisfy the difference form of the Reynolds Equation), the function g(r) shall be required to be of the form

$$g_1(r) = \sum_{j=1}^{n} C_{1j}(r)p_j \tag{4.18}$$

with

$$C_{1j}(r_i) = \delta_{ij} \tag{4.19}$$

Further, in this work, the function $C_{1j}(r)$ are required to be piecewise polynomials of degree 1. Note that the requirement (4.19) assures the independence of the values $\underline{p}$ except in the Reynolds Equation.

The functions $C_{1j}(r)$ may be called the Cardinal Interpolating Polynomials of degree 1. (c.f. RHODE and OH ,1975). They are called cardinal due to the property that equation (4.19) holds.

Piecewise polynomial-functions are chosen in preference to other types (for example, Langrangian interpolation) as they are well behaved and do not oscillate in an alarming manner between the node points. Indeed, using Langrangian interpolation of high order is likely to increase the interpolating errors.

4.5.2 The Form of $C_{1j}(r)$ for Differing 1.

If 1=0, then for $1<j<n$, and defining $r_0=0$ here

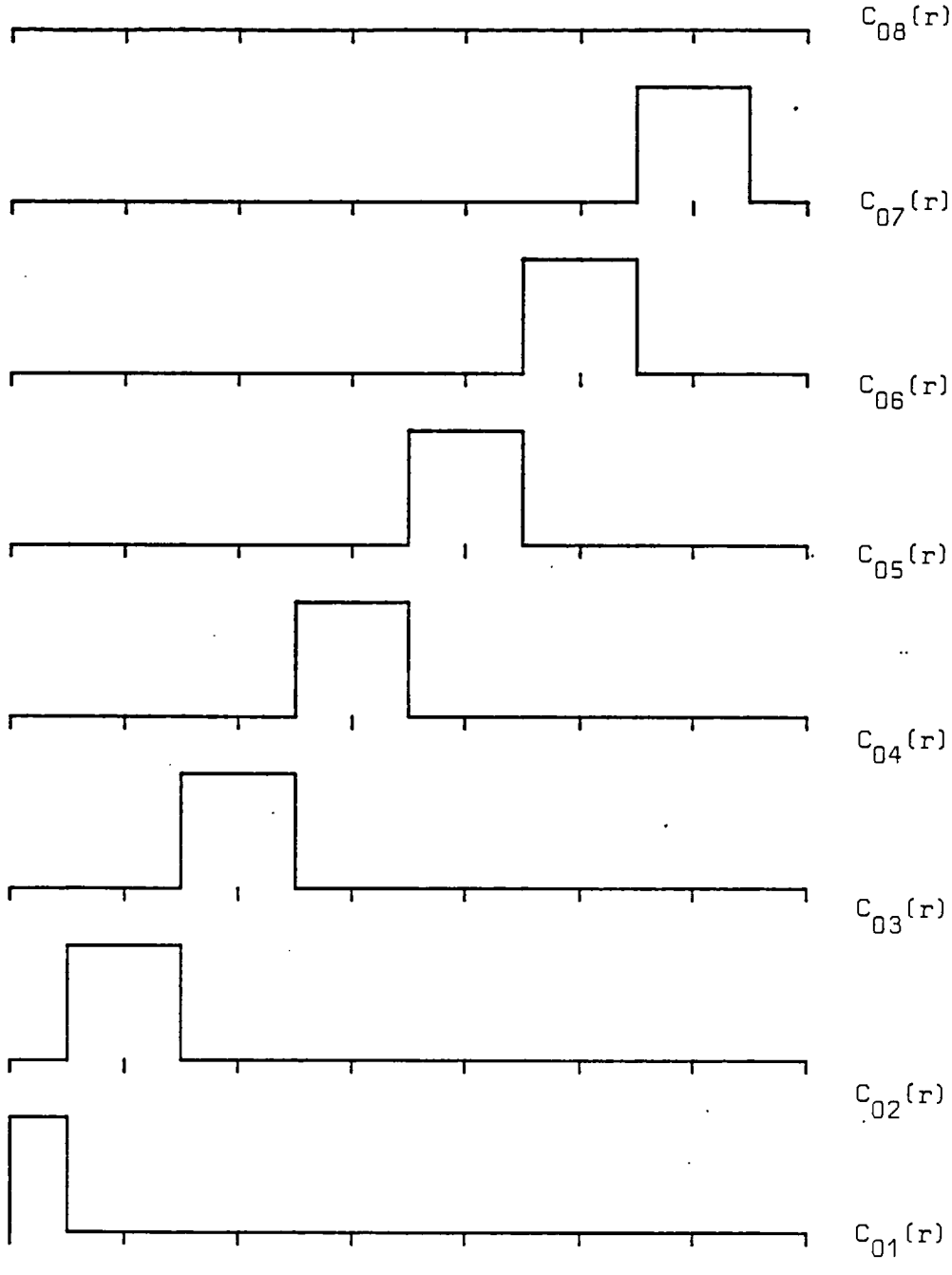

Figure 4.1. Cardinal Interpolating Polynomial of Degree 0.

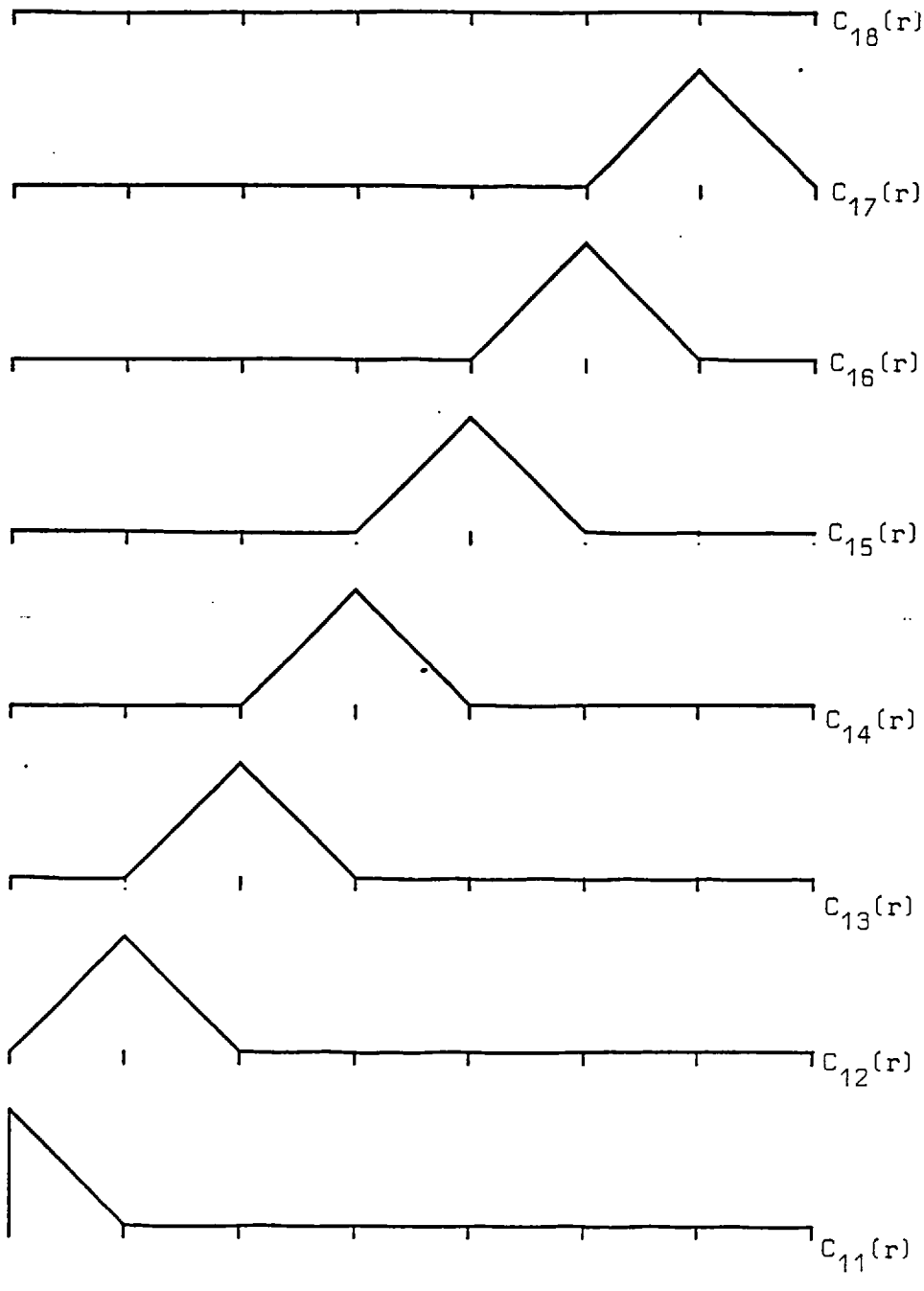

Figure 4.2. Cardinal Interpolating Polynomial of Degree 1.

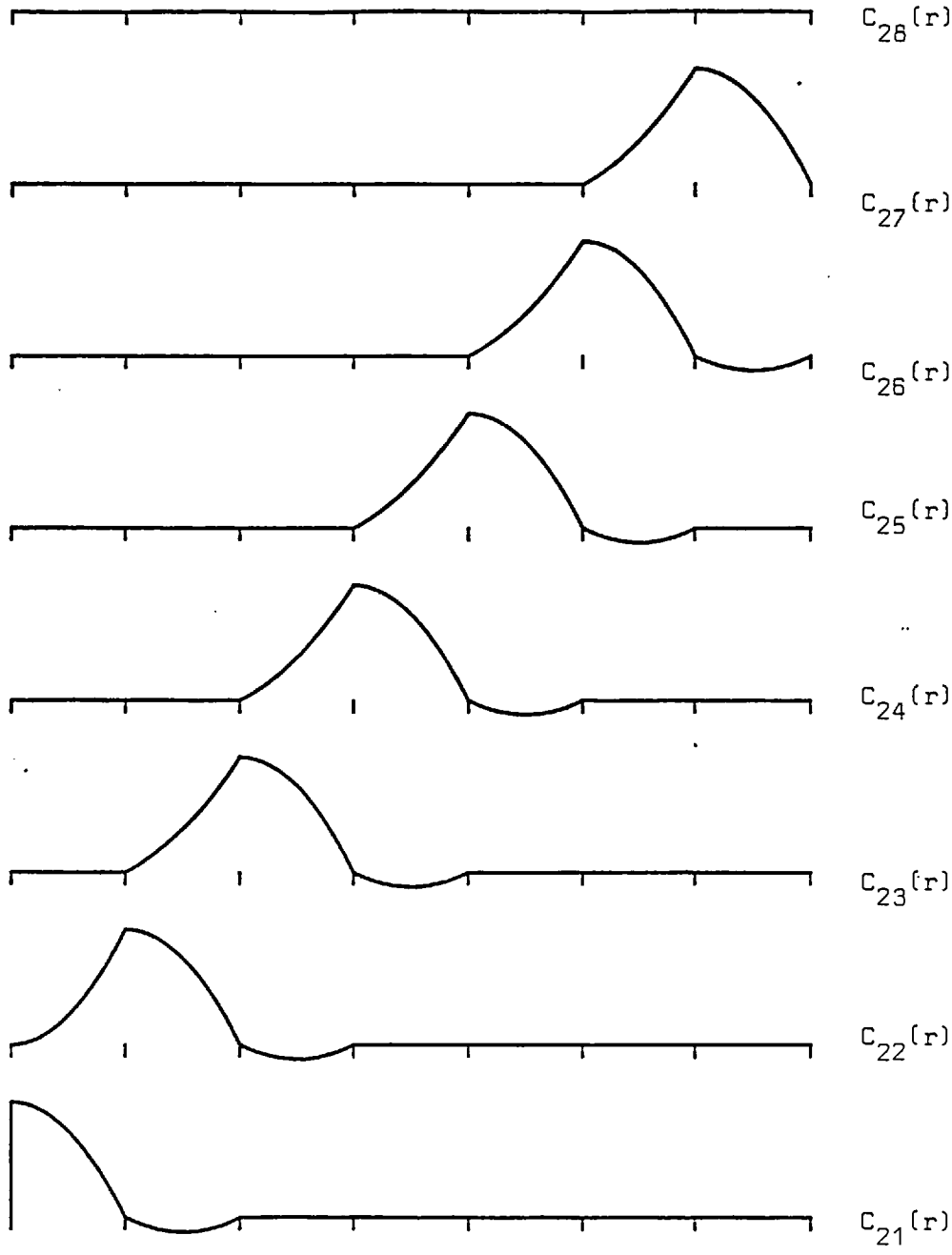

Figure 4.3. Cardinal Interpolating Polynomial of Degree 2.

$$C_{0j}(r) = 0,\ r \leq \tfrac{1}{2}(r_{j-1}+r_j) \qquad (4.20)$$

$$1,\ \tfrac{1}{2}(r_{j-1}+r_j) < r \leq \tfrac{1}{2}(r_j+r_{j+1})$$

$$0,\ r > \tfrac{1}{2}(r_j+r_{j+1})$$

$C_{0n}(r)$ is defined as $p_n=0$, but may be defined as identically zero. These functions are shown diagramatically in Figure 4.1. for a mesh of 8 linearly spaced mesh points.

If l=1, then 'overlapping triangles' are obtained. These are shown in Figure 4.2. Again, $C_{1n}(r)$ is similarly undefined and may be put identically to zero.

If l=2 there is a more complicated system. Requiring a curve to pass through the points at each end gives two conditions for each interval. The third (3 parameters are needed to define a parabolic segment), is that the curve must pass through the mesh point towards the pole from the interval. This was chosen because it is known that the pressure field is symmetrical. That is if the segment is $[r_{j-1},r_j]$, then the curve is to pass through $[r_{j-2},p_{j-2}]$ as well. This process results in a piecewise parabolic curve. For l=2, $C_{2n}(r)$ remains undefined and again is put to zero. This is shown in Figure 4.3 for linearly spaced meshes.

In this work, l=0 is not used, l=1 has been used in the direct differential and direct integral methods, and l=2 is only used in the direct integral method.

4.5.3 The Cubic Spline.

If l=3, a cubic interpolating function is obtained. This could be extended from the case of l=2 by forcing it to go through the point

(r_{j+1},p_{j+1}). However, in this case a cubic spline formulation will be used.

A cubic spline is a continuous piecewise cubic polynomial with the property that the first and second derivatives are continuous across the knots. (A knot is where the third derivative can be discontinuous). If a knot is put at each of the n grid points it can be seen that there are n-1 intervals, thus 4n-4 constants need to be found to uniquely determine the function. 2n-2 constants are obtained by requiring the curve to pass through the knots on either side of the n-1 intervals and a further 2n-4 by requiring the first and second derivatives to be continuous at the interior knots. This leaves 2 conditions to be satisified, normally one at each end of the curve to make it well-conditioned.

These can be of differing types. One, the so-called natural spline end condition, requires that $g''_1=0$. This is not appropriate for this problem as the pressure does not have second derivative zero at r=0 (see the Reynolds equation).

However, $p'(0)=0$, so choosing the end conditions to be given by the end slopes $g'_0=p(0)$, $g'_n=p'(r_s)$, these give the two conditions needed.

$p'(r_s)$ is required in order to solve for the cubic spline uniquely. This may be written as p'_n. Its value could be calculated by writing $p'_n=f(\underline{p},\Delta r)$ for some function f. However, this is not satisfactory for it was found that with Newton's method it gave an oscillating, but only very slowly converging solution. It was decided therefore to extend the system to be solved.

Instead of solving for $\underline{p}$ with n-1 variables unknown ($p_n=0$), this

becomes $\underline{p}^*=(\underline{p}, p'_n\Delta r)$, then

$$g_1(r) = \sum_{j=1}^{n-1} C_{1j}(r)p_j + D_{1n}(r)p'_n\Delta r \qquad (4.21)$$

As $p'(0)=0$, $D_{1n}(r)$ is not required.

Note that for dimensional compatibility instead of using p'_n, $p'_n\Delta r$ is employed. This may be treated as finding the spline over the set of points $\underline{R}$, for the end derivative on this domain is $p'_n\Delta r$.

Only n-1 equations have been used so far to calculate for the pressure distribution. Thus if Reynolds equation is required to be satisfied at r_n, then there are n equations for n unknowns. p'_n may be calculated and the system is solvable.

4.5.4 The Cardinal Cubic Spline Functions.

Recalling that

$$g_1(r) = \sum_{j=1}^{n-1} C_{1j}(r)p_j + D_{1n}p'_n\Delta r$$

then the functions $C_{3j}(r)$ and $D_{3n}(r)$ are defined such that

$$\begin{aligned}
C_{3j}(r_i) &= \delta_{ij}, \quad 1\leq i\leq n \\
C'_{3j}(0) &= 0 \\
C'_{3j}(r_n) &= 0 \\
D_{3n}(r_i) &= 0, \quad 1\leq i\leq n \\
D'_{3n}(0) &= 0 \\
D'_{3n}(r_n) &= 1
\end{aligned} \qquad (4.22)$$

These are known as the Cardinal Cubic Splines [Rhode and Oh, 1975], and

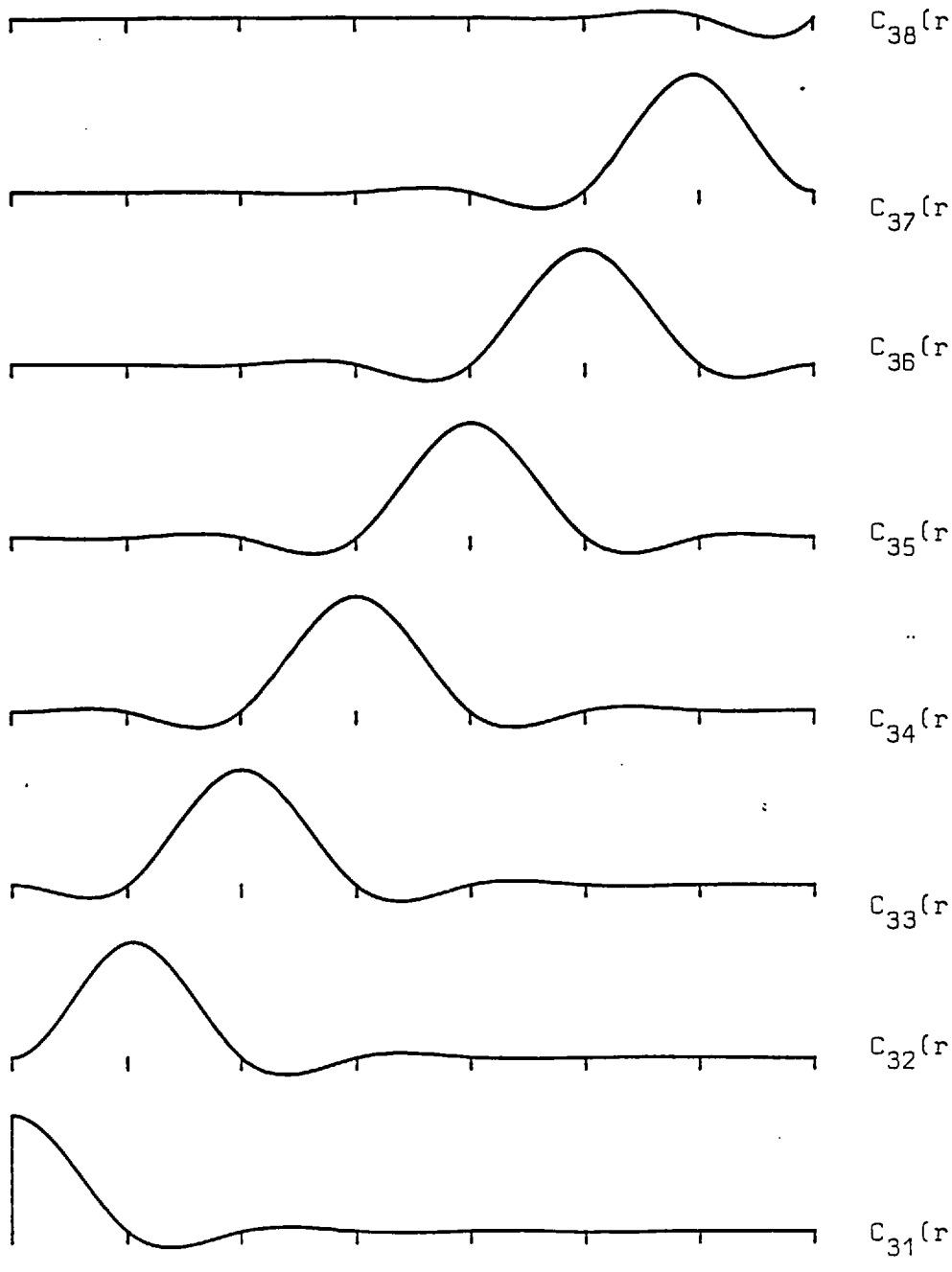

Figure 4.4. Cardinal Interpolating Polynomial of Degree 3.

are shown in Figure 4.4 for 8 linearly spaced mesh points.

The matrices $\underline{\underline{D}}_1$ and $\underline{\underline{D}}_2$ are required (from section 4.1). If the definitions (4.2) and (4.3) are extended so that

$$\frac{d\underline{p}^*}{dr} = \underline{\underline{D}}_1^* \cdot \underline{p}^* \cdot \frac{1}{\Delta r} + O(\Delta r^{k_1})$$

$$\frac{d^2\underline{p}^*}{dr} = \underline{\underline{D}}_2^* \cdot \underline{p}^* \frac{1}{\Delta r^2} + O(\Delta r^{k_2})$$

To simplify the notation, drop asterisks and note that p_n is identically zero and so $C_{1n}(r)$ is not used.

Write

$$\underline{p} = \{p_1, \ldots\ldots, p_{n-1}, p_n' \Delta r\}$$

$$C_{1n}(r) \equiv D_{1n}(r)$$

then

$$g_l(r) = \sum_{j=1}^{n} C_{lj}(r)\, p_j \qquad , l=0,1,2,3 \qquad (4.23)$$

Note that by defining $C_{0n}(r)$, $C_{1n}(r)$, $C_{2n}(r)$ to be identically zero then the new definition of $\underline{p}$ will not alter $g_0(r)$, $g_1(r)$ and $g_2(r)$.

4.5.5 The Cubic Spline Derviative Influence Coefficients.

Remembering that $g_3(r)$ has two continuous derivatives, and differentiating $g_3(r)$ twice gives

$$g_3'(r) = \sum_{j=1}^{n-1} C'_{3j}(r)\, p_j$$

$$g''_3(r) = \sum_{j=1}^{n} C''_{3j}(r)\, p_j$$

Now it is known [Ahlberg, Nilson and Walsh,1967] that

$$g'_3(r) = \frac{dp}{dr} + O(\Delta r^4) \qquad (4.24,i)$$

$$g''_3(r) = \frac{d^2p}{dr^2} + O(\Delta r^2) \qquad (4.24,ii)$$

Thus

$$\frac{d\underline{p}}{dr} = \underline{\underline{D}}_1 \cdot \underline{p}\ \frac{1}{\Delta r} + O(\Delta r^4) \qquad (4.25,i)$$

$$\frac{d^2\underline{p}}{dr^2} = \underline{\underline{D}}_2 \cdot \underline{p}\ \frac{1}{\Delta r^2} + O(\Delta r^2) \qquad (4.25,ii)$$

If

$$\left.\begin{aligned} (\underline{\underline{D}}_k)_{ij} &= C^{(k)}_{3j}(r_i)\ , \quad 1\le j<n \\ &= D^{(k)}_{3n}(r_i)\ , \quad j=n \end{aligned}\right\} \quad 1\le i\le n,\ k=1,2 \qquad (4.26)$$

$(\underline{\underline{D}})_{ij}$ is equal to $\frac{\partial}{\partial p_j}\left(\frac{d^k p}{dr^k}\right)_{r_i}$ if p_n is taken to be $p'_n \Delta r$.

As it was decided to use a relatively fixed grid the matrices $\underline{\underline{D}}_1$ and $\underline{\underline{D}}_2$ could be calculated initially assuming $\Delta r=1$ and remain fixed throughout the run. The appropriate value for Δr was used explicitly where appropriate.

By using cubic splines, a unified method has been obtained in which the complete continuous pressure curve is generated. Further, as Reynolds Equation is a second order differential equation in pressure, the pressure has to have at least continuity in the second derivative. Cubic spline

interpolation gurantees second differential continuity and may be considered to be a finite element method, albeit one-dimensional.

4.5.6 The Calculation of the Jacobian.

It is instructive to write the calculation necessary to solve for the pressure field in the case of an elastic parabola squeezing onto a compressible variable viscosity fluid film.

Let it be assumed here that the deformation $\underline{w}$ may be calculated as

$$\underline{w} = \underline{\underline{F}}.\underline{p} \ .\Delta r \tag{4.27}$$

$$\frac{d\underline{w}}{dr} = \underline{\underline{G}} \ .\underline{p} \tag{4.28}$$

This will be shown to be possible, and a method for calculating $\underline{\underline{F}}$ and and $\underline{\underline{G}}$ given, in the next chapter.

Remember that (equation 4.12)

$$f_i = \left(\frac{d^2p}{dr^2} + \left(\frac{1}{r} + \frac{1}{Y}\frac{dY}{dr}\right) \frac{dp}{dr} - \frac{12\frac{d}{dt}(\rho h)}{Y}\right)_i = 0$$

and

$$(\underline{\underline{J}})_{ij} = \frac{\delta}{\delta p_j}(f_i)$$

Let

$$\frac{d}{dt}(\rho h)_i = \rho_i V_c + \sum_{j=1}^{3} c_j (\rho w)_{ij} \tag{4.29}$$

where $(\rho w)_{i1}$ is to be evaluated at t_i

$(\rho w)_{i2}$ was the value of $(\rho w)_i$ at t_{i-1}

$(\rho w)_{i3}$ was the value of $(\rho w)_1$ at t_{i-2}

and $\underline{c}$ is found from the 3-point Lagrangian interpolation formula.

Note that $(\rho w)_{2i}$ and $(\rho w)_{3i}$ are fixed values as they were solutions at an earlier time. Now from equations 4.2 and 4.3

$$\frac{\partial}{\partial p_j}\left(\frac{d^2p}{dr^2}\right)_i = (\underline{\underline{D}}_2)_{ij}\,\frac{1}{\Delta r^2}$$

and as $\frac{\partial}{\partial p_j}\left(\frac{dp}{dr}\right)_i = (\underline{\underline{D}}_1)_{ij}\,\frac{1}{\Delta r}$

$$\frac{1}{Y}\frac{dY}{dr} = \left(\frac{1}{\rho}\frac{d\rho}{dp} - \frac{1}{\eta}\frac{d\eta}{dp}\right)\frac{dp}{dr} + \frac{3}{h}\frac{dh}{dr}$$

then

$$\frac{\partial}{\partial p_j}\left(\frac{1}{Y}\frac{dY}{dr}\right)_i = \delta_{ij}\,\frac{\partial}{\partial p_j}\left(\frac{1}{\rho}\frac{d\rho}{dp} - \frac{1}{\eta}\frac{d\eta}{dp}\right)_i \frac{dp}{dr} + \left(\frac{1}{\rho}\frac{d\rho}{dp} - \frac{1}{\eta}\frac{d\eta}{dp}\right)_i (\underline{\underline{D}}_1)\quad\frac{1}{\Delta r}$$

$$-\frac{3}{h^2}\frac{dh}{dr}\cdot\underline{\underline{F}}_{ij}\,\Delta r + \frac{3}{h}(\underline{\underline{G}})_{ij}$$

Finally,

$$\frac{\partial}{\partial p_j}\left(-\frac{12(\rho_i v_c + c_1\rho_i w_i + c_2(\rho w)_{i2} + c_3(\rho w)_{i3})}{Y_i}\right) = -\frac{12\delta_{ij}\,\frac{\partial \rho_i}{\partial p_j}\,(v_c + c_1 w_1)}{Y_i}$$

$$-\frac{12\,c_1\rho_i}{Y_i}(\underline{\underline{F}}_1)_{ij}\,r + \frac{12(\rho_i v_c + c_1\rho_i w_i + c_2(\rho w)_{i2} + c_2(\rho w)_{i3}}{Y_i}\cdot$$

$$\left\{\delta_{ij}\left(\frac{1}{\rho}\frac{d\rho}{dp} - \frac{1}{\eta}\frac{d\eta}{dp}\right)_i + \frac{3}{h_i}\,(\underline{\underline{F}})_{ij}\,\Delta r\right\}$$

By elimination this may be written

$$\delta_{ij}\{\frac{12(c_2(\rho w)_{i2}+c_3(\rho w)_{i3})}{Y_i}(\frac{1}{\rho}\frac{d\rho}{dp})_i+\frac{12\frac{d}{dt}(\rho h)}{Y_i}(\frac{1}{\eta}\frac{d\eta}{dp})_i\}+\{\frac{12\frac{d}{dt}(\rho h)}{Y}-$$

$$-\frac{12c_1\rho}{Y}\}\frac{3}{h}(\underline{\underline{F}})_{ij}\Delta r$$

Thence

$$(\underline{\underline{J}})_{ij}=(\underline{\underline{D}}_2)_{ij}\frac{1}{\Delta r^2}+\{(\frac{1}{r}+\frac{1}{Y}\frac{dY}{dr})+(\frac{1}{\rho}\frac{d\rho}{dp}-\frac{1}{\eta}\frac{d\eta}{dp})\}_i(\underline{\underline{D}}_1)_{ij}\frac{1}{\Delta r}+\frac{3}{h_i}(\frac{dp}{dr})_i(\underline{\underline{G}})_{ij}$$

$$+\{\frac{12\frac{d}{dt}(\rho h)}{Y}-\frac{12c_1\rho}{Y}-(\frac{1}{h}\frac{dh}{dr})\}_i\frac{3}{h_i}(\underline{\underline{F}})_{ij}\Delta r+(1-\delta_{in})\delta_{ij}$$

$$\{\frac{\partial}{\partial p_j}(\frac{1}{\rho}\frac{d\rho}{dp}-\frac{1}{\eta}\frac{d\eta}{dp})(\frac{dp}{dr})^2+\frac{12(c_2(\rho w)_{i2}+c_3(\rho w)_{i3}}{Y}(\frac{1}{\rho}\frac{d\rho}{dp})+\frac{12\frac{d}{dt}(\rho h)}{Y}(-\frac{1}{\eta}\frac{d\eta}{dp})_i\}$$

(4.30)

Note that this last term does not appear for i=n, as p'_n has no effect on the density or viscoisty at any grid point.

4.5.7 A Modification to the Newton-Raphson Method.

The Newton-Raphson algorithm gives a method to calculate the changes $\Delta\underline{p}$ that need to be made to the pressure values at the nodes in order to converge to the solution $\underline{f}(\underline{p})=\underline{0}$. The magnitude of the $\Delta\underline{p}$ are absolute values. In the outer regions of the contact the pressures are low and there $\Delta\underline{p}$ are expected to be correspondingly small. Near the centre the pressure values are high and thus large values of $\Delta\underline{p}$ are to be expected.

The equations which are to be solved using the Newton-Raphson method

are linear sums of the $\Delta\underline{p}$. It is possible for large errors to be made in the calculations of the $\Delta\underline{p}$ in the outer regions where they are much smaller in magnitude and are thus liable to be swamped by those of the inner regions.

A possible remedy is to use the fact that the initial estimate is normally quite close to the final solution at all grid points and then to look for a method which solves for relative changes.

A function $y(p)$ will satisfy this requirement if $\Delta y = \frac{\Delta p}{p}$

i.e. if $\frac{dy}{dp} = \frac{1}{p}$, giving $y(p) = \ln p$

Now the problem is reduced to solving $\underline{f}\,(\underline{p}\,) = \underline{\underline{J}}^*(\underline{y}).(-\Delta\underline{y})$

where $$(\underline{\underline{J}}^*)_{ij} = \frac{\partial f_i(\underline{p})}{\partial \ln p_j}$$

$$= \frac{\partial f_i(\underline{p})}{\partial p_j}\ p_j$$

$$= (\underline{\underline{J}})_{ij}\ p_j$$

Note that $\underline{f}\,(\underline{p})$ remains unchanged, and does not need to be written as $f^*(\underline{y})$. Use is made of the fact that $\frac{\partial}{\partial \ln p} = p.\frac{\partial}{\partial p}$

Thus the modified algorithm is to calculate $\underline{f}\,(\underline{p})$ and $\underline{\underline{J}}$. Then for each j, multiply the j-th column of the matrix $\underline{\underline{J}}$ by p_j to obtain $\underline{\underline{J}}^*$. This matrix equation is solved to give $\Delta\ln p_i = \Delta p_i/p_i$ and hence gives $(p_i)_{S+1} = (p_i)_S(1-(\Delta\ln p_i)_S)$ for the (S+1)-th iteration.

This was found to give only a slight improvement to the convergence of the system, and was not pursued. Instead the method described in the next section was employed.

4.6 Vogelpohl Type Substitution.

VOGELPOHL (1937) was aware that due to the h^3 term in the Reynolds Equation the pressure was high where the film thickness was low, and vice versa, so if $s=ph^n$ was substituted into the equation, a more linear distribution would result. He assumed $n=\frac{3}{2}$ in order to eliminate the first derivative in the particular case he was considering. However, there was no great advantage in doing so in the fully varying case, and n=2 was chosen. Also the effect of the viscosity-pressure was to cause greater pressure near the centre than in an isoviscous case making this substitution give

$$\frac{d^2S}{dr^2} + \left(\frac{1}{r} + \frac{1}{Y^*}\frac{dY^*}{dr} - Z\right)\frac{dS}{dr} - \left(\left(\frac{1}{r} + \frac{1}{Y^*}\frac{dY^*}{dr}\right)Z + \frac{dZ}{dr}\right)S = \frac{12\frac{d}{dt}(\rho h)}{Y^*} \qquad (4.31)$$

and by L'Hopital's Rule

$$2\frac{d^2S}{dr^2} - 2\frac{dZ}{dr}S = 12\frac{d}{dt}(\rho h)/Y^* \text{ , at } r=0 \qquad (4.32)$$

where $Y^* = \frac{\rho h^3}{\eta h_0^2}$, $Z = \frac{2}{h_0}\frac{dh_0}{dr}$ with $S=ph_0^2$

$$h_0 = \max(10^{-7}, h_c) + r^2/2R$$

If the body is rigid then $h=h_0$ and so $Y^*=\frac{\rho h}{\eta}$

The substitution $S=ph_0^2$ was used rather than $S=ph^2$, for the elastic case. As h is a function of all the pressures, given a set $\underline{S}$, then the relation between $\underline{S}$ and $\underline{p}$ would be $S_i=p_i(h_i+\underline{F}\underline{p})_i^2$, giving a further non-linear set of equations to be solved for $\underline{p}$ after $\underline{S}$ has been obtained. h_c becomes negative in the elastic case at low film thickness and because the property that h_c is small at the centre and increases like the undeformed film shape outwards is needed, h_c is chosen to have some fixed minimum value, here 10^{-7}.

Note that this process gives a different differential equation and as such is not a solution method but allows us to solve for a more linear function. Most methods that are applicable to solve the Reynolds Equation may be used for this Vogelpohl-Reynolds Equation.

Note that

$$\frac{1}{Y^*}\frac{dY^*}{dr} = \left(\frac{1}{\rho}\frac{d\rho}{dp} - \frac{1}{\eta}\frac{d\eta}{dp}\right)\frac{dp}{dr} + \frac{3}{h}\frac{dh}{dr} - \frac{2}{h_0}\frac{dh_0}{dr}$$

$$= \frac{1}{Y}\frac{dY}{dr} - Z$$

The main attribute of this method is to reduce the difficulty involved due to the centre pressure peak being so high, and it was found by experience to be a very good method. Comparing errors obtained by a method solving for Reynolds Eqaution and those obtained by solving the Vogelpohl-Reynolds equation showed that greatly reduced errors were obtained in about the same time. Thus it was decided that the modified equation was the one to be solved.

The integral solution method cannot be directly used to solve the Vogelpohl-Reynolds equation.

4.7 A Combination Method.

4.7.1 Introduction

The Newton-Raphson method requires the solution of a complete matrix of size (n)*(n) with spline methods or (n-1)*(n-1) with ordinary difference formulae. As the work involved is proportional to n^3, it is worthwhile to look for methods which reduce the size of the system to be solved.

One way to do this is to use two different methods, and join the two together under suitable conditions.

4.7.2 The Method.

In order to solve for the Reynolds Equation using the direct integral method (see section 4.3), the boundary conditions used were:

1) $\frac{dp}{dr} = 0$ at $r=0$

2) $p = 0$ at $r=r_s$

These may be rewritten as

1) $\frac{dp}{dr} = C_N$ at $r=r_a$ (for some $r_a \mid 0 \leq r_a \leq r_s$)

2) $p=0$ at $r=r_s$

and gives $p(r_a) = p_0$

In the normal case, $r_a=0$, so that $C_N = 0$ and $p_0 = p(0)$

Again, in the normal case, $r_a = r_s$, giving $p_N=0$ with $C_N = \frac{dp}{dr}(r_s)$.

The equations were rewritten in the different forms to show that methods already developed may be used with only minimal change to solve with each of the separate domains.

The combination method described here works on the principle that the domain $[0,r_s]$ may be divided into two zones - an inner zone $[0,r_a]$ in which the pressure is high and large relative changes in film thicknesses and viscosity are occurring, thus needing a Newton method (with or without Vogelpohl substitution) and an outer zone $[r_a,r_s]$ in which the pressure is low, the film thickness is large and the effect of the elasticity is small, and thus is amenable to the Direct Integration method.

The algorithm is to use the Newton method with $p(r_a) = p_N$ and obtain $\frac{dp}{dr}(r_a) = C_N$. This value of C_N is used as a boundary condition in the Direct Integration method and a new pressure p_D is generated.

If $p_N=p_D$ (to within an error tolerance), then the solution has been obtained.

With $[0,r_a]$, the pressure field satisfies the Reynolds Equation by Newtons method. It is also satisfied over $[r_a,r_s]$ by the Direct Method. At r_a the pressures match from both methods, the first derivative matches, for C_N, obtained from Newtons method, is used as a boundary condition for the Direct method - and as Reynolds Equation is satisfied on both sides of r_a, the second derivative matches. Hence, all parameters that can be defined using these models have been matched at the junction, so the entire pressure field is the solution required, satisfying (4.7.1) over the whole range.

In general, $p_N \neq p_D$, in this case the solution has not been found, and iterative process needs to be used. The simplest method would be to set $p_D = p_N$ and iterate again. A slight modification to this was made in that instead of just $p(r_a)$ being changed, all pressure values within the inner zone were altered by an amount $\Delta p = p_N - p_D$. As Reynolds Equation is basically an equation relating gradients, if all pressure values were changed, the gradients remain unaltered. This modification guarantees that the complete curve would be continuous.

The advantage of this method is that in the outer zones it uses a computationally cheap method, and an expensive method only in the inner region where it is necessary.

4.7.3 Discussion.

This method was initially thought to be promising as it was far quicker than using Newtons Method over the whole range and it was able to solve for higher pressures than the Direct Method alone. However, at yet still higher pressures, one that are low in EHL terms, the method did not converge. The exact reason for this is difficult to ascertain. It could have been the relative mesh spacing, the position of r_a, or the fact that for large derivatives the method could require under-relaxation, or perhaps some other reasons.

This method was, however, rejected in favour of the next method to be described because, although the pressure is small in the outer regions, it has a disproportionate effect on the load. The load has to be accurate in order to integrate with respect to time in any reasonable computational time (see section 4.2). It has been noted in 4.5.4 that the order of the cubic spline method for Reynolds Equation is $O(\Delta r^2)$. By using the linear spacing it is possible to solve Reynolds

Equation to $O(\Delta r^4)$, however, in the outer zone, the direct method is only accurate to $O(\Delta r^3)$.

It was decided to look for a higher order method that would be more accurate in the outer zones, rather than to track down the reason for the divergence.

4.8 The Quintic Spline Formulation.

Just as a higher order method was obtained by changing interpolating functions from $C_{2j}(r)$ to $C_{3j}(r)$, then this can be further extended by changing the form of the functions from $C_{3j}(r)$ to $C_{5j}(r)$.

Remember that for the cubic spline, in order to evaluate uniquely all the available coefficients, the curve is required to be piecewise cubic with continuity of value first and second derivatives over the knots as well as needing two end conditions. For the quintic spline however, it is required that the function and the first four derivatives be continuous over the domain together with two end conditions being required at each end.

The quartic spline was not considered as it does not always exist for an arbitary spacing (see ALHBERG, NILSON and WALSH, 1967).

What two end conditions may be given?

One may be that the end slope is a given value, as is used for the cubic spline. For the other, ALHBERG, NILSON and WALSH, give a condition that requires the second derivative to be given. This cannot be directly used in this problem, for the Reynolds Equation is used to give a value

for the pressure at r=0 and the derivative at $r=r_s$. That is, there is a (1-1) correspondence between the number of unknown pressure values and points at which the pressure is to be satisfied. To use the second derivative condition means that one equation (Reynolds equation at r=0) has two unknowns at that point; the pressure value and the second derivative.

A solution to this problem would be to require that Reynolds Equation be satisfied at some extra point, say the first mid-point; and that the pressure at that point is not independent but lies on the interpolated pressure curve. This gives an extra equation, but not an extra unknown.

The one used here, however, is that

$$\Delta^3 g_0^{(iv)} = \Delta^3 g_n^{(iv)} = 0 \qquad (4.33)$$

i.e. the third divided difference of the fourth derivative of the interpolating spline function was zero at each end. This is the highest order end condition consistent with using quintic splines. Further, using this allows the function x^5 to be accurately interpolated. The method of calculating $C_{5j}(r)$ is to be found in Appendix I.

Writing as before

$$C_{5n}(r) \equiv D_{5n}(r) \ , \ (\underline{p})_n = \left(\frac{dp}{dr}\right)_{r_s} .\Delta r$$

gives

$$p(r) = \sum_{j=1}^{n} C_{5j}(r)\ p_j$$

and similarly as above

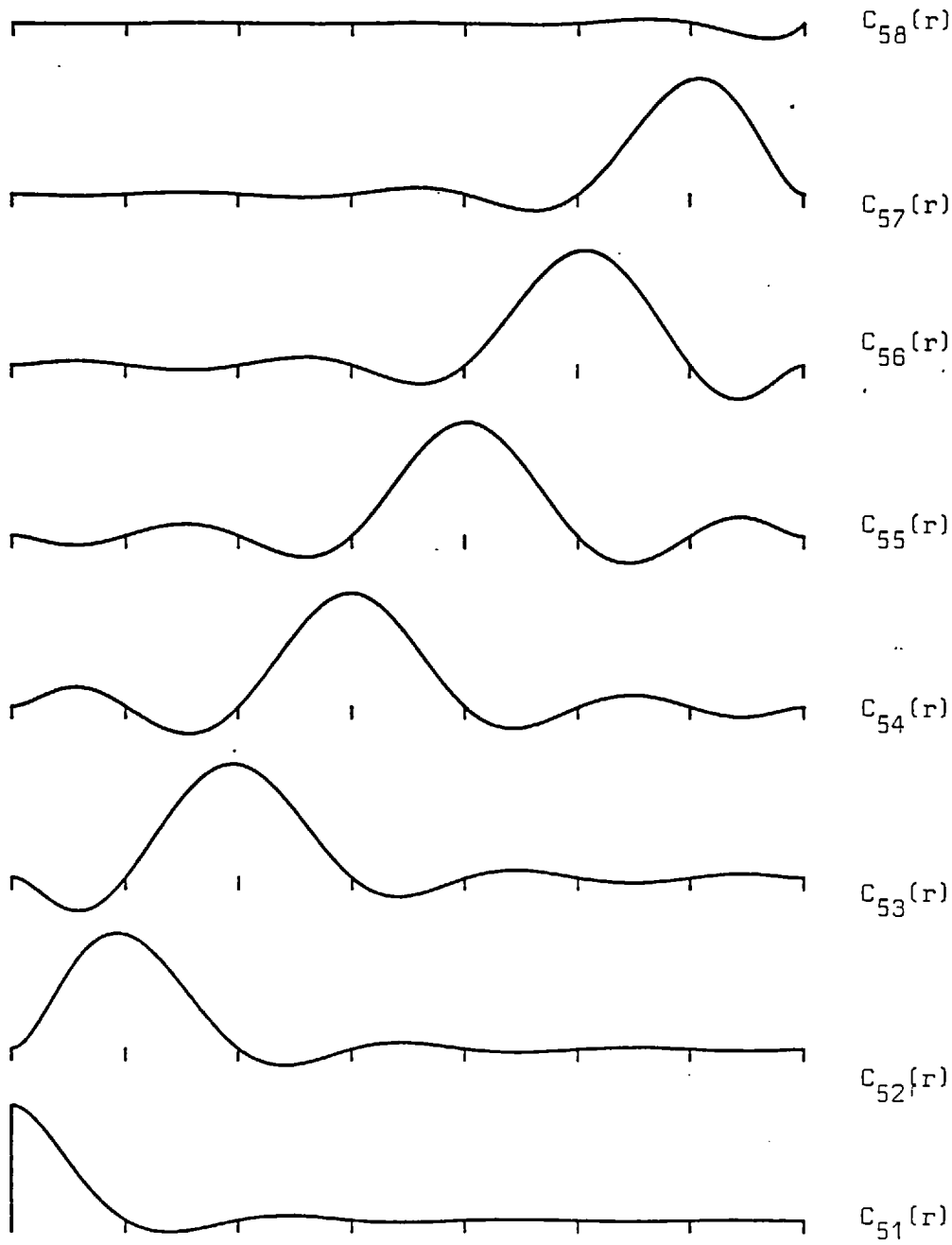

Figure 4.5. Cardinal Interpolating Polynomial of Degree 5.

$$\frac{d\underline{p}}{dr} = \underline{\underline{D}}_1 \underline{p} \frac{1}{\Delta r} + O(\Delta r^{k_1})$$

$$\frac{d^2\underline{p}}{dr^2} = \underline{\underline{D}}_2 \underline{p} \frac{1}{\Delta r^2} + O(\Delta r^{k_2})$$

Here $k_1=6$ and $k_2=4$ and gives a high order system which will help to accurately calculate the load, especially the part obtained in the outer regions. This is very important in the later stages when $2\pi\int_0^{r_s} prdr \rightarrow W$ and the difference between these is required, thus noise in the system becomes increasingly important.

The only difference between the solution method using the cubic spline and that of the quintic spline are small changes in the $\underline{\underline{D}}_1$ and $\underline{\underline{D}}_2$ matrices reflecting the different set-up. A larger curvature in the quintic spline may be observed from Figure 4.5, otherwise the same solution method may be used for the two methods.

Using the standard benchmark test of comparing the solution obtained for a rigid parabola-exponential viscosity oil system by these methods with that obtained by the analytical solution using a fixed time step integrator it was found that the errors obtained for a given mesh were an order of magnitude lower using the quintic spline over that of the cubic spline.

Other conclusions could also be drawn, as during these tests different grid spacings were used in addition to changing the number of grid points. In order to calculate the elastic distortion accurately, it is necessary to solve the system of equations with many points in the middle and more widely spaced towards the outer zones of the contact. However, it was found that when using a non-linear grid spacing, increasing the number of points could increase the errors. Increasing the number of

points should give smaller errors, and this so when using a linearly spaced grid, consequently an explanation was needed.

The answer lay in the effective spacing, i.e. the average length between nodes. If the solution is actually smooth and of the form assumed, then putting in an extra grid point had little effect, so when a non-linear grid was used, putting an an extra grid point in the outer region squeezed several of the central points so close together that no extra information was gained from using them. The solution behaves as if there were less points.

Thus, the choice of grid spacing must be made with great care.

Again, the advantage of using a relatively fixed grid spacing (see section 4.1.3) hold, so the extra overhead of using the quintic spline formulation over the cubic spline is only the extra work involved in finding the load.

Now the number of points may be reduced to reduce the order of the matrix, but to maintain approximately the same truncation error, i.e. 31 grid points down to 26, making the ratio of n^3 to be 1.7:1, so the reduced matrix takes about 60% of the time to solve the larger one. This method, (together with the Vogelpohl substitution) is the one used to obtain the results of Chapter 6. Alternatively if the number of points is kept large the solution may be able to sustain larger time step intervals.

CHAPTER FIVE

THE ELASTIC DEFORMATION

5.1 Introduction

In this chapter an expression will be obtained for the vertical deformation at any point due to an arbitary axisymmetric pressure distribution extending over the contact, (Formulation I). Using this expression a similar formulation for the spatial derivative of the deformation will be calculated. A simple correlation is found in which the derivative is calculated by finding the deformation due to a transformed pressure distribution.

Next the actual pressure distribution that is interpolated from the set of pressure values at the grid points is discussed and then for given pressure distributions of appropriate type the deformations and their derivatives may be calculated exactly (to machine roundoff). These values will be obtained in a different manner (Formulation II) from the initial formulation as it is easier to calculate analytical solutions for the particular pressure functions considered. The relation correlating the derivative with the deformation is used to obtain the spatial derivative. Hence, for a specific grid, the relevant compliance matrices may be obtained.

Finally, the horizontal deformations are similarly calculated and the values of the matrix obtained are seen to be small compared to those of the normal deformation matrix, especially at the centre where the effects of horizontal displacements on the pressure field would be greatest.

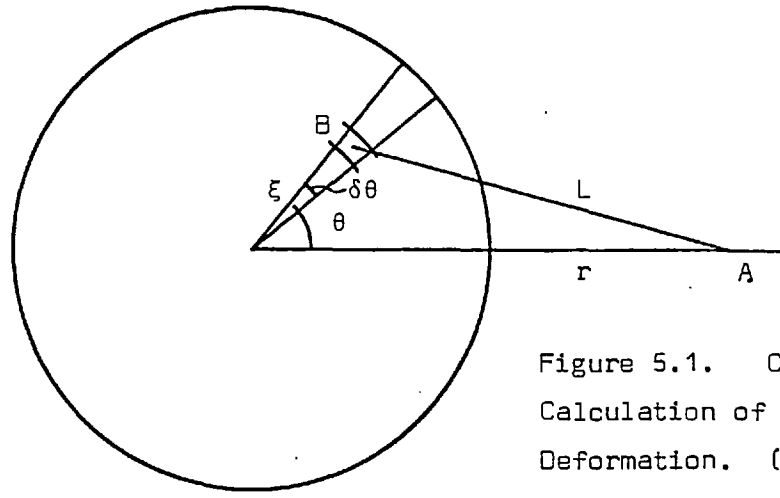

Figure 5.1. Co-ordinates for the Calculation of the Vertical Deformation. (Formulation I).

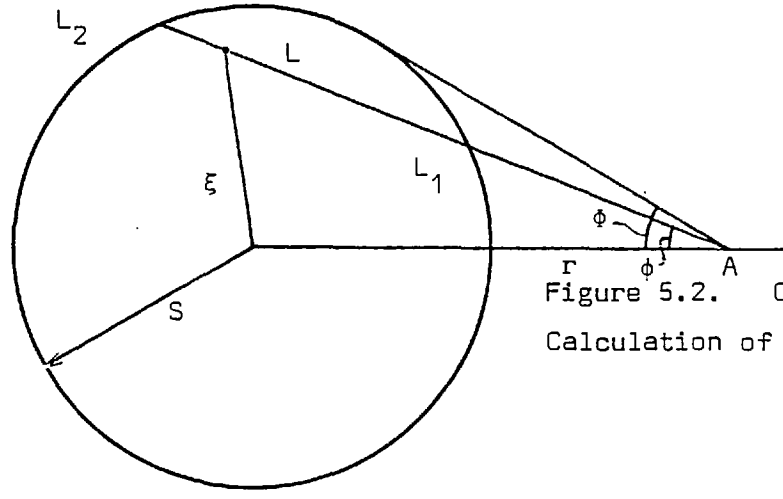

Figure 5.2. Co-ordinates for the Calculation of J^m_{ik}

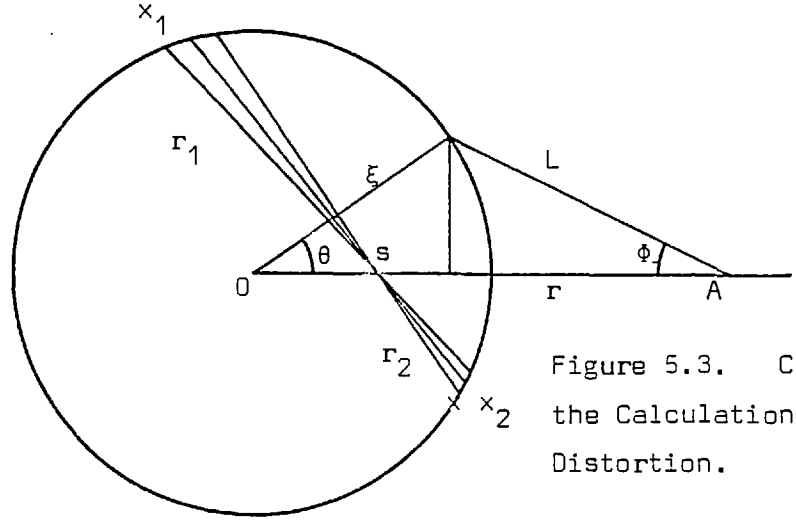

Figure 5.3. Co-ordinates for the Calculation of the Horizontal Distortion.

5.2 The Elastic Deformation (Formulation I)

The deformation produced at any point by the pressure distribution extending over the contact is to be calculated.

Following CHRISTENSEN (1967,1970), the problem consists of finding the deformation at point A on the surface of a semi-infinite solid by a concentrated load $p\xi d\xi d\theta$ applied at an element B (see Figure 5.1). The theory of elasticity (TIMONSHENKO and GOODIER, 1970) predicts that the local vertical deformation is

$$\delta w = \frac{1}{\pi E'} \frac{p\xi d\xi}{L} d\theta \qquad (5.1)$$

From the cosine rule

$$L = (r^2+\xi^2-2r\xi\cos\theta)^{\frac{1}{2}}$$

Now if this is substituted in the above equation and then integrated with the appropriate boundary conditions, (θ runs from 0 to 2π and the pressure is non-zero only on $[0,r_s]$. At any given time r_s is fixed).

$$w(r) = \frac{1}{\pi E'} \int_0^{r_s} p(\xi) \int_0^{2\pi} \frac{\xi d\theta}{\sqrt{r^2+\xi^2-2r\xi\cos\theta}} d\xi \qquad (5.2)$$

Consider first the inner integral, then

$$\int_0^{2\pi} \frac{\xi d\theta}{\sqrt{r^2+\xi^2-2r\xi\cos\theta}} = \frac{4\xi}{r+\xi} \int_0^{\frac{\pi}{2}} \frac{d\theta}{\sqrt{1-\frac{4r\xi}{(r+\xi)^2}\sin^2\theta}}$$

$$= \frac{4\xi}{r+\xi} K\left[\left(\frac{4r\xi}{(r+\xi)^2}\right)^{\frac{1}{2}}\right]$$

where $K(k)$ is the complete elliptic integral of the first kind.

Hence,

$$w(r) = \frac{1}{\pi E'} \int_0^{r_s} p(\xi) \frac{4\xi}{r+\xi} K\left[\frac{2\sqrt{r\xi}}{r+\xi}\right] d\xi$$

$$= \frac{1}{\pi E'} \int_0^{r_s} p(\xi) . F(r,\xi) d\xi \qquad (5.3)$$

where $F(r,\xi) = \frac{4\xi}{r+\xi} K\left[\frac{2\sqrt{r\xi}}{r+\xi}\right]$

Note that this expression is different to that obtained by CHRISTENSEN, 1967,1970, who using another integral transform, obtained

$$\int_0^{2\pi} \frac{\xi d\theta}{\sqrt{r^2+\xi^2-2r\xi\cos\theta}} = 4K\left(\frac{r}{\xi}\right)$$

5.3 The Derivative of the Elastic Deformation.

5.3.1 Transformation

Given the expression above for $w(r)$, $\frac{dw}{dr}(r)$ may now be calculated: this is needed for the solution of Reynolds Equation.

$$\frac{dw(r)}{dr} = \frac{d}{dr}\left(\frac{1}{\pi E'} \int_0^{r_s} p(\xi) F(r,\xi) d\xi\right) \qquad (5.4)$$

Differentiating under the integral sign, noting that the limits are not functions of r.

$$\pi E' \frac{dw}{dr}(r) = \int_0^{r_s} p(\xi) \frac{-4\xi}{(r+\xi)^2} K\left[\frac{2\sqrt{r\xi}}{r+\xi}\right] + p(\xi) \frac{4\xi}{r+\xi} \frac{d}{dr}\left(K\left[\frac{2\sqrt{r\xi}}{r+\xi}\right]\right) d\xi \qquad (5.5)$$

Now if $r \neq 0$

$$\frac{d}{dr} K\left[\frac{2\sqrt{r\xi}}{r+\xi}\right] = \frac{dK}{dk} \cdot \frac{dk}{dr}, \qquad \text{if } k = \frac{2\sqrt{r\xi}}{r+\xi}$$

$$= \frac{dK}{dk} \cdot \frac{\xi - r}{(r+\xi)^2} \sqrt{\frac{\xi}{r}}$$

And if $\xi \neq 0$

$$\frac{d}{d\xi} K\left[\frac{2\sqrt{r\xi}}{r+\xi}\right] = \frac{dK}{dk} \cdot \frac{dk}{d\xi}$$

$$= \frac{dK}{dk} \cdot \frac{r-\xi}{(r+\xi)^2} \sqrt{\frac{r}{\xi}}$$

Hence

$$\frac{dK}{dr} = -\frac{\xi}{r} \frac{dK}{d\xi} \qquad (5.6)$$

Substituting this result in the equation 5.5

$$\pi E' \frac{dw}{dr}(r) = \int_0^{r_s} p(\xi) \frac{-4\xi}{(r+\xi)^2} K\left[\frac{2\sqrt{r\xi}}{r+\xi}\right] d\xi + \int_0^{r_s} p(\xi) \frac{4\xi}{r+\xi} \cdot \frac{-\xi}{r} \frac{d}{d\xi} K\left[\frac{2\sqrt{r\xi}}{r+\xi}\right] d\xi$$

Integrating this second integral by parts.

$$\pi E' \frac{dw}{dr}(r) = \int_0^{r_s} p(\xi) \frac{-1}{r+\xi} F(r,\xi) d\xi - \left(p(\xi) \frac{4\xi^2}{(r+\xi)r} K\left[\frac{2\sqrt{r\xi}}{r+\xi}\right] \right)_0^{r_s}$$

$$+ \int_0^{r_s} \left(\frac{dp}{d\xi}(\xi) \frac{4\xi^2}{(r+\xi)r} + p(\xi) \frac{8\xi}{(r+\xi)r} - p(\xi) \frac{4\xi^2}{(r+\xi)^2 r} \right) K\left[\frac{2\sqrt{r\xi}}{r+\xi}\right] d\xi$$

$$= -\left(p(\xi) \frac{4\xi^2}{(r+\xi)r} K\left[\frac{2\sqrt{r\xi}}{r+\xi}\right] \right)_0^{r_s} + \int_0^{r_s} \frac{dp}{d\xi}(\xi) \frac{\xi}{r} F(r,\xi) + p(\xi) \left[\frac{-1}{r+\xi} + \frac{2}{r} \frac{-\xi}{r(r+\xi)}\right] F(r,\xi) d\xi$$

$$= -\frac{1}{r}\left(p(\xi)\, \xi F(r,\xi) \right)_0^{r_s} + \frac{1}{r} \int_0^{r_s} \left(p(\xi) + \frac{dp}{d\xi}(\xi).\xi \right) F(r,\xi)\, d\xi$$

However, at $\xi = 0$, $\xi F(r,\xi) = 0$, and at $\xi = r_s$, $p(\xi) = 0$, so that

$$[p(\xi)\xi F(r,\xi)]_0^{r_s} = 0$$

Hence

$$\pi E' \frac{dw}{dr}(r) = \frac{1}{r}\int_0^{r_s}\left(p(\xi) + \frac{dp}{d\xi}(\xi)\xi\right)F(r,\xi)d\xi \quad , \quad r\neq 0$$
$$= 0 \quad , \quad r=0 \qquad (5.7)$$

To obtain this relation, it is necessary that $p(\xi)$ is continuous. If it is not, several partial integrations are performed, and terms of the form $[p(\xi)\xi F(r,\xi)]_{r_x}$ are found. Only continuous pressure functions are used in this work.

5.3.2 The Derivative as a Transform of the Deformation.

It may be seen by inspection that the formula for $\frac{dw}{dr}(r)$ requires the calculation of an integral term of the same form as in the formula for $w(r)$, (equation 5.3). Let the pressure distribution $p(\xi)$ be given. It gives rise to a deformation distribution $w_p(r)$, and $\frac{dw_p(r)}{dr}$ is to be calculated. Then, all that is necessary is to construct the function $q(\xi)=p(\xi)+\xi\frac{dp}{d\xi}(\xi)$ and, using equation 5.3, calculate $w_q(r)$. This function is the deformation produced by the pressure function $q(\xi)$.

Then substituting for the integral in equation 5.7

$$\frac{dw_p(r)}{dr} = \frac{1}{r}w_q(r) \quad , \quad r\neq 0$$
$$= 0 \quad , \quad r=0 \qquad (5.8)$$

If $p(\xi)$ is a continuous piecewise polynomial of degree L, then $q(\xi)$ is a piecewise polynomial of degree L. Thus, if a method is found that can find the deformation for an arbitary piecewise polynomial of degree L

then the spatial derivative may be immediately found.

If $p(\xi)$ is not only continuous but also has continuity in its first derivative (such as a cubic spline), then $q(\xi)$ is continuous and consequently if $q^*(\xi)=q(\xi)+\xi\frac{dq}{d\xi}(\xi)$ with a corresponding deformation $w_q^*(r)$ then

$$\frac{d^2w_p(r)}{dr^2} = \frac{d}{dr}\left(\frac{1}{r}w_q(r)\right)$$

$$= \frac{1}{r}\frac{dw_q(r)}{dr} - \frac{1}{r^2}w_q(r)$$

Hence

$$\frac{d^2w_p(r)}{dr^2} = \frac{1}{r^2}(w_q^*(r)-w_q(r)) \qquad (5.9)$$

This may be extended so that if $p(\xi)$ has continuity in the m th derivative, then the (m+1)st derivative of the deformation is given by repeated application of equation 5.8, using appropriate forms of $p(\xi)$ and $q(\xi)$.

5.3.3 A Check on the Transformation.

The transformation may be seen to be correct by considering the pressure obtained between two spherical bodies (the Hertzian problem) and also the problem of a rigid, flat die being normally squeezed on to the surface.

The solution for the Hertz problem is given by:
(see TIMONSHENKO and GOODIER)

$$w_p(r) = \frac{1}{E'} \frac{\pi a}{2} p_0 - \frac{r^2}{2R} \qquad , r \leq a$$

$$p(r) = p_0 \frac{\sqrt{(a^2-r^2)}}{a}$$

where

$$a = \frac{1}{E'} \frac{\pi R}{2} p_0$$

Now

$$\frac{dw_p}{dr} = - \frac{r}{R}$$

And

$$p(r) + \frac{dp}{dr}(r).r = 2p(r) - p_0 \frac{a}{\sqrt{a^2-r^2}}$$

If $q^*(r) = p_0 \frac{a}{\sqrt{a^2-r^2}}$ and has associated deformation $w_q^*(r)$ then as

$q(r)=p(r) + \frac{dp}{dr}(r).r$ (Definition of q(r) from equation 5.8).

$= 2p(r) - q^*(r)$ (Differentiating p(r) and definition for $q^*(r)$)

then considering deformations

$$w_q(r)=2w_p(r) - w_q^*(r)$$

But from equation 5.8

$$w_q(r) = r \frac{dw_p(r)}{dr}$$

$$= \frac{r^2}{R}$$

So $w_q^*(r) = 2w_p(r) + \frac{r^2}{R}$

$$= \frac{1}{E'} \pi a p_0$$

This is a constant and the pressure $q^*(r)$ and its associated deformation $w_q^*(r)$ gives the solution for a rigid flat die impressed onto an elastic

half-space.

5.4 The Calculation of The Deformation Matrices. (Formulation II)

5.4.1 The Interpolating Function and the Deformation Matrix.

In section 4.5.4 it was determined that

$$g_l(r) = \sum_{j=1}^{n} C_{lj}(r)p_j$$

where $g_l(r)$ is the interpolated function through the grid points.

So if the actual pressure distribution is approximated by the interpolated one, then

$$\pi E' w(r) = \int_0^{r_s} g_l(\xi)F(r,\xi)d\xi$$

$$= \int_0^{r_s} \sum_{j=1}^{n} C_{lj}(\xi).p_j F(r,\xi)d\xi$$

$$= \sum_{j=1}^{n} \left[\int_0^{r_s} C_{lj}(\xi)F(r,\xi)d\xi\right]. p_j \qquad (5.10)$$

Thus,

$$\pi E'\underline{w}(r) = (\underline{\underline{F}}^l.\underline{p})\Delta r$$

where

$$(\underline{\underline{F}}^l)_{ij}\ \Delta r = \int_0^{r_s} C_{lj}(\xi)F(r_i,\xi)d\xi \qquad (5.11)$$

5.4.2 The Invariance of the F Matrix for a Relatively Fixed Grid.

It has been shown in Chapter Four that in solving the Reynolds Equation a grid has been used in which $r_i(t)=R_i.\Delta r(t)$, that is, the whole grid expands to cover the area of impact. This means that

$$R_j.r_i(t) = R_i.r_j(t) \qquad , \forall \ i,j$$

Now consider

$$\pi E' w(r_i) = \sum_{j=1}^{n} \int_0^{r_s} C_{1j}(\xi) F(r_i,\xi) d\xi$$

and consider the effect of putting $r=\Delta r.R, \xi=\Delta r \Xi$ (i.e. expanding the grid by a constant factor), then, by inspection

$$F(R_i,\Xi) = F(r_i,\xi)$$

and as from Chapter Four

$$\int_0^{r_s} C_{1j}(\xi) d\xi = \int_0^{R_n} C_{1_j}(\Xi) d\Xi . \Delta r$$

(where $C_{1j}(\xi)$ is mapped onto $\underline{r}$ and $C_{1j}(\Xi)$ is onto $\underline{R}$) then if

$$w^*(r_i) = \frac{1}{\pi E'} \int_0^{R_n} C_{1j}(\Xi) F(R_i,\Xi) d\Xi$$

then

$$w(r_i) = w^*(R_i).\Delta r \qquad (5.12)$$

Thus it may be seen that if a relatively fixed grid $\underline{R}$ is used to calculate for the elements of $\underline{\underline{F}}$, then $\underline{\underline{F}}$ is invariant with time and these elements can be calculated once only, finally giving equation 5.10 for the actual deformation with real spacing Δr.

5.4.3 The $\underline{\underline{F}}$ Matrix

The problem is to calculate the $\underline{\underline{F}}^1$ matrix. The interpolating

functions $g_l(r)$ have been chosen to be piecewise polynomials and are continuous if $l \geq 1$. If $l \geq 1$ then the $g_l(r)$ will satisfy the condition of continuity necessary to obtain equation 5.8.

The elements $(\underline{\underline{F}}^l)_{ij}$ of $\underline{\underline{F}}$ are then calculated. As $C_{lj}(r)$ is a piecewise polynomial of degree l, it has an equation of the form

$$C_{lj}(r) = \sum_{m=0}^{l} a_{ljkm}(r-R_k)^m \qquad , r\varepsilon[R_k, R_{k+1}]$$

which may be written as

$$C_{lj}(r) = \sum_{m=0}^{l} A_{ljkm} r^m \qquad , r\varepsilon[R_k, R_{k+1}] \qquad (5.13)$$

by expansion and collection of the terms.

Using the rule of linear superposition

$$\begin{aligned}(\underline{\underline{F}}^l)_{ij} &= \int_0^{R_n} C_{lj}(\Xi)F(R_i,\Xi)d\Xi \\ &= \sum_{k=1}^{n-1} \int_{R_k}^{R_{k+1}} \sum_{m=0}^{l} A_{ljkm}\Xi^m F(R_i,\Xi)d\Xi \\ &= \sum_{k=1}^{n-1} \sum_{m=0}^{l} A_{ljkm} \int_{R_k}^{R_{k+1}} \Xi^m F(R_i,\Xi)d\Xi \\ &= \sum_{k=1}^{n-1} \sum_{m=0}^{l} A_{ljkm}\, \bar{I}_{ik}^m\end{aligned}$$

Thus the problem reduces to that of finding I_{ik}^m where

$$I_{ik}^m = \int_{R_k}^{R_{k+1}} \Xi^m F(R_i,\Xi)d\Xi \qquad (5.14)$$

But if

$$J^m_{ik} = \int_0^{R_k} \Xi^m . F(R_i, \Xi) d\Xi$$

then

$$I^m_{ik} = J^m_{ik+1} - J^m_{ik} \qquad (5.15)$$

Now J^m_{ik} is the deformation (multiplied by $\pi E'$) at R_i due to a disk of pressure with distribution $p(r)=r^m$, extending to R_k. The method used to calculate these will be found in 5.4.5.

The algorithm used to calculate $(\underline{\underline{F}}^l)_{ij}$ is:-

Choose a grid $\underline{R}$ and an order of interpolation l

For each value of i, $1 \leq i \leq n$

Set R_i

For each value of k, $1 \leq k < n$

Set R_k

For each value of m, $0 \leq m \leq l$

Find I^m_{ik}

End loop m

End loop k

For each value of j, $1 \leq j \leq n$

Set $(\underline{\underline{F}}^l)_{ij}=0$

Find $C_{lj}(r)$

For each k, $1 \leq k < n$

For each m, $0 \leq m \leq l$

Find a_{ljkm} from $C_{lj}(r)$

Hence A_{ljkm}, by expansion

Set $(\underline{\underline{F}}^l)_{ij} = (\underline{\underline{F}}^l)_{ij} + A_{ljkm} . I^m_{ik}$

End loop m

End loop k

End loop j

End loop i

Indentation has been used to show the loop structure of the algorithm. The final summation is at the fourth level of nesting.

5.4.4 The G Matrix

To calculate the $\underline{G}$ matrix, use if made of equation 5.8

As

$$(\underline{F})_{ij} = \int_0^{R_s} C_{lj}(\Xi)F(R_i,\Xi)d\Xi$$

and

$$\frac{dw_p(r)}{dr} = \frac{1}{r} w_q(r)$$

$$(\underline{G}^1)_{ij} = \frac{1}{R_i} \int_0^{R_s} \left\{ C_{lj}(\Xi) + \Xi \frac{d}{d\Xi} C_{lj}(\Xi) \right\} .F(R_i,\Xi)d\Xi$$

But

$$C_{lj}(\Xi) = \sum_{m=0}^{l} A_{ljkm} \Xi^m$$

So

$$C_{ij}(\Xi) + \Xi \frac{d}{d\Xi} C_{ij}(\Xi) = \sum_{m=0}^{l} (m+1)A_{ljkm} \Xi^m$$

Hence

$$(\underline{G})_{ij} = \frac{1}{R_i} \sum_{k=1}^{n-1} \sum_{m=0}^{l} (m+1)A_{ljkm} \int_{R_k}^{R_{k+1}} \Xi^m F(R_i,\Xi)d\Xi$$

$$= \frac{1}{R_i} \sum_{k=1}^{n-1} \sum_{m=0}^{l} (m+1)A_{ljkm} I_{ik}^m \qquad (5.16)$$

Thus the $\underline{G}$ matrix elements may easily be obtained as a by-product of calculating the $\underline{F}$ matrix.

5.4.5 The Calculation of J_{ik}^{m}

J_{ik}^{m} is the deformation produced at r_i due to a pressure field of radial extent r_k and of form r^m. Figure 5.2 is used for the coordinates.

Taking the origin to be the point at which the deformation is required (point A), a distance r away from the centre. Let the disk be of radius s, and an arbitary point in the disc has coordinates (L,Φ) and pressure ξ^m. Equation 5.1 becomes, as the origin is point A

$$\delta w = \frac{1}{\pi E'} \frac{p(L)dLd\theta}{L} = \frac{1}{\pi E'} \xi^m dLd\theta$$

Thus, the deformation w is given by

$$\pi E'w = 2\int_0^{\Phi} \int_{L_1}^{L_2} \xi^m dLd\phi \qquad (5.17)$$

There are three cases to be considered for each value of m,

i) $r<s$. The point A is within the disc. Here $\Phi = \frac{\pi}{2}$.

ii) $r=s$. The point A is on the edge of the disc. Also $\Phi = \frac{\pi}{2}$.

iii) $r>s$. The point A is outside the disc. $\Phi = \sin^{-1}\frac{s}{r}$.

From the cosine rule

$$\xi = (L^2+r^2-2rL\cos\phi)^{\frac{1}{2}}$$

Hence

$$\pi E'w = 2\int_0^{\Phi} \int_{L_1}^{L_2} (L^2+r^2-2rL\cos\phi)^{m/2} dLd\phi$$

But the limits, L_1 and L_2, are given by

$$s = (L^2+r^2-2rL\cos\phi)^{\frac{1}{2}}$$

i.e. $L_1, L_2 = r\cos\phi \pm \sqrt{s^2 - r^2\sin^2\phi}$

Put $b = L - r\cos\phi$

$$\int_{L_1}^{L_2} (L^2 + r^2 - 2rL\cos\phi)^{m/2} dL = 2\int_0^{\sqrt{s^2 - r^2\sin\phi}} (b^2 + r^2\sin^2\phi)^{m/2} db$$

Hence

$$\pi E' w = 4\int_0^{\Phi}\int_0^{\sqrt{s^2 - r^2\sin^2\phi}} (b^2 + r^2\sin^2\phi)^{m/2}\, db\, d\phi \qquad (5.18)$$

These integrals are given in Appendix II.

5.5 The Horizontal Deflection

5.5.1 Derivation

Consider a point S inside an axisymmetric ring of pressure. Whereas the vertical deflection is positive for any positive pressure applied at a point on the plane, the horizontal deflection has an associated direction, that is, it will move towards the applied pressure element.

Again the Boussinesq solution (TIMONSHENKO and GOODIER, 1970) is used. This gives the deformation produced at a point L distant from an applied point load W is $\frac{-1}{2\pi E^*}\frac{W}{L}$

Consider a sector subtending small angle $\delta\phi$, it intersects the circle of radius ξ in two places. The pressure at X_1 tends to deflect the point S towards it by $\frac{-1}{2\pi E^* r_1} Pr_1\delta\phi dr_1$ and that at X_2 towards X_2 by $\frac{-1}{2\pi E^* r_2} Pr_2\delta\phi dr_2$. (See Figure 5.3).

In the limit as the width of the pressure ring tends to zero these

are equal and opposite in direction, thus they cancel each other out. This process may be applied to all such sectors, so as to cover the surface outside the point S.

Hence the horizontal deflection at a point wholly inside an axis-ymmetric pressure field is zero.

This result is analagous to that of the gravitation field inside a uniform spherical shell due to that shell.

For a point T outside the ring, the same process may be performed as for the vertical deformation, but remembering that as direction is involved the distortion may be resolved into two directions, one along the radial line OA and the other perpendicular to it. The deflection perpendicular must be zero as the line is a line of symmetry, so only radial deflection need be considered.

$$\delta u = \frac{-1}{2\pi E^*} \frac{p\xi d\xi d\theta}{L} \cos\phi$$

but $L^2 = r^2+\xi^2-2r\xi\cos\theta$, $L\cos\phi = r-\xi\cos\theta$

so

$$\delta u = \frac{-1}{2\pi E^*} \frac{p\xi d\xi d\theta}{r^2+\xi^2-2r\xi\cos\theta} (r-\xi\cos\theta)$$

thus

$$u(r) = \frac{-1}{2\pi E^*} \int_0^r 2 \int_0^\pi \frac{p(\xi)\xi d\theta}{r^2+\xi^2-2r\xi\cos\theta} (r-\xi\cos\theta) d\xi$$

The upper limit on ξ is r due to the result obtained above.

Now

$$\int_0^{\pi} 2\,\frac{r-\xi\cos\theta}{r^2+\xi^2-2r\xi\cos\theta}\,d\theta = \frac{1}{r}\{\pi + \int_0^{\pi} \frac{r^2-\xi^2}{r^2+\xi^2-2r\xi\cos\theta}\,d\theta\}$$

$$= \frac{1}{r}\{\pi + [2\tan^{-1}\frac{(r-\xi)\tan\frac{\theta}{2}}{(r-\xi)}]_0^{\pi}\} \quad = \frac{2\pi}{r}$$

from DWIGHT, 1961, thus

$$u(r) = \frac{-1}{\pi E^*}\int_0^r \frac{p(\xi).\xi\pi}{r}\,d\xi \qquad (5.19)$$

Putting $r=r_s$, it may be seen that if W is the instantaneous load

$$u(r_s) = -\frac{1}{\pi E^*}\,\frac{W}{2r_s}$$

5.5.2 An Order of Magnitude Analysis for the Horizontal Deflection.

Now

$$|u| = \frac{1}{\pi E^*}\int_0^r \frac{p(\xi)\xi\pi}{r}\,d\xi$$

$$= \frac{E'}{2E^*}\,\frac{1}{\pi E'}\int_0^r p(\xi)\,\frac{4\xi}{r}\cdot\frac{\pi}{2}\,d\xi$$

$$\leq \frac{E'}{2E^*}\cdot\frac{1}{\pi E'}\int_0^r p(\xi)\,\frac{4\xi}{r}\,K[\frac{2\sqrt{r\xi}}{r+\xi}]d\xi \qquad \text{(equality iff r=0)}$$

$$< \frac{E'}{E^*}\cdot\frac{1}{\pi E'}\int_0^r p(\xi)\,\frac{4\xi}{r+\xi}\,K[\frac{2\sqrt{r\xi}}{r+\xi}]\,d\xi$$

$$\leq \frac{E'}{E^*}\cdot\frac{1}{\pi E'}\int_0^{r_s} p(\xi)\,F(r,\xi)d\xi \qquad \text{(equality iff } r=r_s\text{)}$$

$$= \frac{E'}{E^*}\,w(r)$$

This shows that the magnitude of the horizontal deformation is less than that of the vertical deformation.

The horizontal distortion is zero at the centre and also at an infinite distance out. The maximum value occurs when $\frac{du(r)}{dr} = 0$, and let $r=r_x$ at the maximum value.

$$\text{i.e. } \frac{-1}{\pi E^*} \left\{ \frac{p(r_x) r_x \pi}{r_x} - \int_0^{r_x} \frac{p(\xi)\xi\pi d\xi}{r_x^2} \right\} = 0$$

$$- \frac{1}{\pi E^*} p(r_x).r_x\pi = - \frac{1}{\pi E^*} \int_0^{r_x} \frac{p(\xi)\xi\pi d\xi}{r_x}$$

or

$$u(r_x) = - \frac{1}{\pi E^*} p(r_x).r_x.\pi$$

Hence

$$|u(r)| \leq \frac{1}{\pi E^*} p(r_x).r_x.\pi$$

Given an arbitary pressure distribution, not much more may be interpreted from these formulae except by substituting various distributions.

The horizontal deflection was incorporated into the algorithm to find its effect on one run. It was found to have negligble effect.

5.5.3. The $\underline{\underline{U}}$ Matrix

Now from 5.4.1, if

$$p(r) = \sum_{j-1}^{n} C_{ij}(r) p_j$$

and it is desired to calculate $\underline{\underline{U}}$, where

$$-\pi E^* \underline{u}(r\ ) = \underline{\underline{U}} \cdot \underline{p} \cdot \Delta r$$

or

$$-\pi E^* u(r_i) = \sum_{j=1}^{n} u_{ij} \cdot P_j \qquad (p_n = p'_n \Delta r)$$

Hence by (5.19)

$$u_{ij} = \frac{1}{r_i} \int_0^{r_i} C_{1j}(\xi) \xi \pi \, d\xi$$

But, using the Cardinal Cubic Splines $C_{3j}(r)$

$$\int_0^{r_i} C_{3j}(\xi) \xi d\xi = 0, \qquad i=1$$

$$= \sum_{k=1}^{i-1} \int_0^{r_{k+1}} \xi \left[a_{jk} + b_{jk}(\xi - r_k) + C_{jk}(\xi - r_k)^2 + d_{jk}(\xi - r_k)^3\right] d\xi \quad , \quad i \neq 1$$

Performing the integration and eliminating c_{jk} and d_{jk} gives the following formula when $\Delta_k = R_{k+1} - R_k$,

$$u_{ij} = 0 \qquad , \quad i=1$$

$$= \frac{\pi}{60R_i} \sum_{k=1}^{i-1} \left(\begin{array}{l} a_{jk}(30R_k + 9\Delta_k) + b_{jk}\Delta_k(5R_k + 2\Delta_k) \\ + a_{jk+1}(30R_{k+1} - 9\Delta_k) - b_{jk+1}\Delta_k(5R_{k+1} - 2\Delta_k) \end{array} \right) \Delta_k \quad , \quad i>1$$

(5.20)

5.6. Effective Storage of the Compliance Matrices.

It may be seen that the compliance matrices are written so that

$$\pi E' \, \underline{w}(r) = (\underline{F}.\underline{p}) \, \Delta r$$

$$\pi E' \, \frac{d\underline{w}}{dr}(r) = \underline{G}.\,\underline{p}$$

$$-\pi E' \, \underline{u}(r) = (\underline{U}.\underline{p}).\,\Delta r$$

It has already been shown that if $r_i(t) = R_i.\Delta r(t)$, then the matrix

need be calculated once only, but further, by keeping the elastic constants E' and E* out of the expression for $\underline{\underline{F}}$, $\underline{\underline{G}}$ and $\underline{\underline{U}}$, then these matrices may be calculated in a separate program and read in during program initialisation. These internally stored values are then scaled by the appropriate elastic constant giving

$$\underline{w}(r) = (\underline{\underline{F}}'.\underline{p})\Delta r$$

$$\frac{d\underline{w}(r)}{dr} = \underline{\underline{G}}'.\underline{p}$$

$$\underline{u}(r) = (\underline{\underline{U}}'.\underline{p})\Delta r$$

if $\underline{\underline{F}}' = \frac{1}{\pi E'} \cdot \underline{\underline{F}}$

$$\underline{\underline{G}}' = \frac{1}{\pi E'} \cdot \underline{\underline{G}}$$

$$\underline{\underline{U}}' = -\frac{1}{\pi E^*} \cdot \underline{\underline{U}}$$

5.7 Visualisation of the Matrices

The procedure set out above for calculating the matrices may be extended to any order continuous piecewise polynomial interpolating function. For the calculations in this thesis cubic splines were used, giving truncation errors comparable with those of solving Reynolds Equation, rather than the quintic splines as it was felt that roundoff errors could distort the results, especially in the outer regions.

A linearly spaced grid of 61 points in $\underline{R}$ was defined such that $R_i = i-1$ and then using the methods described above the matrices were calculated

and are shown in Figures 5.1, 5.2 and 5.3, in the following manner.

The horizontal plane represents a pair of co-ordinates (i,j), $1 \leq i \leq 61$, $1 \leq j \leq 61$ and the vertical height represents the value of the matrix elements $(\underline{\underline{F}})_{ij}$, $(\underline{\underline{G}})_{ij}$ and $(\underline{\underline{U}})_{ij}$ respectively. The zero plane is marked explicity.

The matrices are each viewed from a height 20 above the zero plane and from two directions. These are given by:

direction 1

$$\begin{pmatrix} \underline{w} \end{pmatrix} = \begin{pmatrix} \underline{\underline{F}} \end{pmatrix} \begin{pmatrix} \underline{p} \end{pmatrix} \Delta r$$

direction 2

where $w_i = \sum_{i=1}^{n} F_{ij} p_j \Delta r$

The range in values of the matrices are:-

	Minimum	Maximum
$\underline{\underline{F}}$	-1.3053	15.756
$\underline{\underline{G}}$	-3.8837	3.621
$\underline{\underline{U}}$	-0.2608	3.298

Note that the last element in each row is the coefficient that multiplies $p_n' \Delta r$.

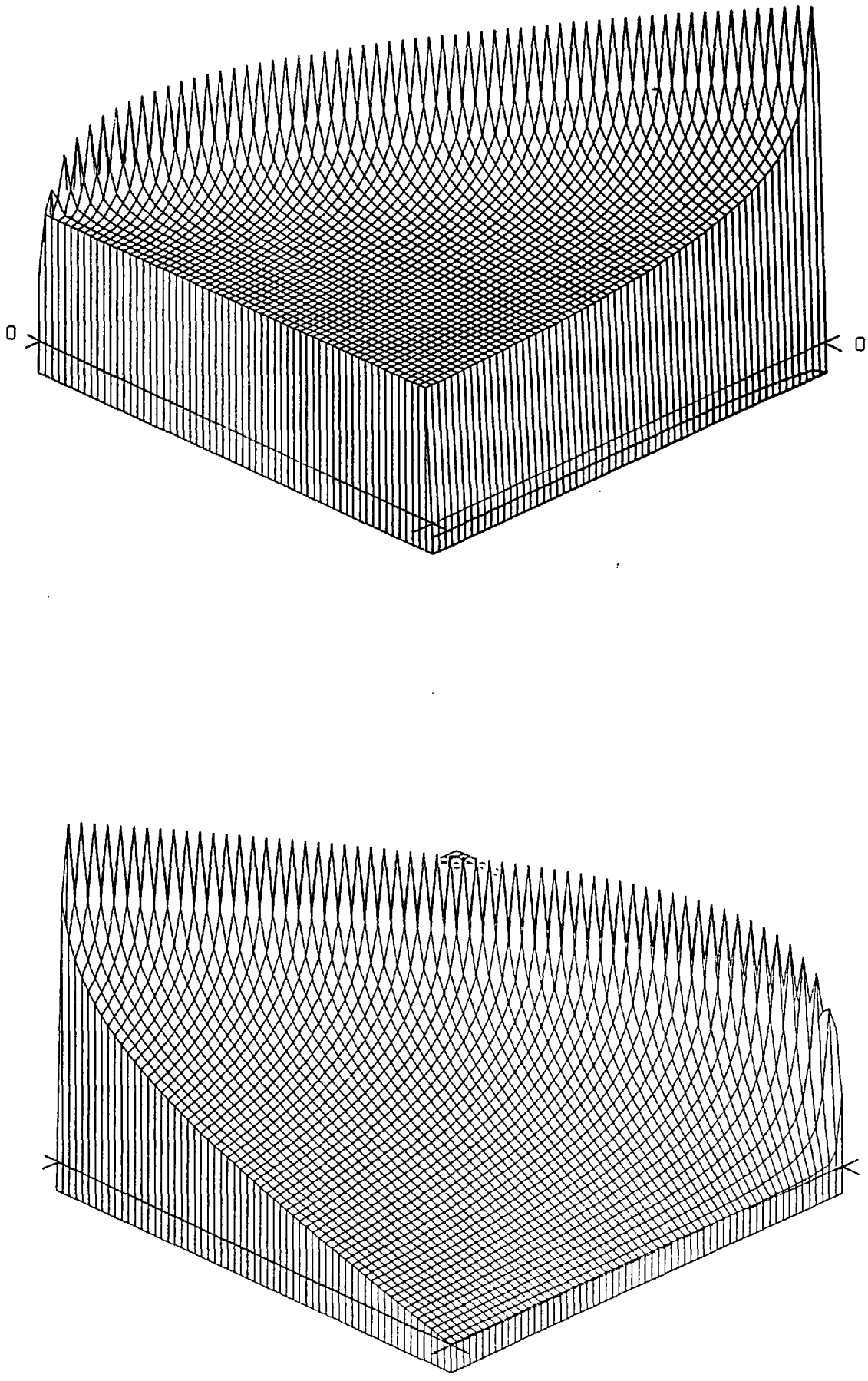

Figure 5.4 The $\underline{\underline{F}}$ Matrix

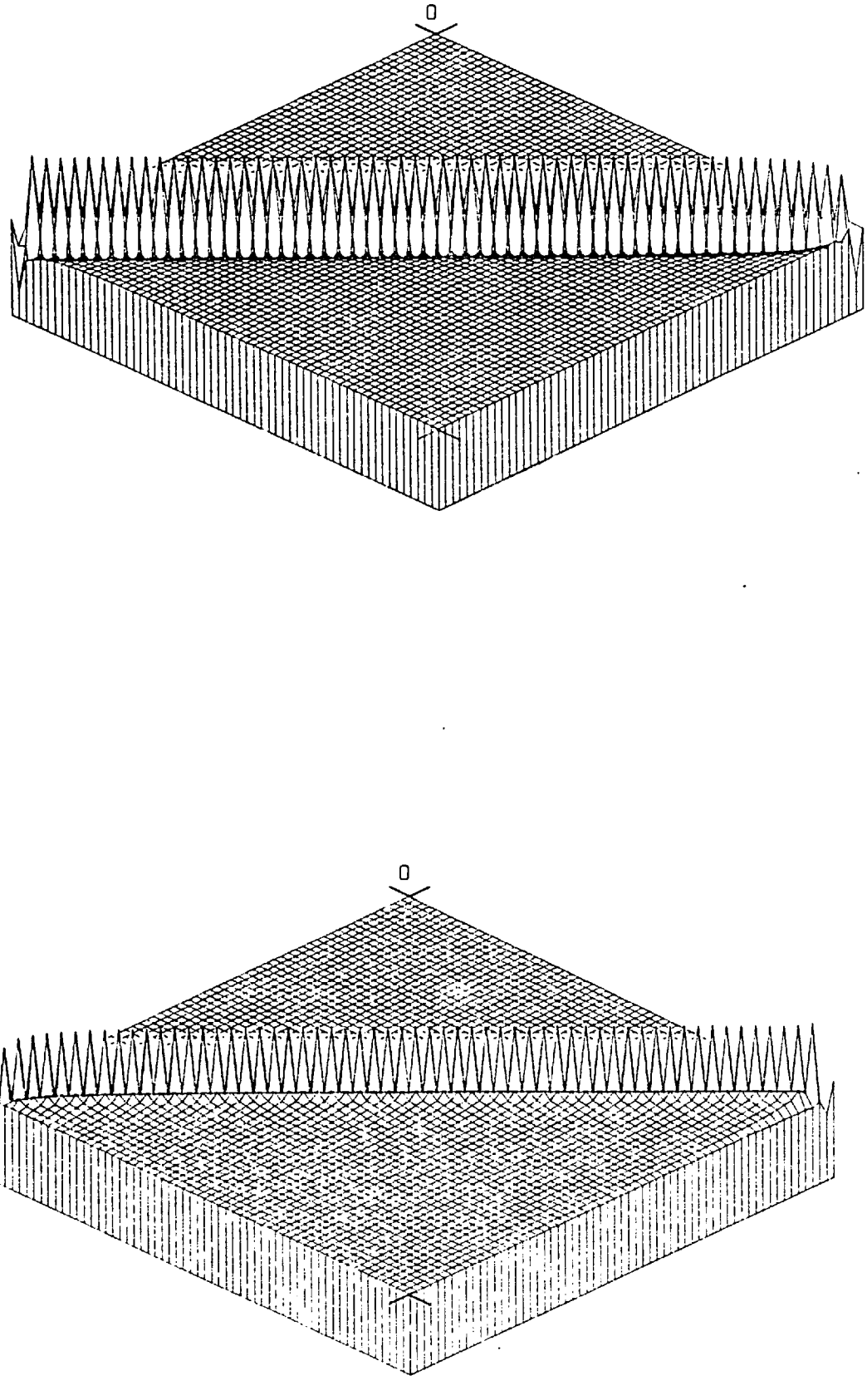

Figure 5.5. The $\underline{G}$ Matrix

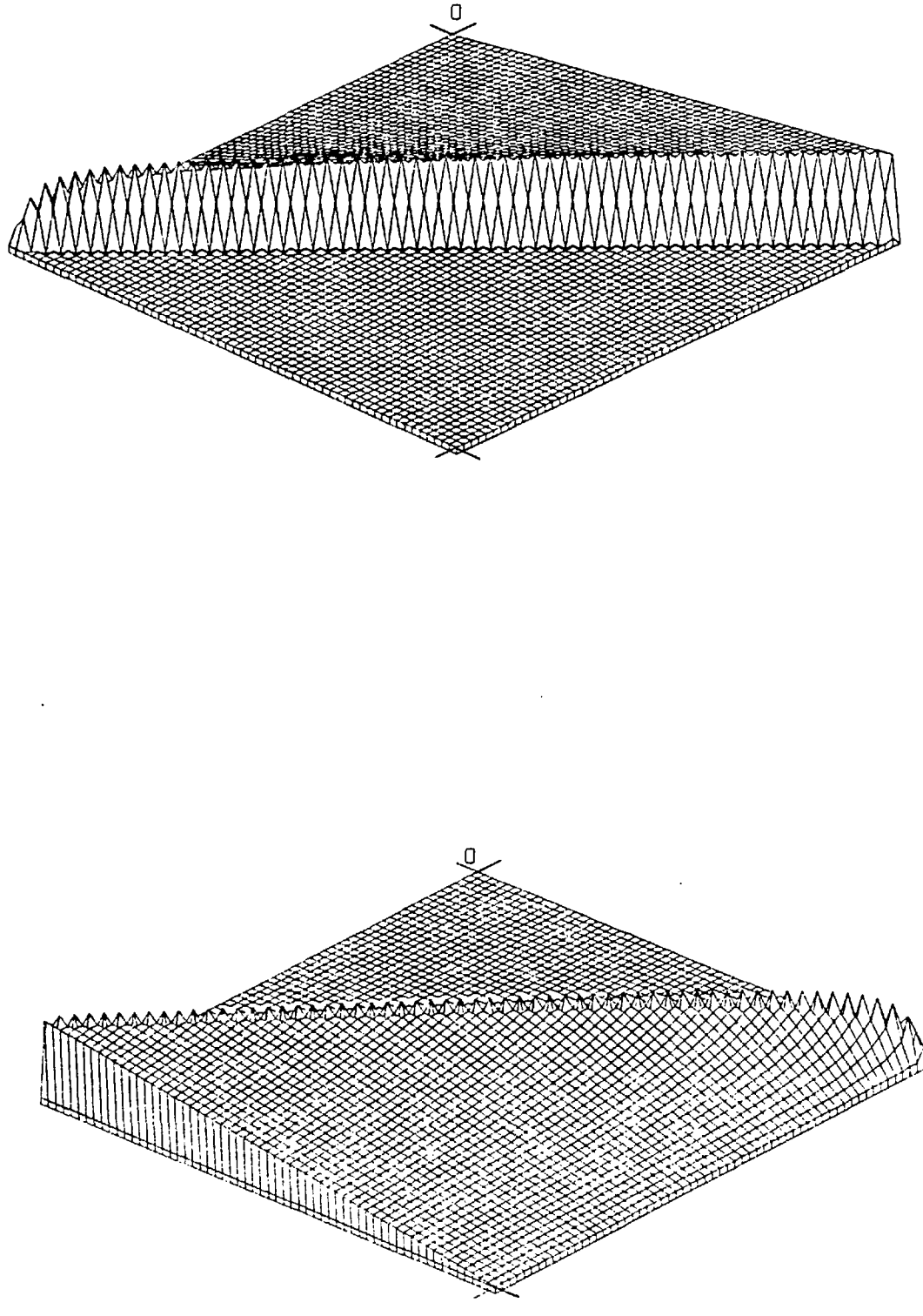

Figure 5.6. The $\underline{\underline{U}}$ Matrix

CHAPTER SIX

THE RESULTS FOR THE FULLY VARYING CASE

6.1 The Method Used to Integrate the Equations.

The results presented in this chapter have all been obtained using the same algorithm. The Vogelpohl-Reynolds equation (4.31) was integrated in the space domain using the quintic spline formulation and the integration with time was performed using Runge-Kutta-Merson. The program incorporated checkpoint and restart features so that it could be restarted if the instability in the time integration method required the time step to be decreased; and because the solution time required per run was of the order of 5000 sec. on the CDC 6400, in which time about 11000 solutions to the Reynolds equation had been found. The maximum time used in any one run was about 75000 sec. during which time about 170000 instantaneous pressure and deformation solutions were found.

There are two points to note concerning the time integration method used. Firstly, having discovered that the trajectory gives rise to stiff equations, the method used does not account for this behaviour; and secondly, the method of solving for constant load (see section 3.5.7) is not used in the latter part of the solution. The reason for both these methods being rejected is implicit in the assumptions used for the model, that is, that the effect of the local velocity of the deformation being taken into account. This has a serious effect on the stability of the solution algorithm. It was mentioned in section 3.5.1 that the solution is well conditioned, in that an overestimate in the load at one point in time will give an underestimate in the next. This gives confidence that the solution is correct and not sensitive to truncation and roundoff errors. However, when local elastic effects are included, then

this possible oscillation is very undesirable. For when attempting to calculate the local deformation velocity, alternate over- and under-estimates of the pressure distribution obtained give large errors in the values of the derivatives obtained. These themselves affect subsequent solutions.

It was therefore necessary to use small time steps in order to integrate this system, ones that were comparable to those necessary to integrate using Runge-Kutta-Merson. Hence there was no reason to use any of the stiffly stable methods as there was nothing to be gained and there was extra computational overhead in using them.

A very similar effect was noted when solving for constant load, though its manifestation was different. It may be recalled that this method was to "drop" the ball a distance Δh and find the velocity of the ball, v_c, such that the load is equal to the weight of the ball. It should be remembered that the local approach velocity is the sum of the elastic deformation velocity and the velocity of the centre of gravity of the ball. These latter two values tend to become equal in magnitude and opposite in sign. With this method, the effect of using large time steps was to start oscillations in the velocity calculated for the ball as $v_c = v - \frac{dw}{dt}$.

6.2 The Cases Considered.

All cases discussed here are to solve for a compressible Mark II viscosity-pressure type oil. It was assumed that the ball shape was initially parabolic. There were two values of α that were considered, and two values of E'; one approximates to steel on steel, the other to glass on glass, (the type used by PAUL, 1971).

If G is defined as $2\alpha E'$, so that G is the same as that of other workers, (e.g. CHENG and LEE, 1971) then G has the following values:-

	$\alpha(Pa^{-1})$	E'(Pa)	$\alpha E'$	G
High α, High E'	6.1E-8	1.1374E11	6938	13876
High α, Low E'	6.1E-8	3.9063E10	2578	5156
Low α, High E'	2.0E-8	1.1374E11	2275	4550
Low α, Low E'	2.0E-8	3.9063E10	781	1563

This is quite a large range compared with other work given in the literature.

Results are presented for these four sets at two different combinations of ball mass, radius, and oil initial viscosity. These are:

	Mass (kg)	Radius (m)	η_0(Pas)	K_1 (s)	K_2(Pasm)
Low Mass	0.0325	0.01	0.7	2.196×10^{-4}	0.007
High Mass	0.65	0.02	3.5	2.196×10^{-4}	0.07

The low mass cases were integrated using initial conditions of v_s=-0.1 ms^{-1}, and h_s=0.0005m. The low mass, high α, cases were also integrated with initial conditions of v_s=0 ms^{-1}, h_s=0.0005m. The high mass cases were integrated using initial conditions of v_s=0 ms^{-1}, h_s=0.0005m.

These may be summarised as:

Run No.	m	α	E'	v_s/R
1	0.65	6.1E-8	1.1374E11	0
2	0.65	6.1E-8	2.9063E10	0

3	0.65	2.0E-8	1.1374E11	0
4	0.65	2.0E-8	3.9063E10	0
5	0.0325	6.1E-8	1.1374E11	0
6	0.0325	6.1E-8	1.1374E11	-10
7	0.0325	6.1E-8	3.9063E10	0
8	0.0325	6.1E-8	3.9063E10	-10
9	0.0325	2.0E-8	1.1374E11	-10
10	0.0325	2.0E-8	3.9063E10	-10

Four further runs were made to test other features of the system. They were all run on the high mass case with $\alpha=6.1\times10^{-8}$ Pa^{-1} and $E'=3.9063\times10^{10}$ Pa. They were to:-

1. Account for the horizontal deflection by setting the film thickness to be:

$$\underline{h}_i=h_c+((\underline{r}-\underline{\underline{U}}\underline{p})_i)^2/2R+\underline{w}_i$$

Otherwise the standard algorithm is used. This was run number 11.

2. Solve the rigid compressible case by setting $\frac{1}{E'}=0$. As there was no instability due to the local deformation velocity, this was solved successfully using stiffly stable methods. (Problems could have arisen due to the $\frac{d\rho}{dt}$ term in the Reynolds Equation, but this effect is much smaller than that in $\frac{dw}{dt}$; also the equation has $\frac{d\rho}{dt}$ multiplied by $h=0(10^{-4}).R$ whereas $\frac{dw}{dt}$ is multiplied by ρ^* which is of order 1.) (Run 12).

3. A run was made accounting for the deformation but its

velocity is ignored. This gave a halfway case between the rigid case and the fully-varying case. Again it was successfully integrated using the stiffly stable methods. (Run 13).

4. Check whether the results depended on the Vogelpohl substitution method (section 4.6). It was noted that the substitution made was $S=ph_0^2$. A run was made to determine whether the particular choice of h_0 had a strong effect on the solution obtained. For this run (run 14)

$$h_o(r)=0.1 * \max(h_c,10^{-7})+r^2/2R$$

This meant that the value of S at the centre was 1% of its value when using the normal method.

It should be noted that as all velocities and film thicknesses are non-dimensionalised with respect to the ball radius, the value of h_s^* is 0.05 for the low mass case, and 0.025 for the high mass.

6.3 The Grid Mesh Used.

There were two different meshes used in this work, one, with 26 points, was used for the low load cases, the other, with 31 points, was used for the high load cases. The great advantage of using a grid that expands with the domain on $[0,r_s]$ is that the compliance matrix may be pre-calculated. This allows for a fast computation time, but, on the other hand, denies flexibility and use of adaptive methods.

The 26 point mesh has values at (remembering $R_2-R_1=\Delta r=1$)

0 1 2 3 4 5 7 10 14 19 25 33
44 59 79 105 140 190 270 500 750 1000 1250 1500
1750 2000

The 31 point mesh similarly has:-

0 1 3 7 10 13 20 30 43 70 102 145
190 250 300 360 420 490 560 640 720 810 900 1000
1100 1200 1300 1400 1550 1700 1850 2000

The 31 point mesh has more points in the outer regions than the 26 point mesh. This was because the solutions are limited by the ability to accurately calculate the force. This point is further discussed in Section 6.9. It was also used for the large mass case, where greater radial spread of the pressure field is to be found.

6.4 The Solutions

It is obvious from the graphs that during the first stages of impact the solution is virtually identical to that obtained for the rigid parabola-incompressible case. This is because the pressure generated is low and the elastic effects small compared with the rigid body effects. There is a slight decrease in the maximum values of pressure and force at the force peak, due to elastic effects. This is only apparent for the high load case.

Many of the graphs are plotted against the central deformed film thickness, h(0). This is to facilitate comparison with the work of CHENG and LEE and CHRISTENSEN.

Figure	Ordinate(s)	Abscissae	Run No(s).	Comment
6.1	$\log_{10} p_c$, $\frac{h_c}{R}$, $\frac{v_c}{R}$, $\frac{\dot{v}_c}{Rg}$	t	5	
6.2	"	"	8	
6.3	"	"	6,8	
6.4	"	"	9,10	
6.5	"	"	5,6	
6.6	"	"	7,8	
6.7	"	"	6,8,R	R-Rigid Incompressible Solution
6.8	"	"	1,3	
6.9	"	"	2,4	
6.10	"	"	1,2,R	Ignore i) E' ii) $\frac{\partial w}{\partial t}$
6.11	"	"	3,4,R	
6.12	"	"	1,12,13	
6.13	"	"	4	Different time scale
6.14	$\log_{10}(p_c)$	h(0)/R	1,2,3,4,R	
6.15	"	"	1,2,3,4,R	
6.16	"	"	5,7,9,10,R	
6.17	v(0)/R	h(0)/R	1,2,3,4,R	Phase-plane diagrams
6.18	"	"	1,2,3,4,R	
6.19	"	"	5,7,9,10,R	
6.20	$\frac{v(a/4)}{v(0)}$, $\frac{v(a/2)}{v(0)}$, $\frac{v(a)}{v(0)}$	h(0)/R	4	Spatial change of relative velocity
6.21	v_c/R	h_c/R	1,2,3,4,R	Phase-plane diagrams
6.22	"	"	1,2,3,4,R	
6.23	"	"	5,7,9,10,R	
6.24	w(0)/R	h(0)/R	1,2,3,4,R	
6.25	"	"	5,7,9,10,R	
6.26	Depth of pocket/R	h(0)	4	i.e. sup (h(0)-h(r))
6.27	$\dot{v}_c$/ Rg	h(0)/R	1,2,3,4,R	
6.28	"	"	5,7,9,10,R	
6.29	$\frac{v(a/4)}{v(0)}$, $\frac{v(a/2)}{v(0)}$, $\frac{v(a)}{v(0)}$	h(0)/R	4	Different scale in h(0) to 6.20
6.30	Depth of pocket/R	h(0)/R	4	Different scale in h(0) to 6.26.

TABLE 6.1

Elastic Parabola. m= 0.0325Kg
R= 0.01m E' = 1.1374x10^11Pa.
Compressible Mark II Viscosity Oil.
ρa= 5.828x10^-10Pa^-1 ρb= 16.84x10^-10Pa^-1
α= 6.1x10^-8Pa^-1 αpL= 25.0 ηo= 0.7Pas.
Log10 (Pc)
- vc
hc
Net Force / W
LOG PRESSURE
TIME (MS)
0.00
3.00
6.00
9.00
12.00
15.00
18.00
21.00
24.00
27.00
30.00
33.00
36.00

Figure 6.1

NET FORCE/WEIGHT
H (C.O.G.) x10⁻¹
- V (C.O.G.)
LOG PRESSURE
TIME (MS)
Elastic Parabola. m= 0.0325Kg
R= 0.01m E'= 3.9063x10¹⁰Pa.
Compressible Mark II Viscosity Oil.
ρa= 5.828x10⁻¹⁰Pa⁻¹ ρb= 16.84x10⁻¹⁰Pa⁻¹
α= 6.1x10⁻⁸Pa⁻¹ αpL= 25.0 ηo= 0.7Pas.
Log10 (Pc)
- vc
hc
Net Force / W

Figure 6.2.

NET FORCE/WEIGHT
H (C.O.G.) ×10⁻¹
- V (C.O.G.)
LOG PRESSURE
TIME (MS)
α=6.1x10⁻⁸Pa⁻¹
α=2.0x10⁻⁸Pa⁻¹
Elastic Parabola. m= 0.0325Kg
R= 0.01m E'= 1.1374x10¹¹Pa.
Compressible Mark II Viscosity Oil.
ρa= 5.828x10⁻¹⁰Pa⁻¹ ρb= 16.84x10⁻¹⁰Pa⁻¹
α= Varying αpL= 25.0 ηo= 0.7Pas.
Log10 (Pc)
- vc
hc
Net Force / W

Figure 6.3.

NET FORCE/WEIGHT
H (C.O.G.) ×10⁻¹
- V (C.O.G.)
LOG PRESSURE
TIME (MS)
α=6.1x10⁻⁸Pa⁻¹
α=2.0x10⁻⁸Pa⁻¹
Elastic Parabola. m= 0.0325Kg
R= 0.01m E' = 3.9063x10¹⁰Pa.
Compressible Mark II Viscosity Oil.
ρa= 5.828x10⁻¹⁰Pa⁻¹ ρb= 16.84x10⁻¹⁰Pa⁻¹
α= Varying apL= 25.0 ηo= 0.7Pas.
Log10 (Pc)
- vc
hc
Net Force / W

Figure 6.4.

NET FORCE/WEIGHT
H (C.O.C.) *10⁻¹
- V (C.O.C.)
LOG PRESSURE
TIME (MS)
Elastic Parabola. m= 0.0325Kg
R= 0.01m E' = 1.1374x10¹¹Pa.
Compressible Mark II Viscosity Oil.
ρa= 5.828x10⁻¹⁰Pa⁻¹ ρb= 16.84x10⁻¹⁰Pa⁻¹
α= 6.1x10⁻⁸Pa⁻¹ αpL= 25.0 ηo= 0.7Pas.
Log10 (Pc)
- vc
hc
Net Force / W

Figure 6.5.

NET FORCE/WEIGHT
H (C.O.G.) *10⁻¹
- V (C.O.G.)
LOG PRESSURE
TIME (MS)
Elastic Parabola. m= 0.0325Kg
R= 0.01m E'= 3.9063x10¹⁰Pa.
Compressible Mark II Viscosity Oil.
ρa= 5.828x10⁻¹⁰Pa⁻¹ ρb= 16.84x10⁻¹⁰Pa⁻¹
α= 6.1x10⁻⁸Pa⁻¹ αpL= 25.0 η0= 0.7Pas.
Log10 (Pc)
- vc
hc
Net Force / W

Figure 6.6

NET FORCE/WEIGHT
H (C.O.G.) *10⁻¹
- V (C.O.G.)
LOG PRESSURE
TIME (MS)
E'=∞
ρa=0
E'=1.1374x10¹¹Pa
E'=3.9063x10¹⁰Pa
Elastic Parabola. m= 0.0325Kg
R= 0.01m E' = Varying.
Compressible Mark II Viscosity Oil.
ρa= 5.828x10⁻¹⁰Pa⁻¹ ρb= 16.84x10⁻¹⁰Pa⁻¹
α= 6.1x10⁻⁸Pa⁻¹ αpL= 25.0 η0= 0.7Pas.
Log10 (Pc)
vc
hc
Net Force / W

Figure 6.7

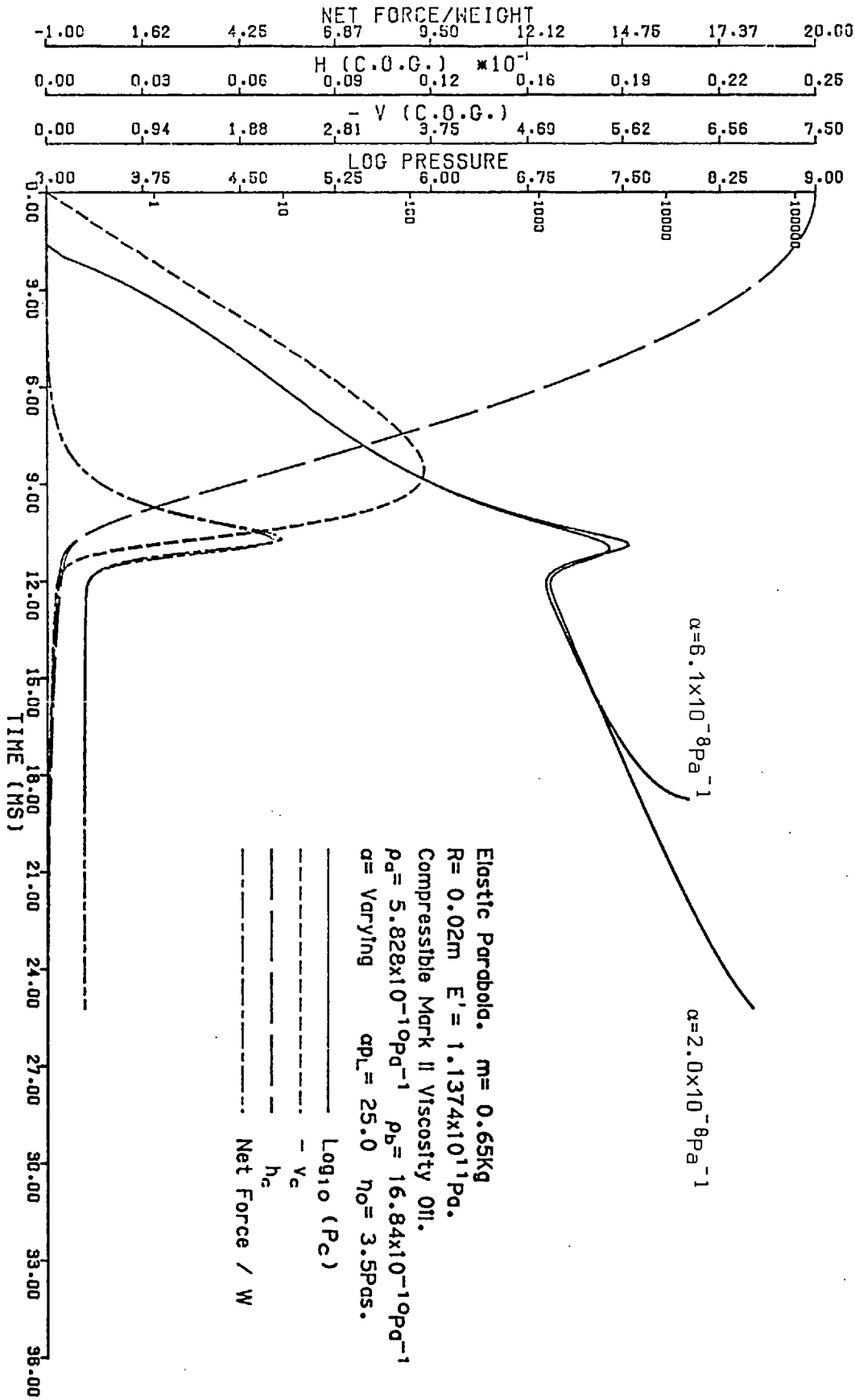
NET FORCE/WEIGHT
-1.00 1.62 4.25 6.87 9.50 12.12 14.75 17.37 20.00
H (C.O.G.) *10⁻¹
0.00 0.03 0.06 0.09 0.12 0.16 0.19 0.22 0.25
- V (C.O.G.)
0.00 0.94 1.88 2.81 3.75 4.69 5.62 6.56 7.50
LOG PRESSURE
3.00 3.75 4.50 5.25 6.00 6.75 7.50 8.25 9.00
1 10 150 1000 10000 100000
0.00 3.00 6.00 9.00 12.00 15.00 18.00 21.00 24.00 27.00 30.00 33.00 36.00
TIME (MS)
α=6.1x10⁻⁸Pa⁻¹
α=2.0x10⁻⁸Pa⁻¹
Elastic Parabola. m= 0.65Kg
R= 0.02m E'= 1.1374x10¹¹Pa.
Compressible Mark II Viscosity Oil.
ρa= 5.828x10⁻¹⁰Pa⁻¹ ρb= 16.84x10⁻¹⁰Pa⁻¹
α= Varying αL= 25.0 η0= 3.5Pas.
Log10 (Pc)
- Vc
hc
Net Force / W

Figure 6.8.

NET FORCE/WEIGHT
H (C.O.G.) *10⁻¹
- V (C.G.G.)
LOG PRESSURE
TIME (MS)
α=6.1x10⁻⁸Pa⁻¹
α=2.0x10⁻⁸Pa⁻¹
Elastic Parabola. m= 0.65Kg
R= 0.02m E' = 3.9063x10¹⁰Pa.
Compressible Mark II Viscosity Oil.
ρa= 5.828x10⁻¹⁰Pa⁻¹ ρb= 16.84x10⁻¹⁰Pa⁻¹
α= Varying apL= 25.0 η0= 3.5Pas.
Log10 (Pc)
- vc
hc
Net Force / W

Figure 6.9.

NET FORCE/WEIGHT
H (C.O.G.) *10⁻¹
- V (C.O.G.)
LOG PRESSURE
TIME (MS)
(1) E'=∞
(2) E'=1.1374x70^11 Pa
(3) E'=3.9063a10^10 Pa
Elastic Parabola. m= 0.65Kg
R= 0.02m E' = Varying.
Compressible Mark II Viscosity Oil.
ρa= 5.828x10⁻¹⁰Pa⁻¹ ρb= 16.84x10⁻¹⁰Pa⁻¹
α= 6.1x10⁻⁸Pa⁻¹ αpL= 25.0 ηo= 3.5Pas.
Log10 (Pc)
- vc
hc
Net Force / W

Figure 6.10

NET FORCE/WEIGHT
H (C.O.G.) *10⁻¹
- V (C.O.G.)
LOG PRESSURE
TIME (MS)
E'=∞
p_a=0
E'=1.1374x10^11Pa
E'=3.9063x10^10Pa
Elastic Parabola. m= 0.65Kg
R= 0.02m E' = Varying.
Compressible Mark II Viscosity Oil.
p_a= 5.828x10^-10Pa^-1 p_b= 16.84x10^-10Pa^-1
α= 2.0x10^-8Pa^-1 αp_L= 25.0 η_o= 3.5Pas.
Log10 (P_c)
- v_c
h_c
Net Force / W

Figure 6.11

NET FORCE/WEIGHT
H (C.O.G.) *10⁻¹
- V (C.O.G.)
LOG PRESSURE
TIME (MS)
0.00
3.00
6.00
9.00
12.00
15.00
18.00
21.00
24.00
27.00
30.00
33.00
36.00
(1)
(2)
(3)
1) E'=∞
2) E'=1.1374x10^11Pa Ignore dw/dt
3) E'=1.1374x10^11Pa Fully Varying
Elastic Parabola. m= 0.65Kg
R= 0.02m E' = 1.1374x10^11Pa.
Compressible Mark II Viscosity Oil.
ρa= 5.828x10^-10Pa^-1 ρb= 16.84x10^-10Pa^-1
α= 6.1x10^-8Pa^-1 αpL= 25.0 η0= 3.5Pas.
Log10 (Pc)
- vc
hc
Net Force / W

Figure 6.12.

Figure 6.13

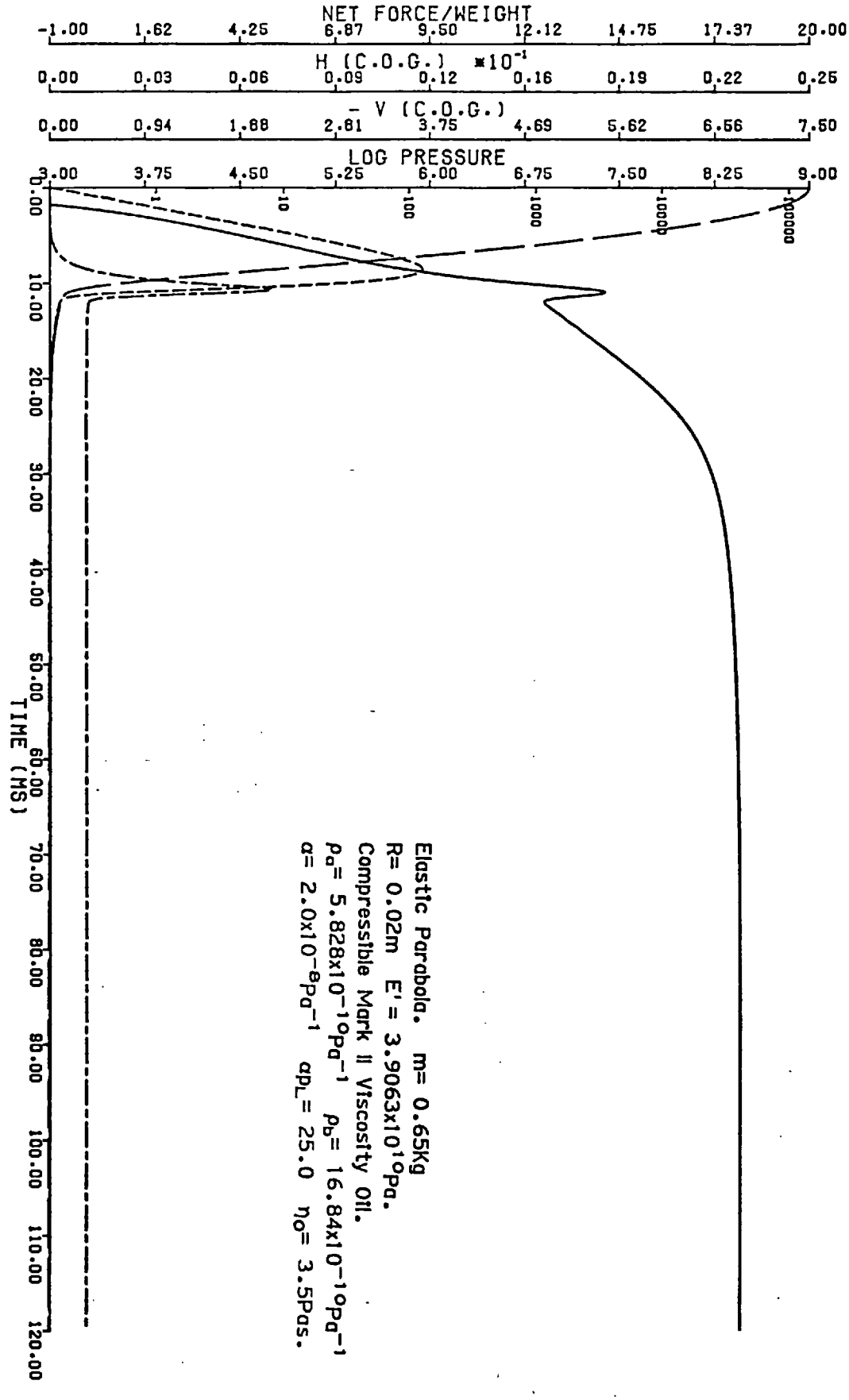

Elastic Parabola. m= 0.65Kg
R= 0.02m E' = 3.9063×10^{10}Pa.
Compressible Mark II Viscosity Oil.
$\rho_a = 5.828 \times 10^{-10} Pa^{-1}$ $\rho_b = 16.84 \times 10^{-10} Pa^{-1}$
$\alpha = 2.0 \times 10^{-8} Pa^{-1}$ $\alpha_L = 25.0$ $\eta_o = 3.5$Pas.

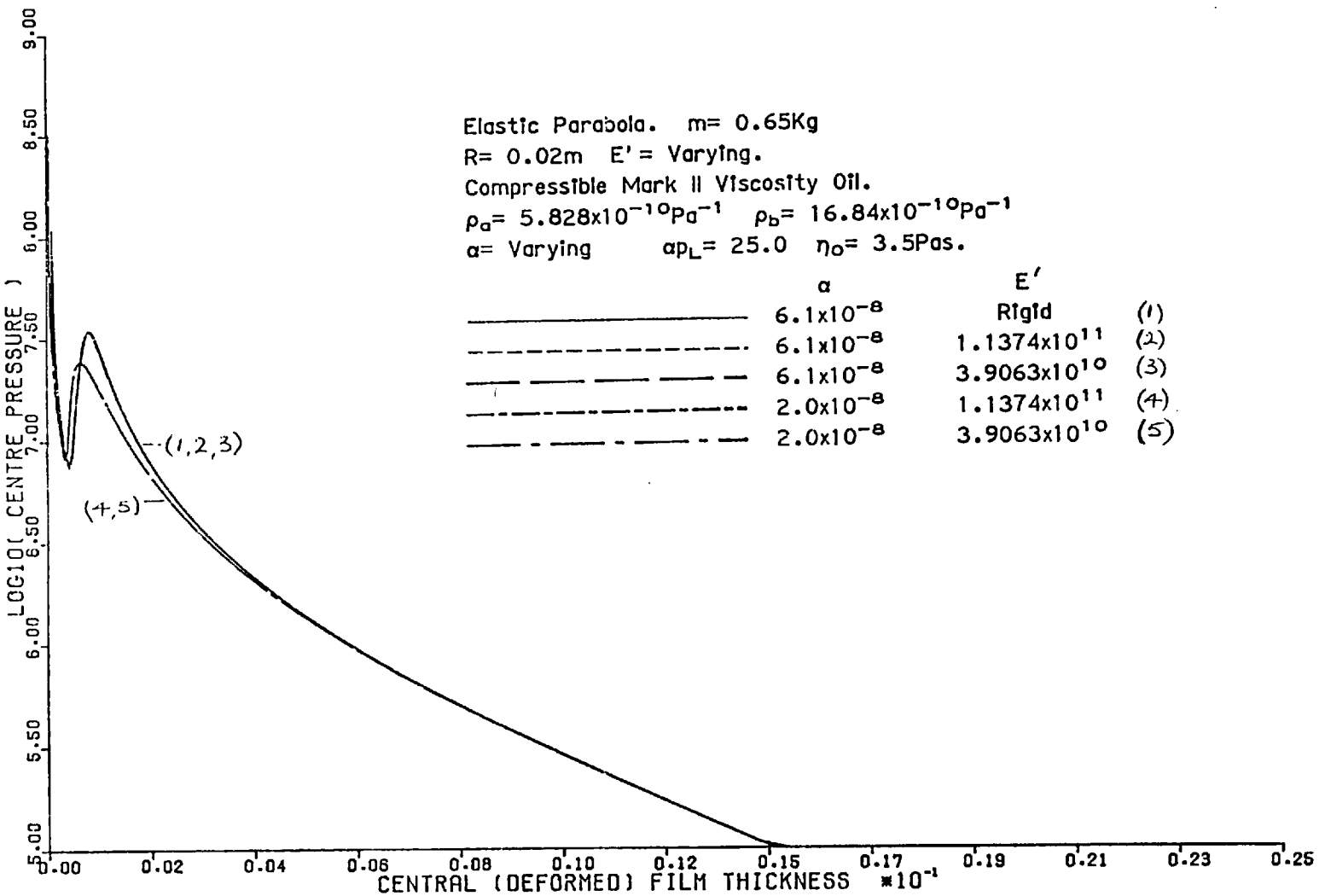
Elastic Parabola. m= 0.65Kg
R= 0.02m E' = Varying.
Compressible Mark II Viscosity Oil.
ρ_a= 5.828x10^{-10}Pa^{-1} ρ_b= 16.84x10^{-10}Pa^{-1}
α= Varying αp_L= 25.0 η_o= 3.5Pas.
α E'
6.1x10^{-8} Rigid (1)
6.1x10^{-8} 1.1374x10^{11} (2)
6.1x10^{-8} 3.9063x10^{10} (3)
2.0x10^{-8} 1.1374x10^{11} (4)
2.0x10^{-8} 3.9063x10^{10} (5)
(1,2,3)
(4,5)
LOG10(CENTRE PRESSURE)
9.00
8.50
8.00
7.50
7.00
6.50
6.00
5.50
5.00
0.00
0.02
0.04
0.06
0.08
0.10
0.12
0.15
0.17
0.19
0.21
0.23
0.25
CENTRAL (DEFORMED) FILM THICKNESS *10^{-1}

Figure 6.14.

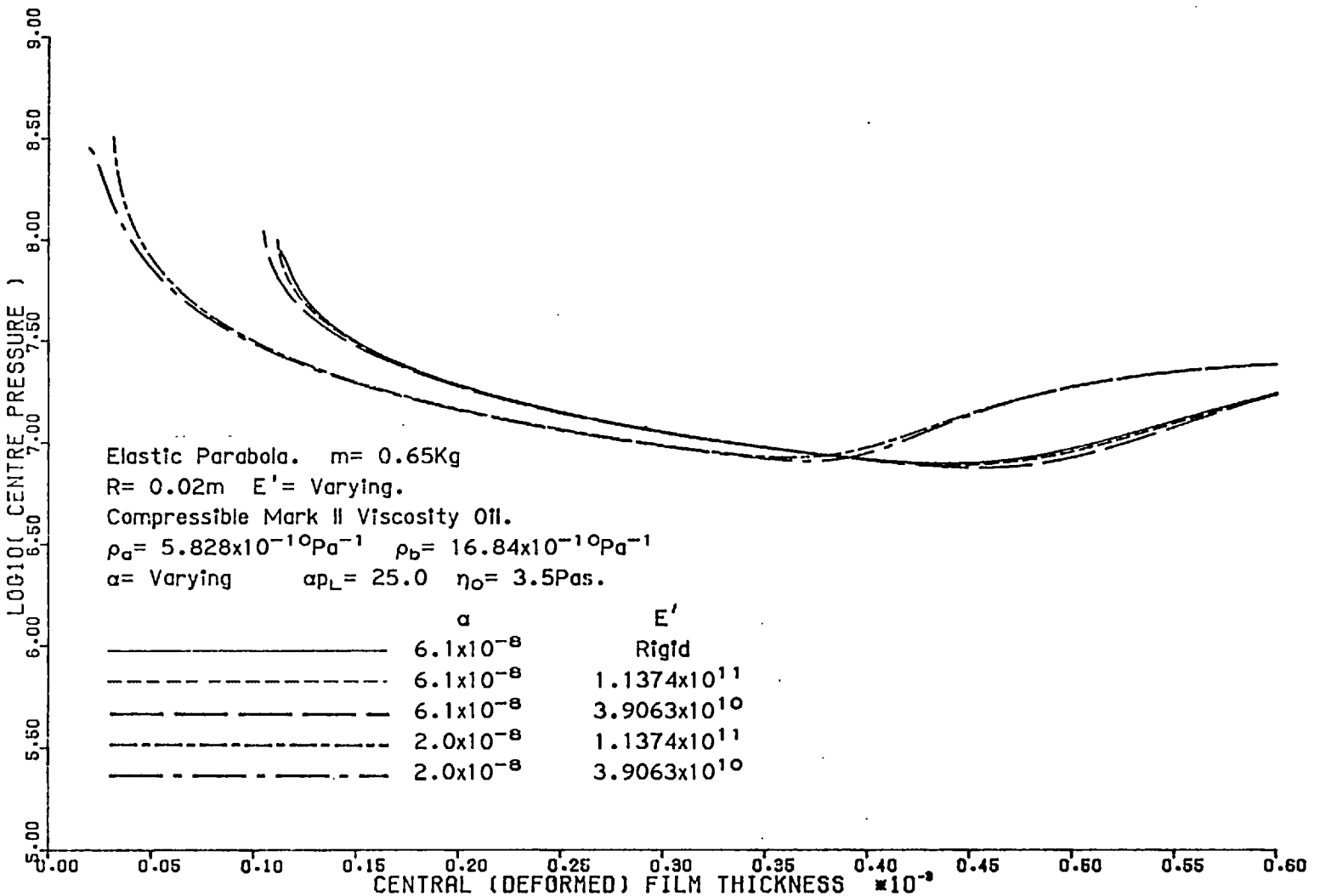
LOG10(CENTRE PRESSURE)
9.00
8.50
8.00
7.50
7.00
6.50
6.00
5.50
5.00
0.00
0.05
0.10
0.15
0.20
0.25
0.30
0.35
0.40
0.45
0.50
0.55
0.60
CENTRAL (DEFORMED) FILM THICKNESS *10⁻³
Elastic Parabola. m= 0.65Kg
R= 0.02m E'= Varying.
Compressible Mark II Viscosity Oil.
ρa= 5.828x10⁻¹⁰Pa⁻¹ ρb= 16.84x10⁻¹⁰Pa⁻¹
α= Varying αpL= 25.0 ηo= 3.5Pas.
α E'
6.1x10⁻⁸ Rigid
6.1x10⁻⁸ 1.1374x10¹¹
6.1x10⁻⁸ 3.9063x10¹⁰
2.0x10⁻⁸ 1.1374x10¹¹
2.0x10⁻⁸ 3.9063x10¹⁰

Figure 6.15

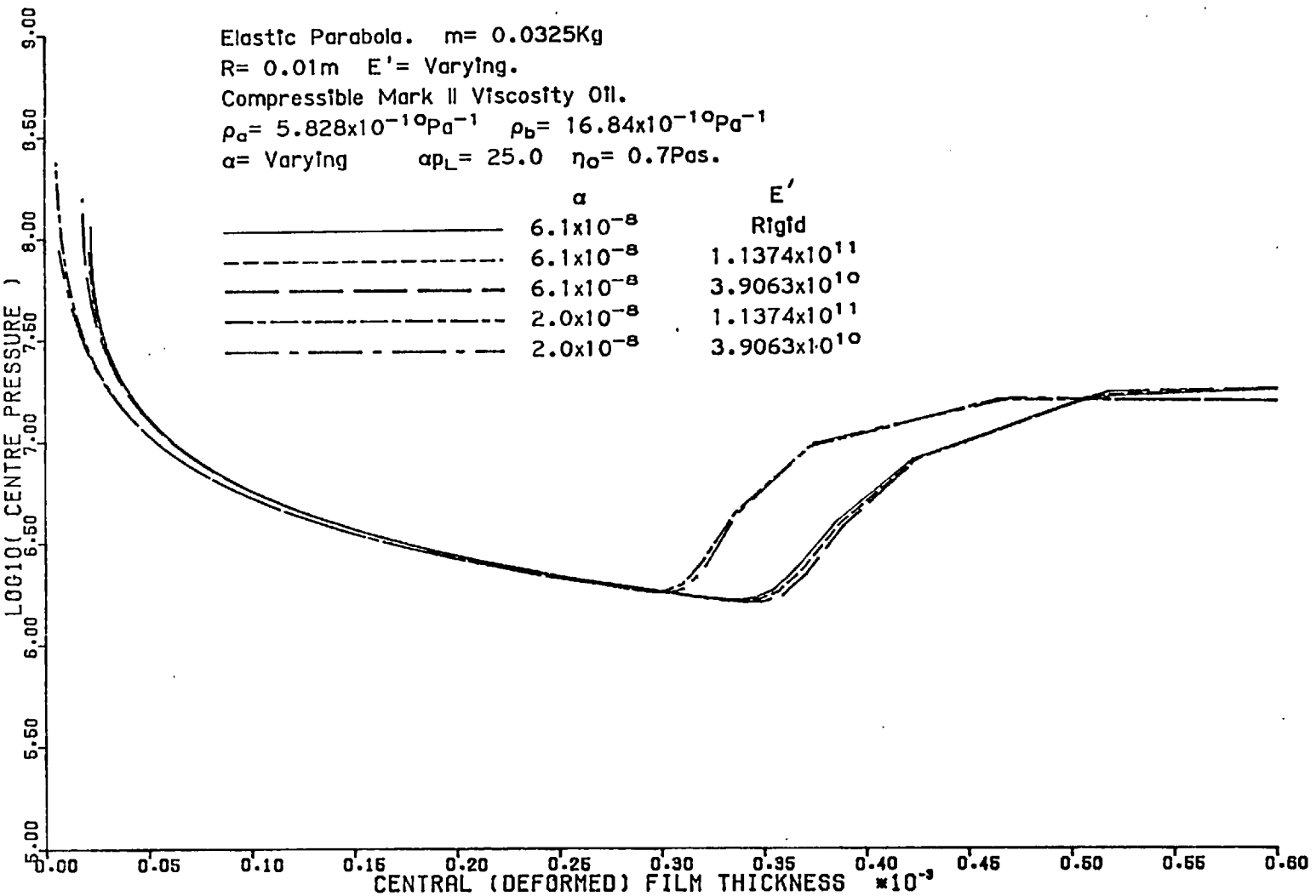
Elastic Parabola. m= 0.0325Kg
R= 0.01m E'= Varying.
Compressible Mark II Viscosity Oil.
ρ_a= 5.828x10^{-10}Pa^{-1} ρ_b= 16.84x10^{-10}Pa^{-1}
α= Varying αp_L= 25.0 η_o= 0.7Pas.
α
E'
6.1x10^{-8} Rigid
6.1x10^{-8} 1.1374x10^{11}
6.1x10^{-8} 3.9063x10^{10}
2.0x10^{-8} 1.1374x10^{11}
2.0x10^{-8} 3.9063x10^{10}
LOG10(CENTRE PRESSURE)
5.00
5.50
6.00
6.50
7.00
7.50
8.00
8.50
9.00
0.00
0.05
0.10
0.15
0.20
0.25
0.30
0.35
0.40
0.45
0.50
0.55
0.60
CENTRAL (DEFORMED) FILM THICKNESS *10^{-3}

Figure 6.16.

VELOCITY OF CENTRAL (DEFORMED) POINT
0.00
0.50
1.00
1.50
2.00
2.50
3.00
3.50
4.00
0.00
0.02
0.04
0.06
0.08
0.10
0.12
0.15
0.17
0.19
0.21
0.23
0.25
CENTRAL (DEFORMED) FILM THICKNESS *10⁻¹
Elastic Parabola. m= 0.65Kg
R= 0.02m E'= Varying.
Compressible Mark II Viscosity Oil.
ρa= 5.828x10⁻¹⁰Pa⁻¹ ρb= 16.84x10⁻¹⁰Pa⁻¹
α= Varying αpL= 25.0 ηo= 3.5Pas.
α
E'
6.1x10⁻⁸
Rigid
6.1x10⁻⁸
1.1374x10¹¹
6.1x10⁻⁸
3.9063x10¹⁰
2.0x10⁻⁸
1.1374x10¹¹
2.0x10⁻⁸
3.9063x10¹⁰

Figure 8.17

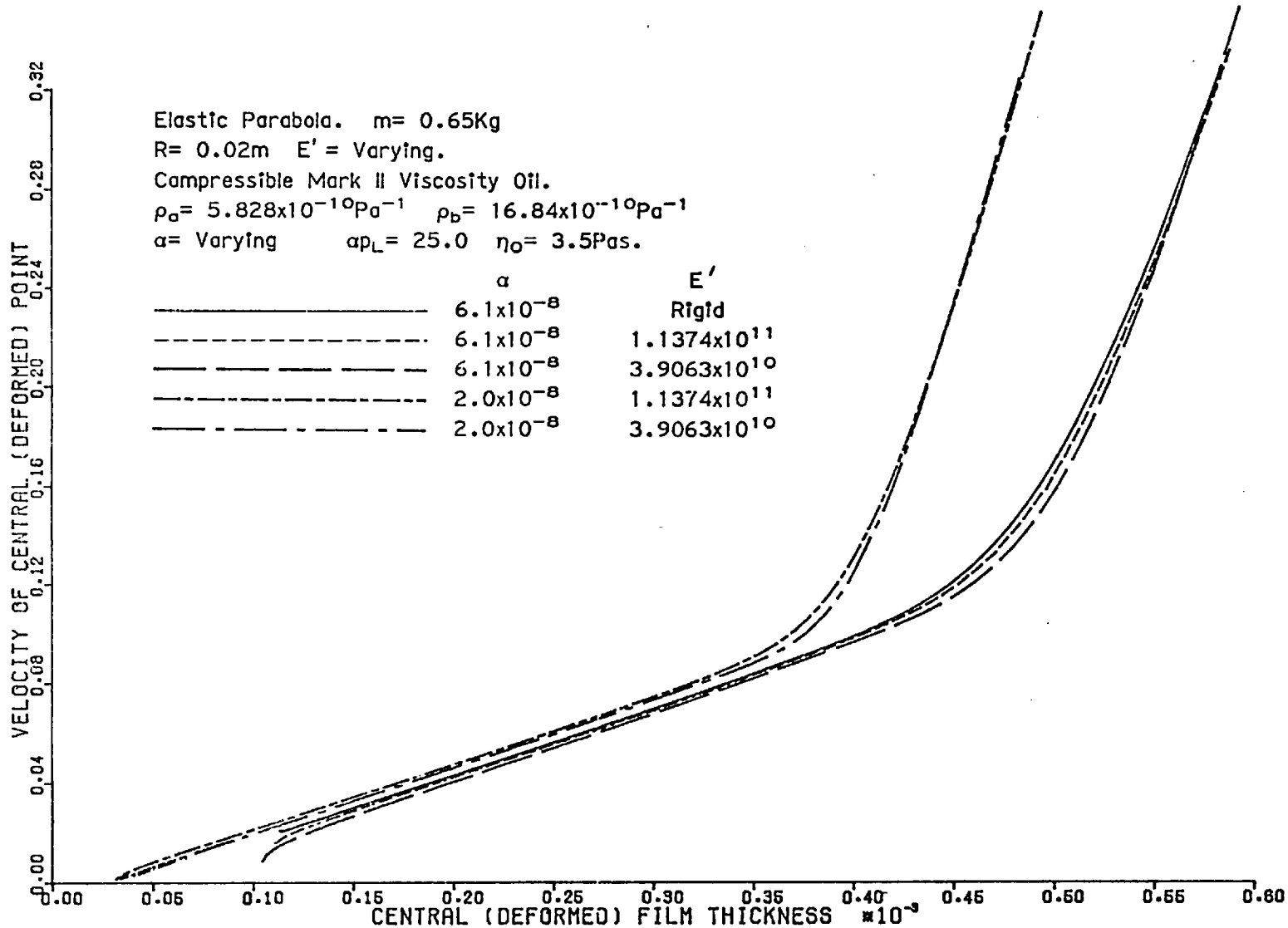
Elastic Parabola. m= 0.65Kg
R= 0.02m E' = Varying.
Compressible Mark II Viscosity Oil.
ρ_a= 5.828x10^{-10}Pa^{-1} ρ_b= 16.84x10^{-10}Pa^{-1}
α= Varying αp_L= 25.0 η_o= 3.5Pas.
α
E'
6.1x10^{-8} Rigid
6.1x10^{-8} 1.1374x10^{11}
6.1x10^{-8} 3.9063x10^{10}
2.0x10^{-8} 1.1374x10^{11}
2.0x10^{-8} 3.9063x10^{10}
VELOCITY OF CENTRAL (DEFORMED) POINT
0.00
0.04
0.08
0.12
0.16
0.20
0.24
0.28
0.32
0.00
0.05
0.10
0.15
0.20
0.25
0.30
0.35
0.40
0.45
0.50
0.55
0.60
CENTRAL (DEFORMED) FILM THICKNESS *10^{-9}

Figure 6.18.

Figure 6.19.

Elastic Parabola. m= 0.0325Kg
R= 0.01m E'= Varying.
Compressible Mark II Viscosity Oil.
ρ_a= 5.828x10^{-10}Pa^{-1} ρ_b= 16.84x10^{-10}Pa^{-1}
α= Varying αp_L= 25.0 η_o= 0.7Pas.
α
E'
6.1x10^{-8} Rigid
6.1x10^{-8} 1.1374x10^{11}
6.1x10^{-8} 3.9063x10^{10}
2.0x10^{-8} 1.1374x10^{11}
2.0x10^{-8} 3.9063x10^{10}
VELOCITY OF CENTRAL (DEFORMED) POINT
0.00
0.04
0.08
0.12
0.16
0.20
0.24
0.28
0.32
0.00
0.05
0.10
0.15
0.20
0.25
0.30
0.35
0.40
0.45
0.50
0.55
0.60
CENTRAL (DEFORMED) FILM THICKNESS *10^{-3}

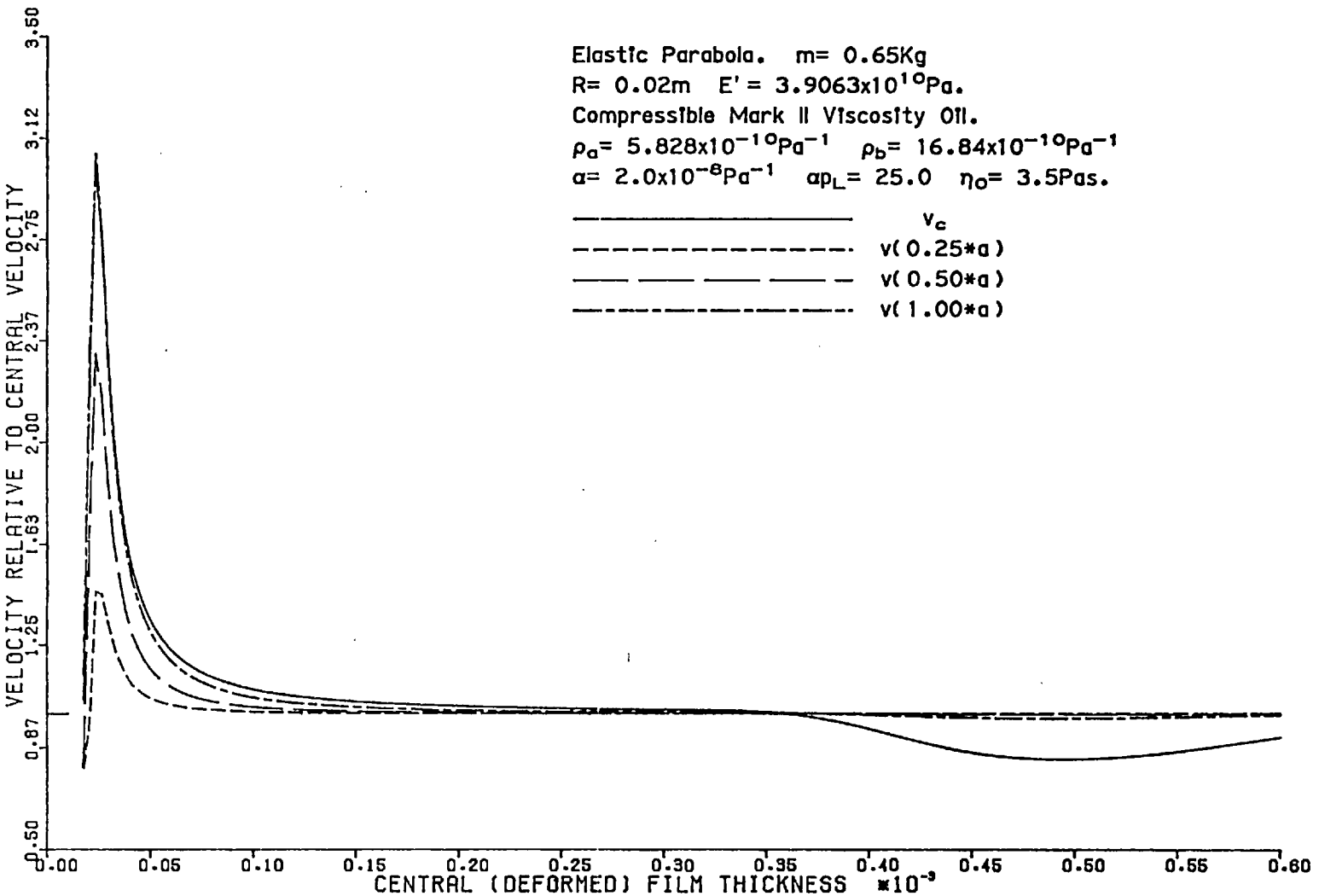
Elastic Parabola. m= 0.65Kg
R= 0.02m E' = 3.9063x10^10Pa.
Compressible Mark II Viscosity Oil.
ρa= 5.828x10^-10Pa^-1 ρb= 16.84x10^-10Pa^-1
α= 2.0x10^-8Pa^-1 αpL= 25.0 ηo= 3.5Pas.
vc
v(0.25*a)
v(0.50*a)
v(1.00*a)
VELOCITY RELATIVE TO CENTRAL VELOCITY
0.50
0.87
1.25
1.63
2.00
2.37
2.75
3.12
3.50
0.00
0.05
0.10
0.15
0.20
0.25
0.30
0.35
0.40
0.45
0.50
0.55
0.60
CENTRAL (DEFORMED) FILM THICKNESS *10^-3

Figure 6.20.

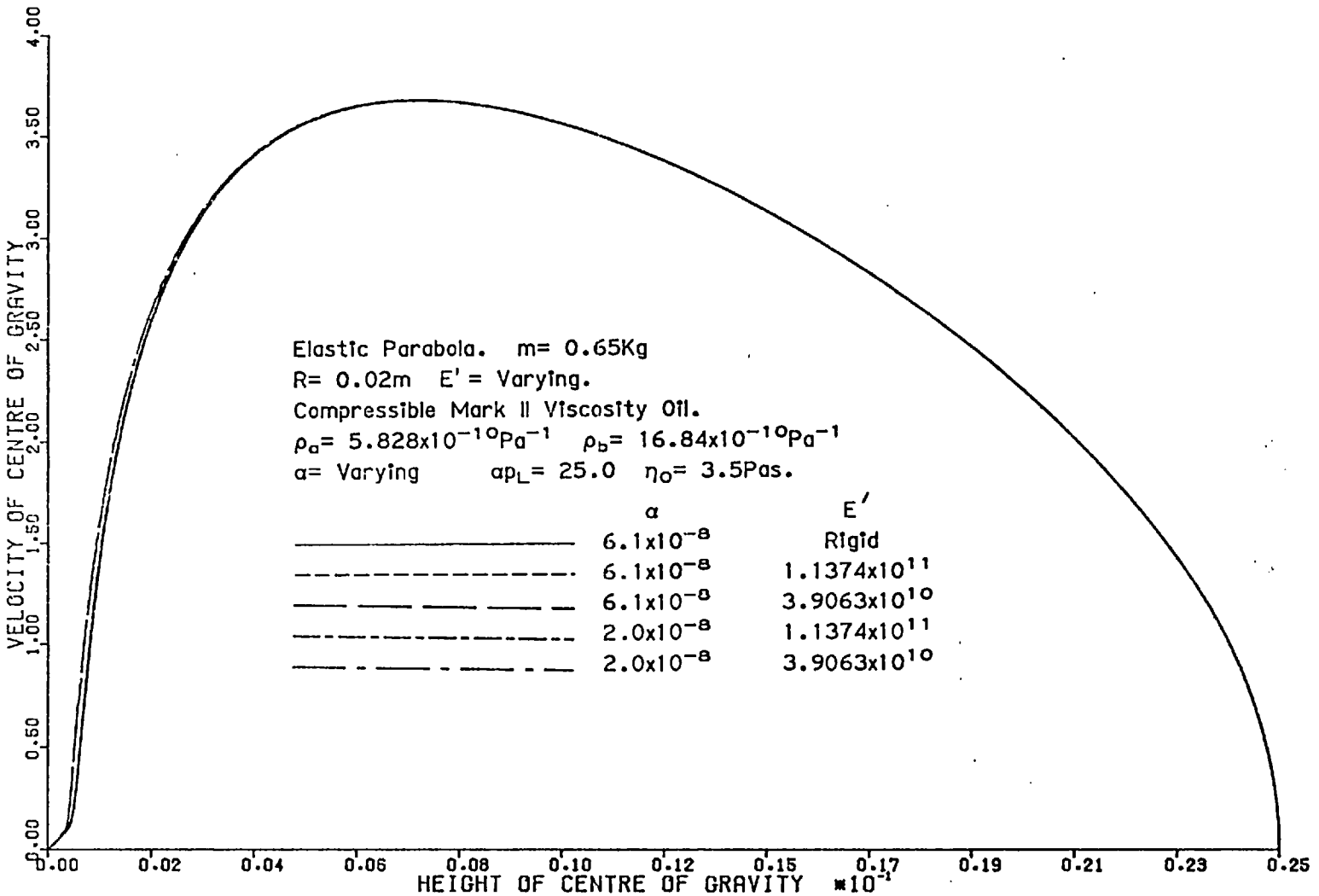
VELOCITY OF CENTRE OF GRAVITY
0.00
0.50
1.00
1.50
2.00
2.50
3.00
3.50
4.00
0.00
0.02
0.04
0.06
0.08
0.10
0.12
0.15
0.17
0.19
0.21
0.23
0.25
HEIGHT OF CENTRE OF GRAVITY *10⁻¹
Elastic Parabola. m= 0.65Kg
R= 0.02m E' = Varying.
Compressible Mark II Viscosity Oil.
ρa= 5.828x10⁻¹⁰Pa⁻¹ ρb= 16.84x10⁻¹⁰Pa⁻¹
α= Varying αpL= 25.0 ηo= 3.5Pas.
α
E'
6.1x10⁻⁸ Rigid
6.1x10⁻⁸ 1.1374x10¹¹
6.1x10⁻⁸ 3.9063x10¹⁰
2.0x10⁻⁸ 1.1374x10¹¹
2.0x10⁻⁸ 3.9063x10¹⁰

Figure 6.21.

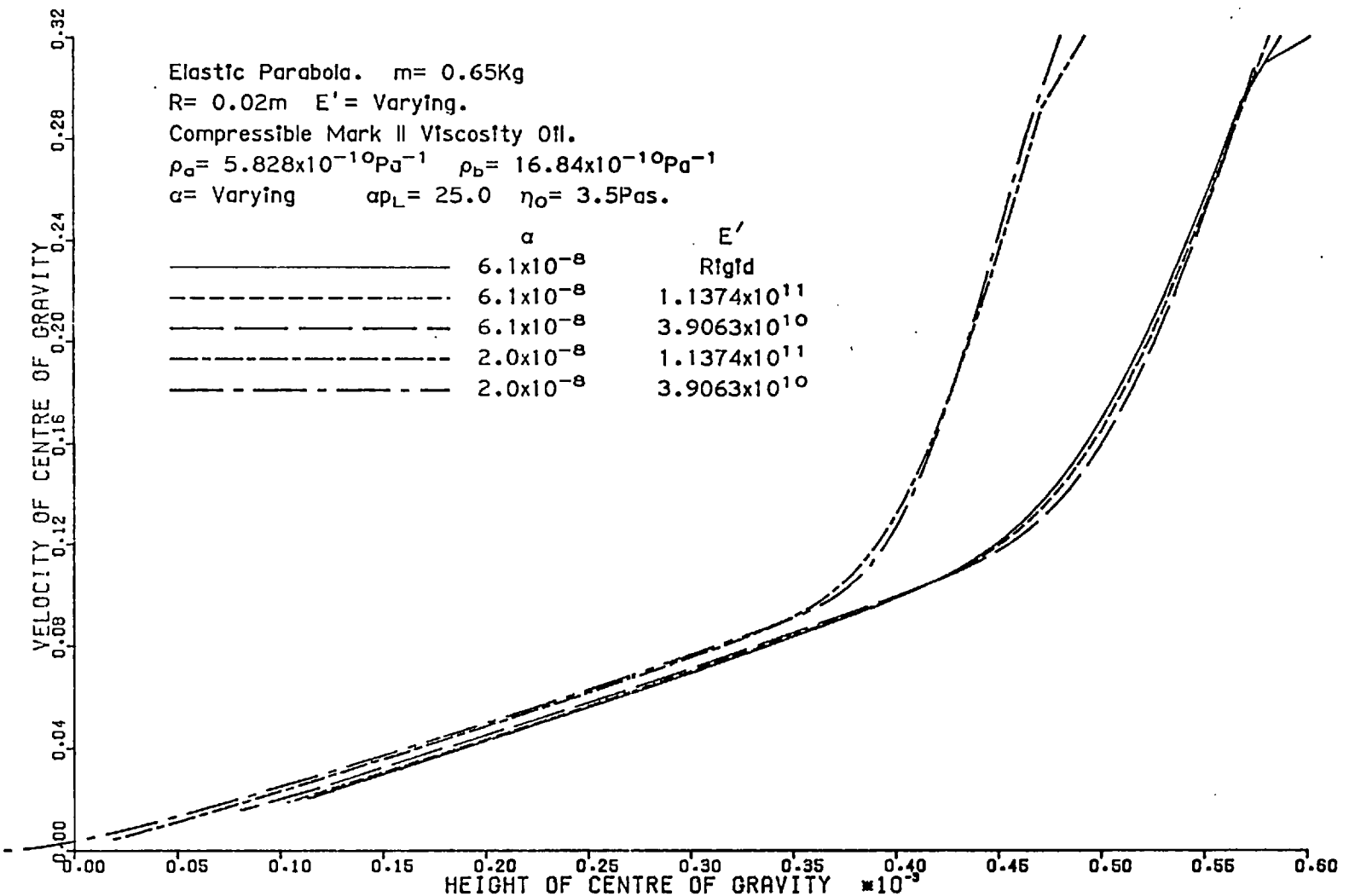
Elastic Parabola. m= 0.65Kg
R= 0.02m E'= Varying.
Compressible Mark II Viscosity Oil.
ρ_a= 5.828x10^{-10}Pa^{-1} ρ_b= 16.84x10^{-10}Pa^{-1}
α= Varying αp_L= 25.0 η_o= 3.5Pas.
α
E′
6.1x10^{-8} Rigid
6.1x10^{-8} 1.1374x10^{11}
6.1x10^{-8} 3.9063x10^{10}
2.0x10^{-8} 1.1374x10^{11}
2.0x10^{-8} 3.9063x10^{10}
VELOCITY OF CENTRE OF GRAVITY
0.00 0.04 0.08 0.12 0.16 0.20 0.24 0.28 0.32
0.00 0.05 0.10 0.15 0.20 0.25 0.30 0.35 0.40 0.45 0.50 0.55 0.60
HEIGHT OF CENTRE OF GRAVITY *10^{-3}

Figure 6.22.

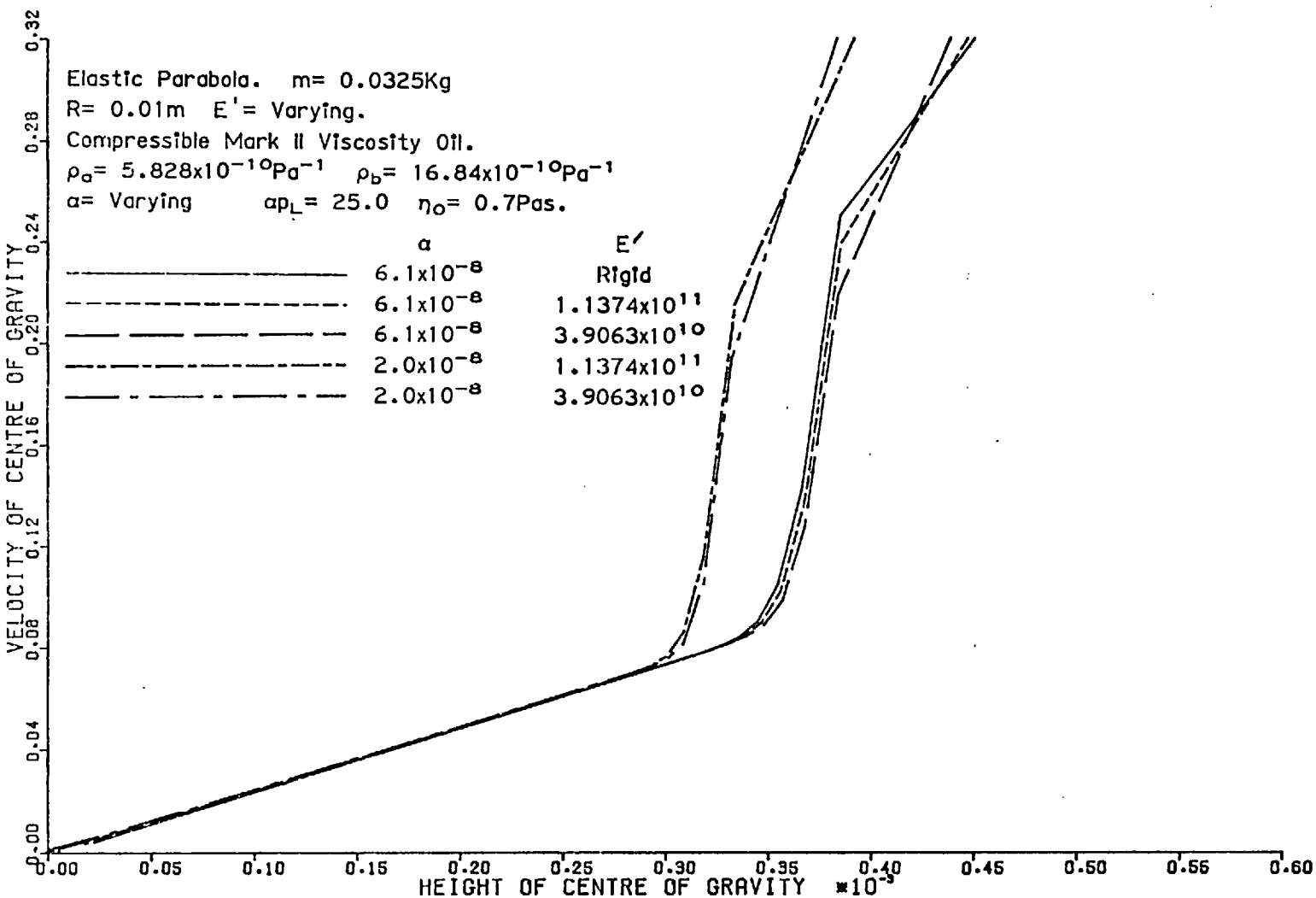
Elastic Parabola. m= 0.0325Kg
R= 0.01m E'= Varying.
Compressible Mark II Viscosity Oil.
ρ_a= 5.828x10^{-10}Pa^{-1} ρ_b= 16.84x10^{-10}Pa^{-1}
α= Varying αp_L= 25.0 η_o= 0.7Pas.
α
E'
6.1x10^{-8} Rigid
6.1x10^{-8} 1.1374x10^{11}
6.1x10^{-8} 3.9063x10^{10}
2.0x10^{-8} 1.1374x10^{11}
2.0x10^{-8} 3.9063x10^{10}
VELOCITY OF CENTRE OF GRAVITY
0.00
0.04
0.08
0.12
0.16
0.20
0.24
0.28
0.32
0.00
0.05
0.10
0.15
0.20
0.25
0.30
0.35
0.40
0.45
0.50
0.55
0.60
HEIGHT OF CENTRE OF GRAVITY *10^{-9}

Figure 6.23.

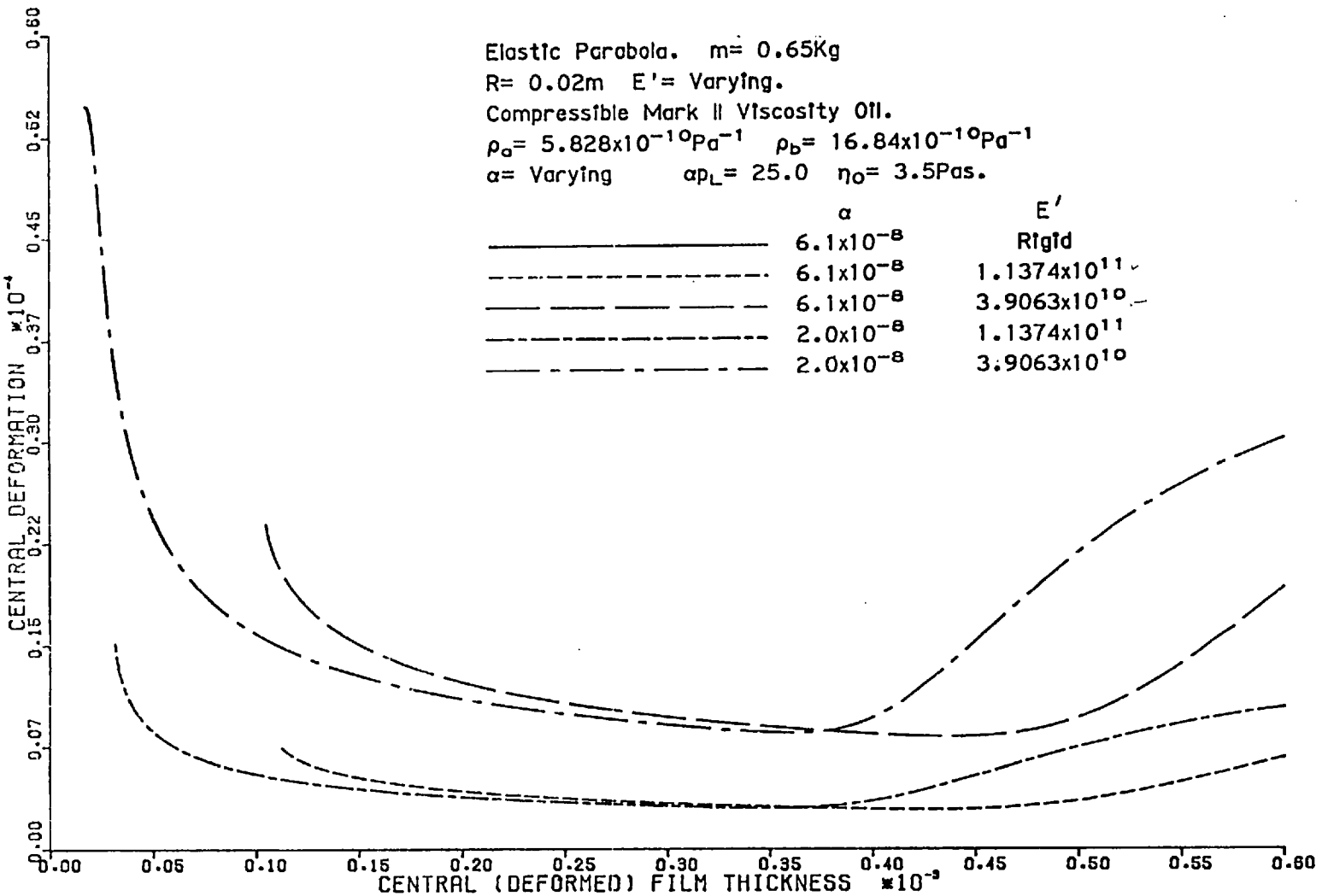
Elastic Parabola. m= 0.65Kg
R= 0.02m E'= Varying.
Compressible Mark II Viscosity Oil.
ρ_a= 5.828x10^{-10}Pa^{-1} ρ_b= 16.84x10^{-10}Pa^{-1}
α= Varying αp_L= 25.0 η_o= 3.5Pas.
α
E'
6.1x10^{-8} Rigid
6.1x10^{-8} 1.1374x10^{11}
6.1x10^{-8} 3.9063x10^{10}
2.0x10^{-8} 1.1374x10^{11}
2.0x10^{-8} 3.9063x10^{10}
CENTRAL DEFORMATION x10^{-4}
0.00
0.07
0.15
0.22
0.30
0.37
0.45
0.52
0.60
0.00
0.05
0.10
0.15
0.20
0.25
0.30
0.35
0.40
0.45
0.50
0.55
0.60
CENTRAL (DEFORMED) FILM THICKNESS x10^{-3}

Figure 6.24.

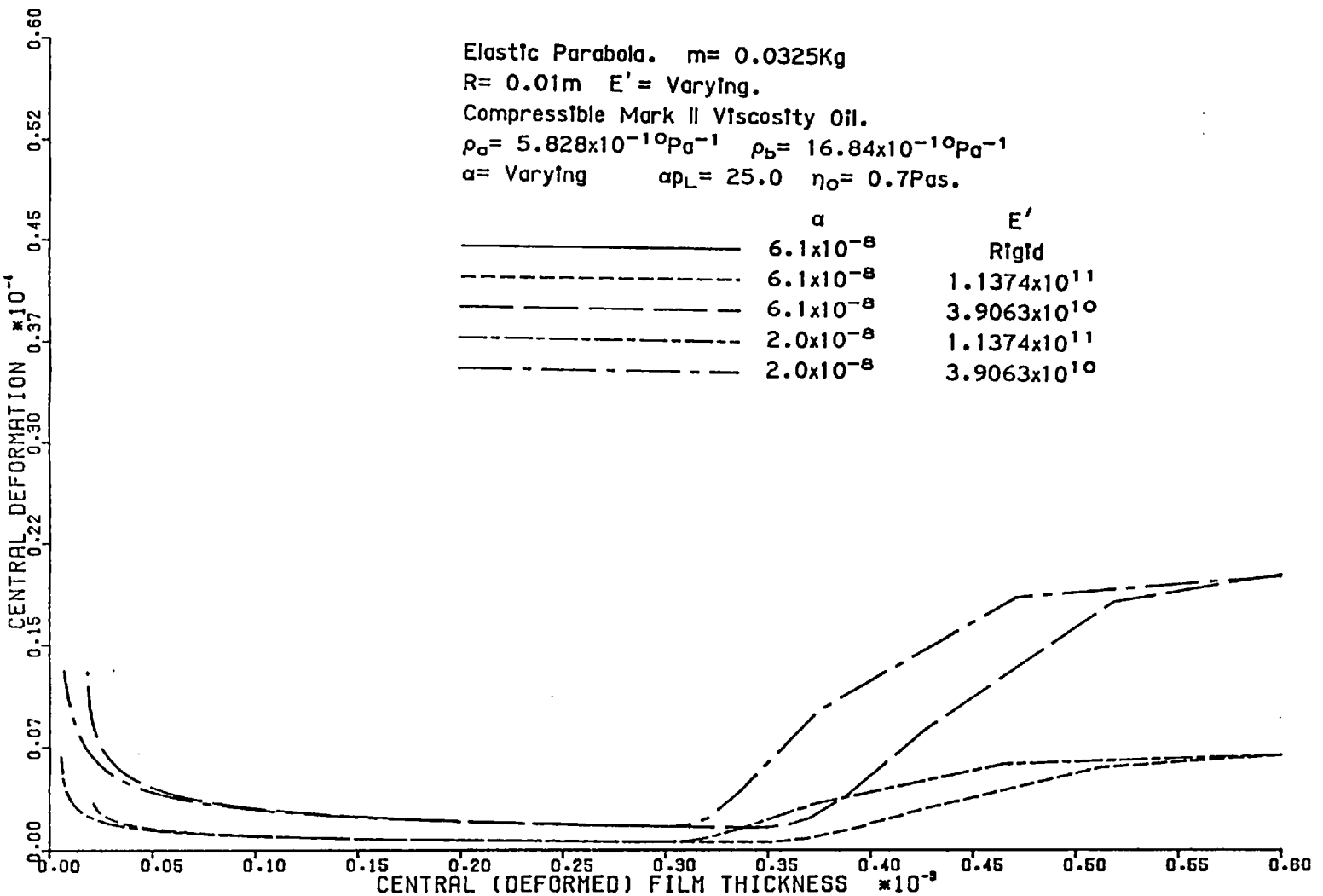
Elastic Parabola. m= 0.0325Kg
R= 0.01m E' = Varying.
Compressible Mark II Viscosity Oil.
ρ_a= 5.828x10^{-10}Pa^{-1} ρ_b= 16.84x10^{-10}Pa^{-1}
α= Varying αp_L= 25.0 η_o= 0.7Pas.
α
E'
6.1x10^{-8} Rigid
6.1x10^{-8} 1.1374x10^{11}
6.1x10^{-8} 3.9063x10^{10}
2.0x10^{-8} 1.1374x10^{11}
2.0x10^{-8} 3.9063x10^{10}
CENTRAL DEFORMATION *10^{-4}
0.00
0.07
0.15
0.22
0.30
0.37
0.45
0.52
0.60
0.00
0.05
0.10
0.15
0.20
0.25
0.30
0.35
0.40
0.45
0.50
0.55
0.60
CENTRAL (DEFORMED) FILM THICKNESS *10^{-9}

Figure 6.25.

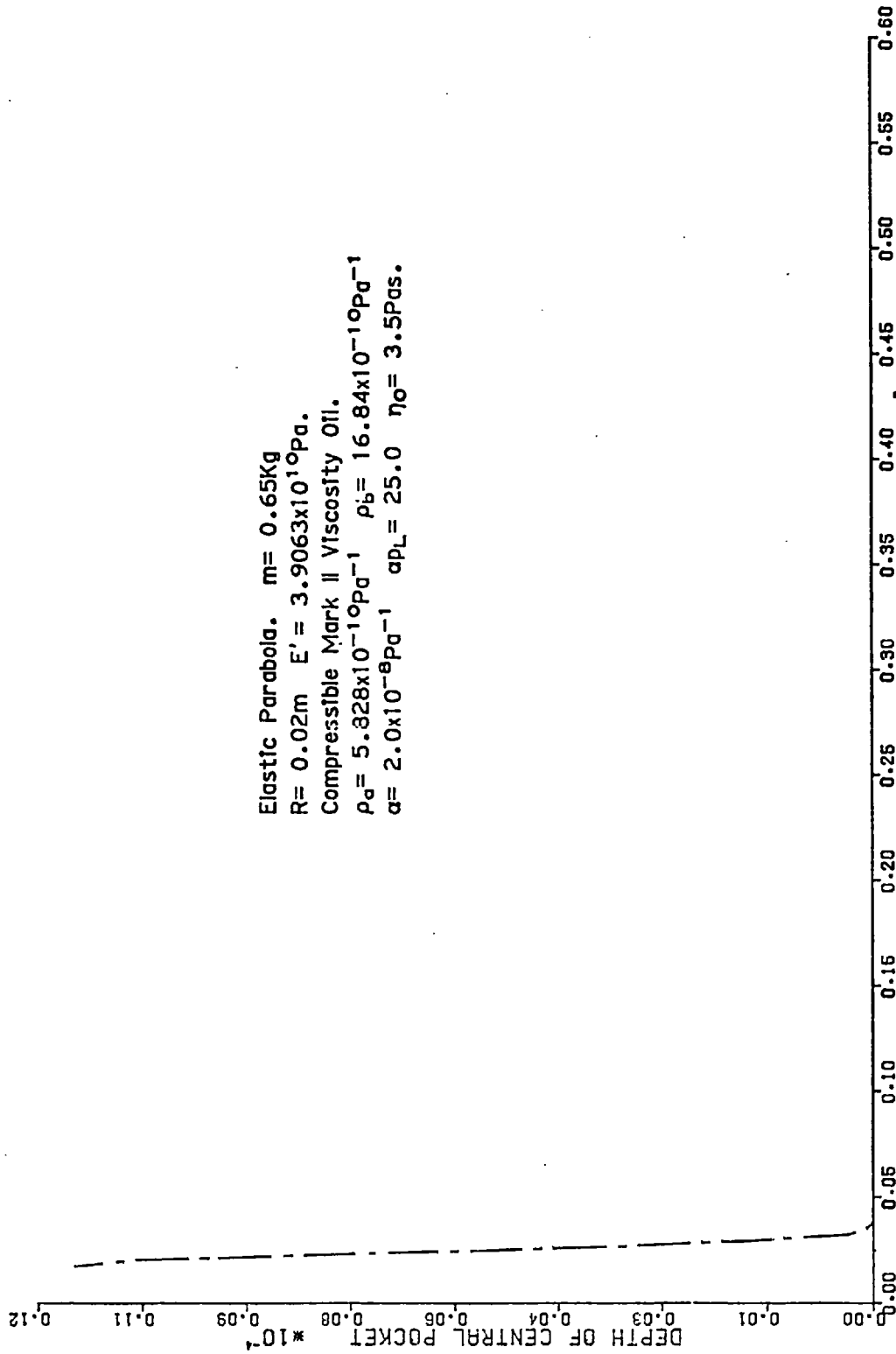
Elastic Parabola. m= 0.65Kg
R= 0.02m E'= 3.9063x10^10Pa.
Compressible Mark II Viscosity Oil.
ρa= 5.328x10^-10Pa^-1 ρb= 16.84x10^-10Pa^-1
α= 2.0x10^-8Pa^-1 αpL= 25.0 η0= 3.5Pas.
DEPTH OF CENTRAL POCKET *10^-4
0.00
0.01
0.03
0.04
0.06
0.08
0.09
0.11
0.12
0.00
0.05
0.10
0.15
0.20
0.25
0.30
0.35
0.40
0.45
0.50
0.55
0.60
CENTRAL (DEFORMED) FILM THICKNESS *10^-3

Figure 6.26.

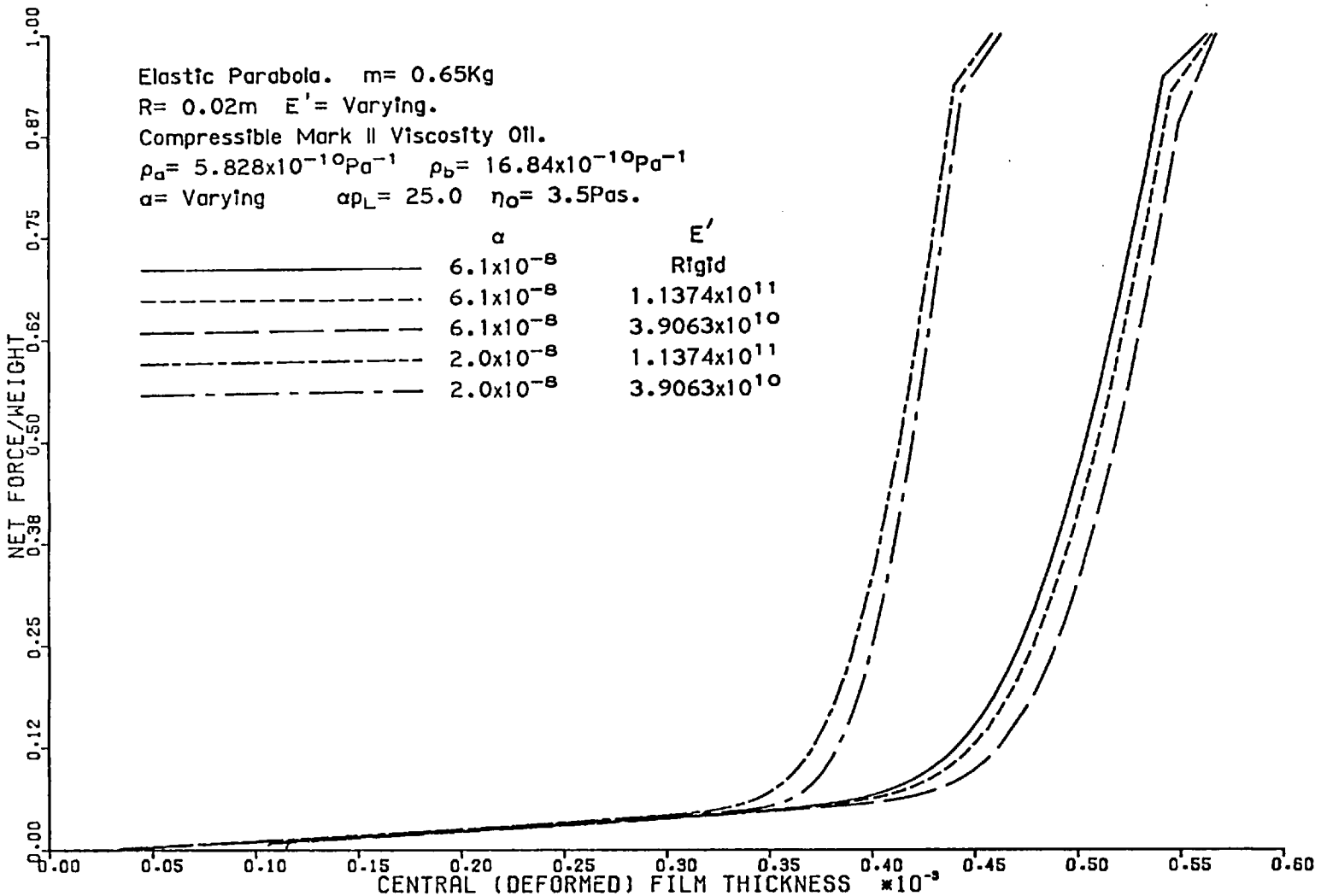
Elastic Parabola. m= 0.65Kg
R= 0.02m E'= Varying.
Compressible Mark II Viscosity Oil.
ρ_a= 5.828x10^{-10}Pa^{-1} ρ_b= 16.84x10^{-10}Pa^{-1}
α= Varying αp_L= 25.0 η_o= 3.5Pas.
α E'
6.1x10^{-8} Rigid
6.1x10^{-8} 1.1374x10^{11}
6.1x10^{-8} 3.9063x10^{10}
2.0x10^{-8} 1.1374x10^{11}
2.0x10^{-8} 3.9063x10^{10}
NET FORCE/WEIGHT
0.00
0.12
0.25
0.38
0.50
0.62
0.75
0.87
1.00
0.00
0.05
0.10
0.15
0.20
0.25
0.30
0.35
0.40
0.45
0.50
0.55
0.60
CENTRAL (DEFORMED) FILM THICKNESS *10^{-3}

Figure 6.27.

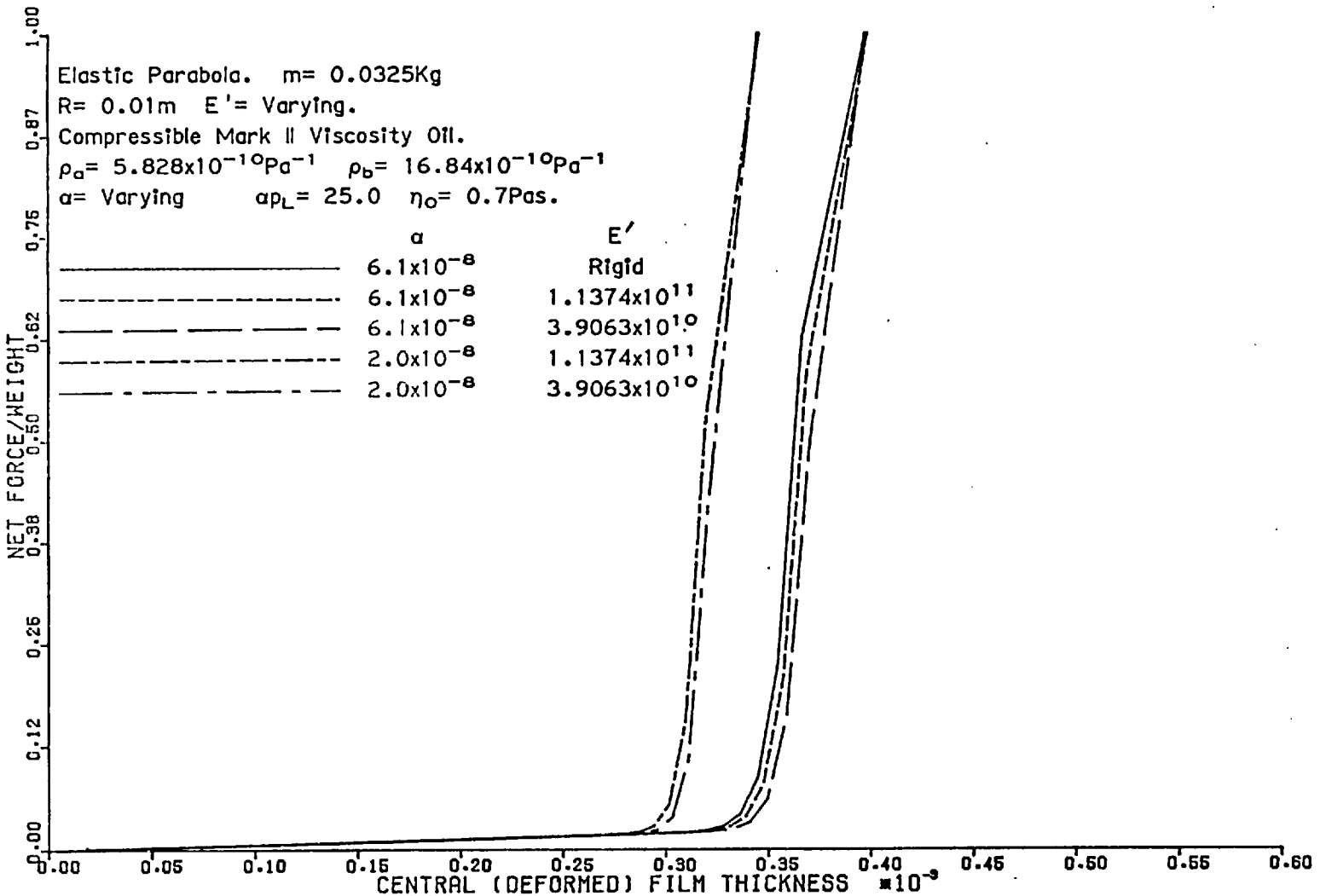
Elastic Parabola. m= 0.0325Kg
R= 0.01m E'= Varying.
Compressible Mark II Viscosity Oil.
ρ_a= 5.828x10^{-10}Pa^{-1} ρ_b= 16.84x10^{-10}Pa^{-1}
α= Varying αp_L= 25.0 η_o= 0.7Pas.
α
E'
6.1x10^{-8} Rigid
6.1x10^{-8} 1.1374x10^{11}
6.1x10^{-8} 3.9063x10^{10}
2.0x10^{-8} 1.1374x10^{11}
2.0x10^{-8} 3.9063x10^{10}
NET FORCE/WEIGHT
0.00
0.12
0.25
0.38
0.50
0.62
0.75
0.87
1.00
0.00
0.05
0.10
0.15
0.20
0.25
0.30
0.35
0.40
0.45
0.50
0.55
0.60
CENTRAL (DEFORMED) FILM THICKNESS *10^{-3}

Figure 6.28.

Elastic Parabola. m= 0.65Kg
R= 0.02m E'= 1.1374x10^11Pa.
Compressible Mark II Viscosity Oil.
ρa= 5.828x10^-10Pa^-1 ρb= 16.84x10^-10Pa^-1
α= 2.0x10^-8Pa^-1 αpL= 25.0 ηo= 3.5Pas.
vc
v(0.25*a)
v(0.50*a)
v(1.00*a)
VELOCITY RELATIVE TO CENTRAL VELOCITY
0.50
0.87
1.25
1.63
2.00
2.37
2.75
3.12
3.60
0.00
0.10
0.20
0.30
0.40
0.50
0.60
0.70
0.80
0.90
1.00
1.10
1.20
CENTRAL (DEFORMED) FILM THICKNESS *10^-4

Figure 6.29.

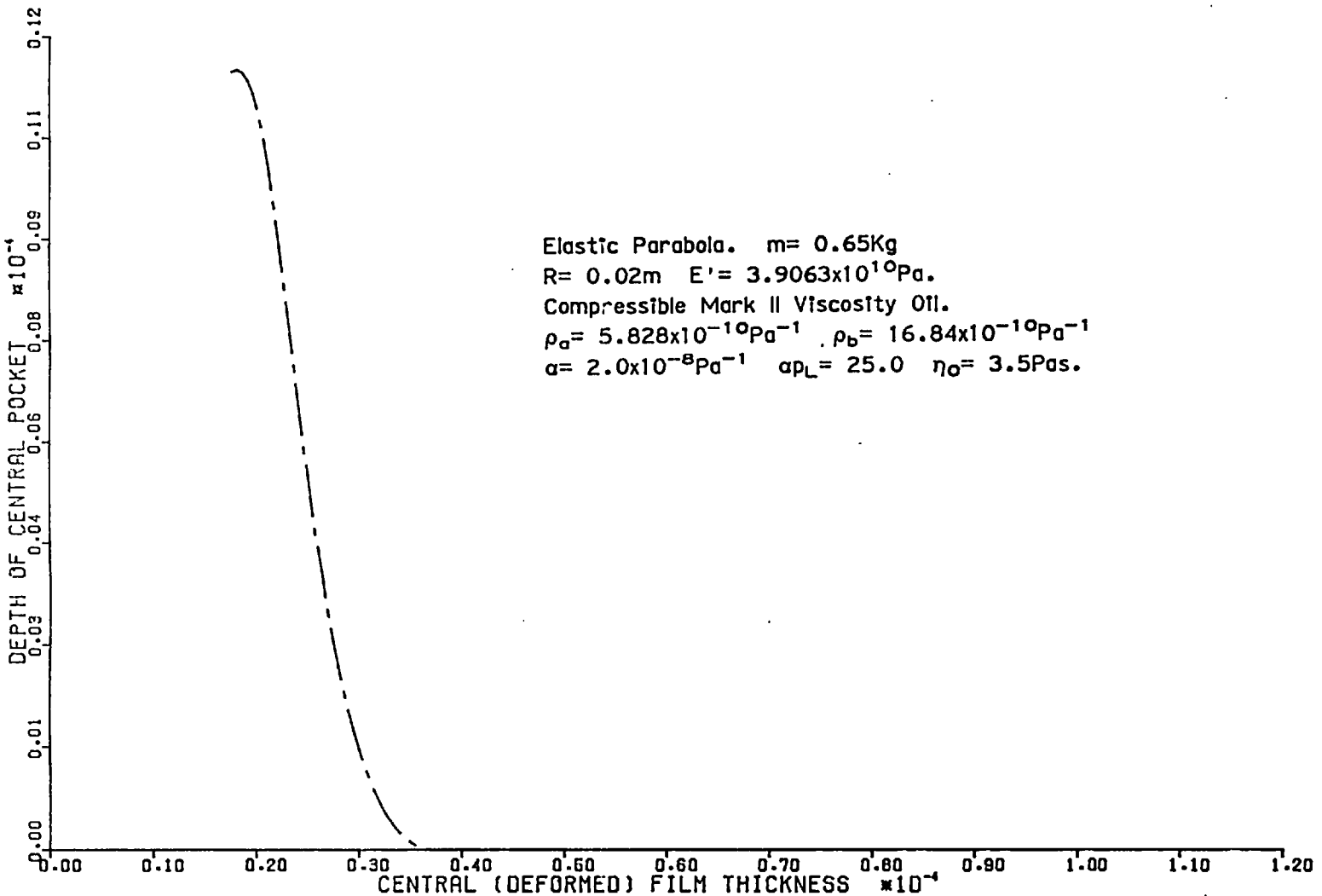
Elastic Parabola. m= 0.65Kg
R= 0.02m E'= 3.9063x10^10Pa.
Compressible Mark II Viscosity Oil.
ρa= 5.828x10^-10Pa^-1 ρb= 16.84x10^-10Pa^-1
α= 2.0x10^-8Pa^-1 αpL= 25.0 ηo= 3.5Pas.
DEPTH OF CENTRAL POCKET *10^-4
0.00
0.01
0.03
0.04
0.06
0.08
0.09
0.11
0.12
0.00
0.10
0.20
0.30
0.40
0.50
0.60
0.70
0.80
0.90
1.00
1.10
1.20
CENTRAL (DEFORMED) FILM THICKNESS *10^-4

Figure 6.30.

The graphs are grouped together according to the major axes rather than the run number. Figures 6.1 - 6.13 show $\log_{10}p_c$, v_c/R, h_c/R, $m\dot{v}_c/W$ plotted against time for different initial velocities as well as physical parameters. Figure 6.12 shows the effect of ignoring the elasticity of the ball completely and also of ignoring just the local deformation velocity, $\frac{dw}{dt}$.

Figures 6.14 - 6.16 show the central pressure plotted against the central (deformed) film thickness ($h(0)=h_c+w(0)$). Figures 6.17 - 6.19 give phase plane diagrams of $h(0)$, i.e. $v(0)$ vs. $h(0)$. Figure 6.20 shows the ratio of velocity of several points on the surface relative to v_c against $h(0)$, Figure 6.29 gives the same graph plotted to a different horizontal scale.

Figures 6.21 - 6.23 are phase plane diagrams of h_c, i.e. v_c vs. h_c. Figures 6.24 and 6.25 have the central deformation, $w(0)$, plotted against the central film thickness $h(0)$; Figure 6.26 gives the depth of the entrapment plotted against $h(0)$. The depth of the entrapment is given by $\sup(h(0)-h(r))$. This graph is also replotted as Figure 6.30 with a different horizontal scale. Figures 6.27 and 6.28 give $m\bar{v}_c/W$ plotted against $h(0)$.

6.5 Central Pressure

This is the most sensitive of the derived quantities and thus gives the best indication of slight differences in changes of algorithms or parameters.

The effect of elasticity is to relieve the pressure, thus making the pressure distribution less spiked: the amount of relief is determined

by the elastic coeeficient. As the pressure becomes more spiked, in the later stages of impact, more of the load is concentrated in the middle of the contact, thus tending to invalidate the assumption of no horizontal deformation.

Where the pressure diverges from the straight power law, (isoviscous solution), the elastic results diverge from the rigid results. Thus, it is concluded that whenever the effect of α needs to be accounted for, so does the elasticity of the body, for the range of α and E' considered in this work.

By increasing the elasticity of the ball, the effect of α may be more than counteracted, and so the pressure increases less than log-linearly (i.e. isoviscous solution). Indeed, for the softest case it appears that a constant peak pressure is obtained.

From Figures 6.5 and 6.6, if the time base is moved then the second stage of the solution curves are superimposed. Hence, for the elastic case as well as the rigid incompressible case the intital velocity does not determine the trajectory in the region of fluid entrapment. (Unless the intitial position of the ball is in this region).

When the central pressure is plotted against $h(0)$, the curves fall into two groups, depending on the value of α (Figures 6.14, 6.15, 6.16). Within a group the curves diverge in the zone of significant distortion. This is to be expected as the ordinate is a function of deformation and thus of pressure.

6.6 Velocity Characteristics

The same remarks that applied to the rigid incompressible case apply

here, i.e. the initial velocity does not significantly influence the eventual trajectory, (see section 3.6.2). Figures 6.17, 6.18, 6.19 show phase-plane diagrams.

The result, by other workers (CHENG and LEE; CHRISTENSEN) that $v_c \sim h_c^2$ does not hold here due to the different assumptions made for the impacting process. Again, two groups are found, depending on α, though for the light mass, they are virtually inseparable when h(0) is small.

The figures show that the centre velocity is tending to zero at a finite film thickness indicating the existence of an entrapped pool of liquid. There is some noise in the results which is due to (1) a breakdown of the solution algorithm, and (2) the velocity being calculated from values written to a data file with only five significant figures.

In the low mass case, the extrapolated entrapment thickness is small, but the effect of a slight bounce may be seen. (Figure 6.19). This occurs just after the peak force and is due to pressure relief.

The approach velocity varies over the surface of contact, Figures 6.20, 6.29 and 6.30 show the local approach velocity non-dimensionalised with respect to the central local approach velocity at various multiples of the Hertzian radius. The relative value for the centre of gravity of the ball is also plotted. At the maximum film thickness shown in Figure 6.20, the centre point is moving faster than the centre of gravity due to the pressure field temporarily decreasing. As the pressure field starts increasing again, this is more than compensated for, and the centre point slows down much more rapidly than the centre of gravity.

The curves obtained are quite different to those obtained by CHENG and Lee for cylinders in that no values are obtained less than 0.8, but

the assumption of CHRISTENSEN that there is only a few percent difference is apparently in error, though this may be due to different assumptions of the trajectory. The maximum value of about 1.1 obtained by HERREBURGH, 1970, for cylinders also seems to be an underestimate.

The accuracy of the last part of Figure 6.20, where the ratios drop, is not known, as here the solution algorithm is breaking down. In this latter part of the solution, radially the local relative velocity is oscillating very rapidly, especially in the region of minimum film thickness. Unfortunately there was only one grid point in the immediate vicinity of the minimum film. Results indicate that the local pressure becomes negative at that point, but that further out radially the pressure field is positive again.

Figures 6.21, 6.22 and 6.23 show v_c plotted against h_c; negative values of h_c exist. Note that as a straight line relation holds, the velocity is an exponentially decaying function of film thickness. The observations regarding h(0) also apply for h_c.

6.7 Deformation

Figures 6.24 and 6.25 show the deformation plotted against the film thickness. The two groups depend on E', one group is about three times larger than the other group, reflecting the different values of E'.

For the low mass case, the maximum deformation is obtained during the force peak at which point large time steps were taken; here the curves are given by straight line segments.

In Figures 6.26 and 6.31, the pocket depth formed is plotted for the large mass, low α, low E' case (Run 4) against h(0). Note that the only

difference between the graphs is the horizontal scale used. The film is extremely thin before the entrapment really starts to form - less than 1 μm - and it rapidly increases in depth and gradually becomes wider as the impact progresses.

The pressure field outside the minimum film thickness is supporting less and less of the load as it is being concentrated near to the pole. This will have the effect of making the horizontal distortion more and more important as time increases, however, the run including horizontal distortion is virtually indistinguishable from the run ignoring it (- a change in peak pressure at any time of less than 0.1%). The form of the horizontal distortion was the same as given in Section 5.5.2 and with the maximum magnitude of the distortion about 20% of the central vertical deformation and occured at about 5 Hertzian radii from the centre.

It is to be expected that as the load is further concentrated at the centre, the point of maximum horizontal distortion will move towards the centre and if it comes close to being within the entrapment zone then this distortion will have a significant effect on the subsequent entrapment.

6.8 Film Force

Figures 6.17 and 6.28 show the net force/weight vs. h(0). The film is quite thin before the net force become small compared to the weight of the ball. Again the two groups are found depending on α. Different values of α cause significant changes in the peak force attained in the high mass case, but not for the low mass case, for higher pressures are generated due to the different value of K_2. Note how close the force lines lie to each other, showing how the force is sensitive to changes in film thickness, so that slight discrepancies are forced back on to the correct curve.

6.9 The Stability of the Algorithm

It is appropriate to discuss here the effect of changing the parameter used in the Vogelpohl substitution and also the points at which the programs were stopped.

A run was performed in which $h_0=0.1*\max(h_c,10^{-7})$, as against $h_0=\max(h_c,10^{-7})$ used for all other runs where the value of $\max(h_c,10^{-7})$ is h_c when $h_c>10^{-7}$, and h_c otherwise. It was found that the curves obtained were identical. This gave confidence in the solution algorithm being accurate for the results shown. It was mentioned in Section 4.7.3 that the load needs to be accurately calculated and it was this that caused the algorithm to break down and hence the solutions were not carried further. Near the end of some force curves there is a small change from the extrapolated line. This error will occur due to the accuracy requirement on the load becoming ever more stringent, as discussed in Section 3.5.1. The effect is exacerbated by the load being concentrated in the centre region, thus essentially solving for the pressure distribution with less than the full number of grid points.

This was the cause of failure for all runs except the high mass, low α, low E' run. This failed due to an insufficient number of points near to the minimum film thickness, as discussed earlier.

It should be realised that the breakdown of the model only occurs when the central film thickness is at most 2.4 μm (6 μin) for the high mass cases or 0.25 μm (0.6 μin) for the low mass cases. These are well within the surface roughness expected on machine components and even on polished components with the lightly loaded cases. Hence, integrating the system further is not really realistic for the model takes no account of asperity interaction, although by using more points integration may proceed.

CHAPTER SEVEN

CLOSURE

7.1 Summary on the Results.

1) The rigid parabola, isoviscous incompressible fluid system gives a good approximation to the fully varying case whilst the centre pressure is less than 10^7 Pa. After that time only the method that takes into account all variations gets close to the correct solution.

2) Machine precision limitations occur at quite low pressures when considering the load coupling effect, i.e. at about 2×10^8Pa and for any system above 5×10^8Pa.

3) For numerical experiments with preset errors, the solution used has to be extremely accurate in order to integrate the system.

4) As long as the initial film thickness is reasonably thick (i.e. about 1mm) then the trajectory followed will be independent of the initial conditions (v_s, h_s) as long as the ball can dissipate its energy by viscous action alone.

5) There are two groups which characterize the behaviour of the rigid imcompressible solution K_1 and K_2. The value of K_1 determines the rate of exponential decay in the second stage.

6) Using the parabolic approximation to the spherical profile of the ball gives negligible error.

7) For an impact which loses its energy by viscous flow the temperature generated will be small (see also Appendix III) and can be ignored.

8) For all elastic impacts a pocket is formed. This grows in size throughout the solution time, forming a pressurized central pocket. This region supports virtually all of the load. Outside this zone the pressure falls to zero.

9) As the effect of pressure dependent viscosity becomes important so does the elasticity. It is not true that the load is more influenced by piezoviscous behaviour than by elastic effects. (CHRISTENSEN).

10) The thickness of the oil film is likely to be strongly affected by the surface roughness of the impacting bodies by the time either elastic or non-isoviscous effects become significant. Consequently many aspects of the behaviour of the problem may be studied by just considering the rigid body isoviscous incompressible fluid system.

11) Pressures, far greater than the Herztian, are generated and maintained within the contact region.

12) For the pressures generated here the horizontal distortion is small and can be safely ignored. It is not, however, significantly difficult to include this effect.

13) The radial distribution of local elastic velocity cannot be ignored when the peak pressure is greater than 10^8Pa, which is shortly after the time when elastic and non-isoviscous effects begin to

apply. There is a large change through the contact zone, and it is interesting to note that in the region of minimum film thickness, the local velocity tends to push the surfaces together faster than the velocity of the centre of gravity, due to the changing pressure profile.

14. The solution coupling the ball dynamics produces significantly different results to those obtained assuming fixed central pressure. Such results should be used with caution.

7.2 Summary on the Computational Methods Used.

1) The only methods that are effective in integrating the limited viscosity-rigid body models are stiffly stable ones. However, they are of limited use when employed in the fully varying cases with local velocity variations included.

2) The Newton-Raphson method is needed to obtain results in the high pressure region. However, using it, the Reynolds, Elasticity and State Equations may be solved simultaneously.

3) The Vogelpohl substitution allowed results to be obtained more easily. By changing the substitution it was found that the results obtained were not sensitive to the particular parameter used.

4) The use of quintic spline interpolating polynomials allowed an accurate solution of high order to be obtained with virtually no extra work over that of the cubic spline. (The error in the solution is of the the order Δr^4). If the cubic spline formulation had been used for the pressure field determination, then a completely unified treatment of the problem would have been achieved. The

cubic spline pressure distribution determines the deformation and the $\underline{\underline{D}}_1$, $\underline{\underline{D}}_2$ matrices, and hence the revised pressure. However, in this case it was decided to use methods in which the truncation errors were of the same order. The unified method with a cubic spline formulation has been applied by RHODE and OH to rolling line contact problems. It is possible to use the quintic spline formulation to attain greater accuracy as long as there is no discontinuity in gradient through the domain. The extra curvature of the quintic elements mean that less points are needed in the region of the pressure spike.

5) The method used to obtain the compliance matrix is general in its application. When calculating the deformation due to an arbitrary pressure distribution the only error is that from a possible discretization error in the interpolating polynomial. The spatial derivative of the deformation may be found to the same order as the deformation by use of the given transformation. The form of the equation for the horizontal distortion is particularly amenable to calculation. An application of these matrices to the work of PAUL is given in Appendix V.

6) This model has been applied to the problem of a flat steel pad of area $10^{-6} m^2$ squeezing on air from a height of 0.5 μm (BOWYER, 1977).

7.3 Recommendations for Further Work.

The solution to this problem is not as trivial to obtain as it may at first sight appear.

Proposals to extend this work should be viewed with extreme caution. The solution of the problem, coupled in space and time, requires large

amounts of computer time. To obtain pressures significantly higher than those shown here with viscosity pressure models of an exponential form will require use of a machine with an extended word-length, either by hardware or by software simulation. However, there are very few machines currently available with a word length greater than 60 bits. Also, use of double precision multiplies the computation time by a factor of four.

If it is desired to perform further work, then areas to be explored are:-

1) Changing the grid mesh dynamically as the impact progresses in order to counteract loss of accuracy.

2) Increasing the number of mesh points used in order to gain accuracy in the calculation of the load. However, this enormously increases the amount of work necessary to obtain a solution.

3) The combination method given in 4.7 could be extended so that the outer zone has many more points than were used here. As the pressure and deformations are small in the outer region, two procedures could be used. These are:

   a) To calculate the deformations accurately at a few points and interpolate for the deformations.

   or

   b) Use elements that are of a higher order than the parabolic ones used here to integrate the Reynolds Equation in the outer zone.

   Neither of these procedures are totally satisfactory.

4) All the cases calculated in this work have modelled a ball freely falling and only being retarded by the liquid pool. To obtain higher loads being supported by the contact, a modification could be made, suggested by the experimental conditions of PAUL. It would be necessary to model external viscous damping, i.e.

$$m\dot{v}_c = \int_0^{r_s} 2\pi p r dr - mg - Cv_c$$

This would ensure that the velocity does not become large enough for the ball to bounce.

5) It is known that the fluid viscosity shows time-dependence as well as pressure-dependence. If a satisfactory model could be interpreted from experimental work then this model can be incorporated in the temperature solution method. (See Appendix III).

APPENDIX I

THE CALCULATION OF THE QUINTIC SPLINE

The algorithm is taken from AHLBERG, NILSON and WALSH, 1967, Chapter 4 for a quintic spline over $[0,R_s]$ with knots $\underline{R}$. It has the form

$$g(R)=a_i+b_i(R-R_i)+C_i(R-R_i)^2+d_i(R-R_i)^3+e_i(R-R_i)^4+f_i(R-R_i)^5 \quad , R\varepsilon\,[R_i,\ R_{i+1}] \qquad (A1.1)$$

As it is to have continuity up to the fourth derivative, and on writing $\Delta_i=R_{i+1}-R_i$, and $M_i=g^{iv}(R_i)$ together with $S_\Delta\,[r_1,\ldots r_n]$ as the nth divided difference over the mesh $\underline{\Delta}$, then

$$\frac{1}{120}\quad\frac{\Delta_{i-2}^2}{(\Delta_{i-2}+\Delta_{i-1})(\Delta_{i+2}+\Delta_{i-1}+\Delta_i)}\quad M_{i-2}$$

$$+\quad\frac{1}{120}\ \{\Delta_{i-2}^2+(\Delta_{i-2}+\Delta_{i-1})(3\Delta_{i-2}+\Delta_{i-1}(\frac{\Delta_i}{\Delta_{i-1}+\Delta_i})+2))/(\Delta_{i-2}+\Delta_i+\Delta_{i+1})$$

$$+\frac{\Delta_{i-1}^2(\Delta_i+\Delta_{i+1})}{(\Delta_{i-1}+\Delta_i)(\Delta_{i-1}+\Delta_i+\Delta_{i+1})}\ \}\ M_{i-1}$$

$$+\quad\frac{1}{120}\ \{\Delta_{i-1}\Delta_{i-2}(\frac{\Delta_{i-2}}{\Delta_{i-2}+\Delta_{i-1}}+2)+\frac{\Delta_{i-2}+\Delta_{i-1}}{\Delta_{i-2}+\Delta_{i-1}+\Delta_i}(3(\Delta_{i-1}+\Delta_i)+\Delta_i)\ +$$

$$+\ \Delta_i\ \Delta_{i+1}(\frac{\Delta_{i+1}}{\Delta_i+\Delta_{i+1}}+2)+\frac{\Delta_i+\Delta_{i+1}}{\Delta_{i-1}+\Delta_i+\Delta_{i+1}}(\Delta_{i-1}$$

$$+3(\Delta_{i-1}+\Delta_i)\ \}M_i$$

$$+\ \frac{1}{120}\{\ \Delta_{i+1}^2\ +(\Delta_i+\Delta_{i+1})(3\Delta_{i+1}+\Delta_i(\frac{\Delta_{i-1}}{\Delta_{i-1}+\Delta_i}+2))/(\Delta_{i-1}+\Delta_i+\Delta_{i+1})\ +$$

$$+\frac{\Delta_i^2(\Delta_{i-2}+\Delta_{i-1})}{(\Delta_{i-1}+\Delta_i)(\Delta_{i-2}+\Delta_{i-1}+\Delta_i)}\}M_{i+1}$$

$$+\frac{1}{120}\quad\frac{\Delta_{i+1}^3}{(\Delta_i+\Delta_{i+1})(\Delta_{i-1}+\Delta_i+\Delta_{i+1})}M_{i+2}$$

$$=(\Delta_{i-2}+\Delta_{i-1}+\Delta_i+\Delta_{i+1})\,S_\Delta[R_{i-2},R_{i-1},R_i,R_{i+1},R_{i+2}]\quad,\ 3\leq i\leq n-2 \qquad (A1.2)$$

Two further conditions are needed at each end in order to determine $\underline{M}$ explicitly. As it is required that the spline approximation and the function have the same slope at each end, the formula

$$\frac{\Delta_1^2}{\Delta_1+\Delta_2}\left[\frac{\Delta_2+\Delta_3}{\Delta_1+\Delta_2+\Delta_3}+\frac{2\Delta_1+3\Delta_2}{\Delta_1+\Delta_2}\right]M_1+\{\frac{(4\Delta_1+3\Delta_2)(\Delta_2+\Delta_3)}{\Delta_1+\Delta_2+\Delta_3}+\frac{\Delta_1}{\Delta_1+\Delta_2}(3\Delta_1+4\Delta_2)$$

$$+\frac{\Delta_2\Delta_3(2\Delta_2+3\Delta_3)}{(\Delta_2+\Delta_3)(\Delta_1+\Delta_2+\Delta_3)}\}M_2+\{\frac{\Delta_2(3\Delta_1+2\Delta_2)(\Delta_2+\Delta_3)}{(\Delta_1+\Delta_2)(\Delta_1+\Delta_2+\Delta_3)}+\frac{\Delta_3(3\Delta_2+4\Delta_3)}{\Delta_1+\Delta_2+\Delta_3}+\frac{\Delta_1\Delta_2^2}{(\Delta_1+\Delta_2)^2}\}M_3$$

$$+\frac{\Delta_3^3}{(\Delta_2+\Delta_3)(\Delta_1+\Delta_2+\Delta_3)}M_4=S[R_1,R_2,R_3,R_4]-\frac{\frac{1}{4}(g'(R_1)-S[R_1,R_2])+S[R_1,R_2,R_3])}{\Delta_1+\Delta_2}$$

(A1.3)

and its equivalent may be used. Their other formula for the end condition using $g''(R_1)$ is not applicable directly to this problem (though it could be made so, as outlined above), and the one chosen was that

$$\Delta^3M_1=0 \qquad (A1.4)$$

Similar relations hold for the point R_n.

This was chosen as it is simple to set up, and it enabled the function X^5 to be approximated to within round off error. The complete system to be solved was then a pentadiagonal matrix with two extra non-zero coefficients, these were eliminated first and then a standard method

[CONTE and DE BOOR, 1972] was used to solve the penta-diagonal matrix. Once $\underline{M}$ had been found, the first derivatives (4.1.31 of AHLBERG, NILSON and WALSH) were calculated using the formulae:-

$$\frac{\Delta_{i-1}^2}{30}M_{i-1} + \frac{\Delta_{i-1}^2-\Delta_i^2}{20}M_i - \frac{\Delta_i^2}{30}M_{i+1} = \frac{-2}{\Delta_{i-1}}g'(R_{i-1}) - \left(\frac{4}{\Delta_{i-1}} + \frac{4}{\Delta_i}\right)g'(R_i)$$

$$- \frac{2}{\Delta_i}g'(R_{i+1}) + \frac{6}{\Delta_i}S_\Delta[R_i,R_{i+1}] + \frac{6}{\Delta_{i-1}}S_\Delta[R_{i-1},R_i] \qquad \text{(A1.5)}$$

giving a tridiagonal matrix to solve. Although the first derivatives could have been calculated explicity, since this matrix equation was diagonally dominant, the equations were all well-conditioned and errors would be small. The second and third derivatives could be then calculated as explicit functions of the previously solved values.

Finally it should be noted that:-

$$\begin{aligned} g(R_i) &= a_i \\ g'(R_i) &= b_i \\ g''(R_i) &= 2c_i \\ g'''(R_i) &= 6d_i \\ g^{iv}(R_i) &= 24e_i = M_i \\ g^{v}(R_i) &= 120f_i \end{aligned} \qquad \text{(A1.6)}$$

Testing

It was tested by checking that it could accurately interpolate for $X^n, 0 \leq n \leq 5$ with 11 grid points over the range $[0,10]$ both with equidistant spacing and also with random spacing. It was found that with equidistant spacing, the interpolation was accurate to round off, about 13 significant figures, but using random spacing, the coefficients given in the book gave

erroneous results. This was due to typographical error in the equation for $g'(R_i)$ (e.g. $3h_2+2h_3$ should have read $3h_3+2h_2$); for changing to the formula given above gave results to within roundoff error.

Further tests were conducted showing that that at the grid points $g'(r)$ is correct to $O(\Delta^6)$ and $g''(r)$ to $O(\Delta^4)$, i.e. $k_1=6, k_2=4$.

APPENDIX II

THE CALCULATION OF $4\int_0^{\Phi}\int_0^{\sqrt{s^2-r^2\sin^2\phi}}(b^2+r^2\sin^2\phi)^{m/2}\,db\,d\phi$

A2.1 Introduction

It has been noted in Section 5.4.3 that for each value of m, there are three cases to be considered depending on whether the point whose deformation is required lies inside, on the edge of, or outside the applied pressure disk. As this makes a difference only in the angle subtended by the disk at the point under consideration, it is only the integration limit of it that is altered. Thus the integrals may be written as $\int_0^{\Phi} I_m(\phi)d\phi$, where $I_m(\phi)\equiv\int_0^{\sqrt{s^2-r^2\sin^2\phi}}(b^2+r^2\sin^2\phi)^{m/2}\,db$ depends only on the degree m, once r and s are fixed, then the integration with respect to ϕ is performed using the appropriate boundary conditions.

If the interpolating polynomial is of degree 1 then the integrals $I_m(\phi)$, m=0,1,...l need to be calculated. The highest order polynomial used here for the deformation coefficients is three. For each $I_m(\phi)$, the three further integrals are identified as:

i) $r<s$: $\Phi=\frac{\pi}{2}$, $I=\int_0^{\frac{\pi}{2}} I_m(\phi)\,d\phi$

ii) $r=s$: $\Phi=\frac{\pi}{2}$, $I=\int_0^{\frac{\pi}{2}} I_m(\phi)\,d(\phi)$

iii) $r>s$: $\Phi=\sin^{-1}\frac{s}{r}$ $I=\int_0^{\sin^{-1}\frac{s}{r}} I_m(\phi)\,d\theta\,\phi$

For this last case, to obtain solutions in terms of complete elliptic integrals, the substitution $r\sin\phi=s\sin\theta$ is made. So, $\sqrt{s^2-r^2\sin^2\phi}=s\cos\theta$ and $d\phi=\frac{s}{r}\cdot\frac{\cos\theta}{\sqrt{1-(s/r)^2\sin^2\theta}}\,d\theta$. Then $I=\frac{s}{r}\int_0^{\frac{\pi}{2}} I^*_m(\theta)\,\frac{\cos\theta}{\sqrt{1-(s/r)^2\sin^2\theta}}\,d\theta$, with $I^*_m(\theta)\equiv I_m(\phi)$

A2.2 $\underline{m=0}$

$$I_m(\phi)=4\int_0^{\sqrt{s^2-r^2\sin^2\phi}} db$$

$$= 4\sqrt{s^2-r^2\sin^2\phi}$$

Hence

i) $r<s$: $I=4\int_0^{\frac{\pi}{2}} \sqrt{s^2-r^2\sin^2\phi}\,d\phi = 4sE(\frac{r}{s})$

ii) $r=s$: $I=4s.\frac{\pi}{2}$

iii) $r>s$: $I=4\frac{s}{r}\int_0^{\frac{\pi}{2}} s\cos\theta\sqrt{1-(s/r)\sin^2\theta}\,d\theta$

A.2.3 $\underline{m=1}$

$$I_m(\phi) = \int_0^{\sqrt{s^2-r^2\sin^2\phi}} \sqrt{s^2+r^2\sin^2\phi}\; db$$

On integrating by parts

$$I_m(\phi)=2(s\sqrt{s^2-r^2\sin^2\phi} + r^2\sin^2\phi\sinh^{-1}\frac{\sqrt{s^2-r^2\sin^2\phi}}{r\sin\phi})$$

Hence

i) $r<s$: $I=2\int_0^{\frac{\pi}{2}} (s\sqrt{s^2-r^2\sin^2\phi} + r^2\sin^2\phi\sinh^{-1}\frac{\sqrt{s^2-r^2\sin^2\phi}}{r\sin\phi})\,d\phi$

$$= s^2E(\frac{r}{s}) - (r^2-s^2)K(\frac{r}{s})+r^2\{\frac{\pi}{2}\sinh^{-1}\frac{\sqrt{s^2-r^2}}{r} + \int_0^{\frac{\pi}{2}} \frac{\cos\phi}{\sin\phi\sqrt{1-(r/s)^2\sin^2\phi}}\,d\phi\}$$

ii) $r=s$: $I=s^2(1+\int_0^{\frac{\pi}{2}} \frac{\phi}{\sin\phi}\,d\phi)$

iii) $r>s$: $I=\int_0^{\frac{\pi}{2}} 2(s^2\cos\theta+s^2\sin^2\theta\sinh^{-1}\frac{\cos\theta}{\sin\theta})\frac{s\cos\theta}{r\sqrt{1-(s/r)^2\sin^2\theta}}\,d\theta$

$$= 2\left[\frac{s}{r}(r^2E(\tfrac{s}{r})-(r^2-s^2)K(\tfrac{s}{r})) + \frac{s^3}{r}\int_0^{\frac{\pi}{2}} \frac{\sin^2\theta\cos\theta}{\sqrt{1-(s/r)^2\sin^2\theta}} \sinh^{-1}\frac{\cos\theta}{\sin\theta}\,d\theta\right]$$

A2.4 $\underline{m=2}$

$$I_m(\phi) = 4\int_0^{\sqrt{s^2-r^2\sin^2\phi}} b^2+r^2\sin^2\phi\,d\phi = \frac{4\sqrt{s^2-r^2\sin\phi}}{3}[s^2+2r^2\sin^2\phi]$$

Hence

i) $r<s$: $I = \frac{4}{3}\int_0^{\frac{\pi}{2}} (s^2\sqrt{s^2-r^2\sin^2\phi} + 2r^2\sin^2\sqrt{s^2-r^2\sin^2\phi})\,d\phi$

$$= \frac{4s}{9}\left[(4r^2+s^2)E(\tfrac{r}{s}) - 2(r^2-s^2)K(\tfrac{r}{s})\right]$$

ii) $r=s$: $I = \frac{20s^3}{9}$

iii) $r>s$: $I = \frac{4}{3}\int_0^{\frac{\pi}{2}} s^3[\sin\theta-2\sin^2\theta\cos\theta]\frac{s}{r}\frac{\cos\theta}{\sqrt{1-(s/r)^2\sin^2\theta}}\,d\theta$

$$= \frac{4}{9r}\left[r^2(4r^2+s^2)E(\tfrac{s}{r}) - (3s^2+4r^2)(r^2-s^2)K(\tfrac{s}{r})\right]$$

A2.5 $\underline{m=3}$

$$I_m(\phi) = 4\int^{\sqrt{s^2-r^2\sin^2\phi}} (b^2+r^2\sin^2\phi)^{3/2}\,db$$

$$= s^3\sqrt{s^2-r^2\sin^2\phi} + 3r^2\sin^2\phi\,\frac{1}{2}\left(s\sqrt{s^2-r^2\sin^2\phi} + \phi r^2\sin^2\phi\sinh^{-1}\frac{\sqrt{s^2-r^2\sin^2\phi}}{r\sin\phi}\right)$$

Hence

i) $r<s$: $I=\int_0^{\frac{\pi}{2}} s^3\sqrt{s^2-r^2\sin^2\phi} + \frac{3}{2}r^2\sin^2\phi s\sqrt{s^2-r^2\sin^2\phi} + \frac{3}{2}r^4\sin^4\phi\sinh^{-1}$

$$\frac{\sqrt{s^2-r^2\sin^2\phi}}{r\sin\phi}\,d\phi$$

$$= \frac{1}{16}\left[s^2(4s^2+9r^2)E(\tfrac{r}{s}) - (12s^2+9r^2)(r^2-s^2)K(\tfrac{r}{s})\right]$$

$$+\frac{9r^4}{16}\left[\frac{\pi}{2}\sinh^{-1}\frac{\sqrt{s^2-r^2}}{r}+\int_0^{\frac{\pi}{2}}\frac{\phi\cos\phi}{\sin\phi\sqrt{1-(r/s)^2\sin^2\phi}}\,d\phi\right]$$

ii) $r=s$: $I=\frac{s^4}{16}\left[13+9\int_0^{\frac{\pi}{2}}\frac{\theta}{\sin\theta}\,d\theta\right]$

iii) $r>s$: $I=\int_0^{\frac{\pi}{2}}\frac{s^5}{r}\left(\cos\theta+\frac{3}{2}\sin\theta\cos\theta+\frac{3}{2}\sin^4\theta\sinh^{-1}\frac{\cos\theta}{\sin\theta}\right)\frac{\cos\theta}{\sqrt{1-(s/r)^2\sin^2\theta}}\,d\theta$

$$=\frac{s}{8r}\left[r^2(9r^2+2s^2)E(\tfrac{s}{r})-(r^2-s^2)(8s^2+9r^2)K(\tfrac{s}{r})\right]$$

$$+\frac{9}{8}s^3r\int_0^{\frac{\pi}{2}}\frac{\sin^2\theta\cos\theta\sinh^{-1}\frac{\cos\theta}{\sin\theta}}{\sqrt{1-(s/r)^2\sin^2\theta}}\,d\theta$$

A2.6 Conclusion

For any r,s and m ($m<4$), the integral may be calculated from one of above formulae. The E(k) and K(k) are complete elliptic integrals of the first kind and the integrals that are explicitly written out must be calculated by quadrature, (e.g. Gaussian quadrature).

It should be noted that as a check on the calculations, the various integrals are continuous over the boundary $r=s$ ($\lim_{k\to 1}(1-k^2)K(k)=0$).

APPENDIX III

ON THE THERMODYNAMIC IMPACT OF A RIGID BALL ONTO AN OIL FILM

A3.1 The Problem

A3.1.1 Introduction

Some exploratory work was carried out on the feasibility of calculating the temperature distribution within the oil fim. It was assumed that the ball was of rigid parabolic section, squeezing onto an exponential viscosity pressure temperature-modified oil.

A3.1.2 The Equations to be Solved.

Dynamic

$$m\dot{v}_c = \int_0^{r_s} 2\pi p r dr - mg \qquad (A3.1)$$

Ball Shape

$$h(r) = h_c + r^2/2R \qquad (A3.2)$$

Reynolds Equation

$$\frac{1}{r}\frac{\partial}{\partial r}\left(rM_2\frac{\partial p}{\partial r}\right) = \int_0^h \left(\frac{\partial \rho}{\partial t}\right)dz + [\rho w]_0^h \qquad (A3.3)$$

where $$M_2 = \frac{F_1 M_1}{F_0} - \int_0^h \rho \int_0^z \frac{z'dz'}{\eta} dz$$

$$M_1 = \int_0^h \rho \int_0^z \frac{dz'}{\eta} dz$$

$$F_1 = \int_0^h \frac{z dz}{\eta} = \bar{z} F_0$$

$$F_0 = \int_0^h \frac{dz}{\eta}$$

Thermodynamic

$$\rho C_p \frac{DT}{Dt} - \left(\frac{\partial v}{\partial T}\right)_p T \frac{Dp}{Dt} = K\nabla^2 T + \Phi \qquad \text{(A3.4)}$$

where $$\Phi = \eta\left[2\left(\left(\frac{u_r}{r}\right)^2 + \left(\frac{\partial u_r}{\partial r}\right)^2 + \left(\frac{\partial u_z}{\partial z}\right)^2\right) + \left(\frac{\partial u_r}{\partial z} + \frac{\partial u_z}{\partial r}\right)^2 - \frac{2}{3}\left[\frac{u_r}{r} + \frac{\partial u_r}{\partial r} + \frac{\partial u_z}{\partial z}\right]^2\right] \qquad \text{(A3.5)}$$

Pressure-Temperature Viscosity

$$\eta = \eta_0 e^{\alpha p + \beta T} \qquad \text{(A3.6)}$$

Pressure-Temperature Density

$$\rho = \rho_0\left(1 + \frac{\rho_a p}{1+\rho_b p} + \varepsilon T\right) \qquad \text{(A3.7)}$$

The thermodynamic equation is from DOWSON and WHITTAKER, 1965, assuming no external heating and the conductivity of the oil is constant. It was decided not to eliminate any of the terms in Φ using an order of magnitude analysis as there were high rates of shear whose relative magnitudes varied greatly from point to point.

A3.1.3 The Fluid Velocity

These are needed in the calculation of the temperature. It is necessary to calculate temperatures outside the contact zone so velocities there are also needed. Two sets of formulae are needed.

I. Within the Contact Zone

For the radial velocity, u_r

$$u_r(z) = \frac{\partial p}{\partial r} \int_0^z \frac{z-\bar{z}}{\eta}\, dz \qquad \text{(A3.8)}$$

The vertical velocity, u_z, is obtained by integrating the continuity equation

$$u_z(z) = -\frac{1}{\rho}\int_0^z \frac{1}{r}\frac{\partial}{\partial r}(ru_r)dz \qquad (A3.9)$$

II Outside the Contact Zone

A more complicated system holds here. This is because the liquid has a free surface, so the assumption that $u_r(h_s)=0$ is invalid. It was decided to model the outer zone by assuming that:

a. Incompressible continuity holds

b. $u_z(z)$ is indentically zero

c. The film is of constant thickness h_s

d. The approximately parabolic velocity profile (at the end of the contract) changes into an exponential one. This will be such that $u_r(r_{max}) = C\frac{1-e^{-x(z/h_s)}}{1-e^{x}}$ where x is chosen to give $1-e^{-x/8}=0.6(1-e^{-x})$ [i.e. the first grid point from the plane has 60% of the maximum velocity] and C is calculated so that continuity holds.

e. If the edge of the contact is at $r=r_s$ then the flow there is $\int_0^{h_s} u_r\,dz\big|_{r_s}$. C is chosen so that $\int_0^{h_s} r_{max}u_r(r_{max})dz = \int_0^{h_s} r_s u_r(r_s)dz$.

The velocity at any intermediate value is calculated from

$$ru_r|_{r_x} = r_s\theta u_z|_{r_s} + r_{max}(1-\theta)u_z|_{r_{max}} \quad , \text{with}\ \theta = \left(\frac{r_x-r_{max}}{r_s-r_{max}}\right)^2$$

This satisfies continuity.

These assumptions for the fluid velocity in the outer region have been made in order to estimate the convection and conduction effects before they (perhaps) become enclosed by the contact zone. It is important to note that these assumptions are made only to obtain answers in the right order of magnitude. It is not suggested in any way that these are definitive conditions. To obtain a complete solution is not feasible.

A3.1.4 Thermal Boundary Conditions

Boundary conditions are needed for the temperature field.

1) Radially $-\frac{\partial T}{\partial r} = 0$ at $r=0$ and $r=r_{max}$

2) Vertically

a) For the free surface $(z=h_s, r\varepsilon[r_s, r_{max}])$

$$\frac{\partial T}{\partial z} = 0$$

b) For the Solid-Oil Interface, there are four main possibilities:

i) Isothermal

$T=0$

ii) Adiabatic

$$\frac{\partial T}{\partial z} = 0$$

iii) Full Thermodynamic

$$(K\frac{\partial T}{\partial z})_{oil} = (K\frac{\partial T}{\partial z})_{solid}$$

iv) Approximation to Thermodynamic

$$(K\frac{\partial T}{\partial z})_{oil} = C, \text{ a constant}$$

The actual surface temperature will be bounded by the Isothermal and Adiabatic conditions.

These were the only conditions considered.

A3.2 Method

The equations were solved by mapping a fixed (in space) finite difference grid of 60 x 15 points. Derivatives of the form $\frac{\partial}{\partial t}$ were approximated by

backward difference formula and all others were approximated by a central difference formulae wherever possible. Truncation errors with respect to space and time were $O(\Delta r^2)$ and $O(\Delta t)$ respectively.

The Stokesian, $\frac{D}{Dt}$, arises as Eulerian co-ordinates are used. The fixed grid is used to represent accurately temperature and time derivatives and to account for the oil being heated outside the contact zone.

The Reynolds, Fluid Velocity and Thermodynamic equations were solved in rotation, converging first the Reynolds Equation, then calculating the velocities and finally the temperature. If any change in temperature were greater than some predetermined amount, the entire process was repeated.

A3.3 Results

The parameters used were

Solid:	$E' = \infty$ Pa^{-1}	R=0.01m	
Oil	$\alpha=6.1\times10^{-8}$ Pa^{-1}	$\rho_0=852.1$ kgm^{-3}	$\rho_a=5.828\times10^{-10}$ Pa^{-1}
	$\rho_b=16.84\times10^{-10}Pa^{-1}$	$C_p=2020$ J $kg^{-1}{}^0C^{-1}$	$\eta_0=0.7$ Pas
	$\varepsilon= -5.5\times10^{-4}{}^0C^{-1}$	$\beta= -0.04$ $^0C^{-1}$	K=0.1308 Wm $^0C^{-1}$
Initial conditions		$h_s=0.0005m$	$v_s= -0.1$ ms^{-1}
Thermal Boundary Conditions		1) Isothermal	2) Adiabatic.

The integration was carried out to a maximum time of 4.7×10^{-3}s. This is after the peak force and pressure have occurred.

When impact first occurs, the temperature profile within the contact was approximately parabolic across the film thickness, with the maximum near the centre-line. Outside of the contact the temperature tends to zero faster along the centre-line than at the edge of the film.

As the impact progresses the form of the distribution changes with the maximum temperature being generated at the exit zone of the contact ($r=r_s$) and near to the boundary solids. This result is conistent with the analysis of section 2.7.

The maximum temperature obtained at the force peak was 0.519^0C for isothermal boundary conditions and $2.24\ ^0C$ for the adiabatic boundary conditions.

APPENDIX IV

THE OPERATOR *

This operator is an extension of the Hadamard Product (see MINC and MARCUS, 1964) and is defined to operate on a vector and either a vector or a matrix. The number of rows in both operands must be equal.

Case 1 Both Operands Vectors

The result is a vector such that

$$\underline{c} = \underline{a} * \underline{b} = \underline{b} * \underline{a}$$

The elements of $\underline{c}$ are given by

$$c_k = a_k \, b_k$$

i.e. the kth element is $\underline{a}$ multiplied by the kth element of $\underline{b}$ to give the kth element of $\underline{c}$.

Case 2 One Operand in a Matrix

The result is a matrix such that

$$\underline{\underline{C}} = \underline{\underline{A}} * \underline{b} = \underline{b} * \underline{\underline{A}}$$

The elements of $\underline{\underline{C}}$ are given by

$$(\underline{\underline{C}})_{jk} = (\underline{\underline{A}})_{jk} (\underline{b})_j$$

i.e. the kth row of $\underline{\underline{A}}$ is multiplied by the kth element of $\underline{b}$ to give the kth row of $\underline{\underline{C}}$.

Note that

$$(\underline{\underline{A}}.\underline{b})*\underline{c} = \underline{c}*(\underline{\underline{A}}.\underline{b}) = (\underline{c}*\underline{\underline{A}}).\underline{b}$$

but

$$(\underline{\underline{A}}.\underline{b})*\underline{c} \neq \underline{\underline{A}}*(\underline{b}.\underline{c})$$

APPENDIX V

AN APPLICATION OF THE COMPLIANCE MATRICES TO THE WORK OF PAUL, 1971

PAUL, 1971 describes an experiment in which the film thickness within an extrapment is measured and, using the theory of elasticity, the applied pressure is calculated. The method of calculation used is given in RANGER, 1974.

The problem consists of finding the pressure at n points, given the film thickness at n + 1 points, the value of h_c being unknown. So the problem reduces to solving the n + 1 equations

$$\underline{h}_i = h_c + s(\underline{r}_i) + \underline{w}_i \qquad , \qquad 1 \leq i \leq n+1 \qquad \text{(A5.1)}$$

A matrix $\underline{\underline{E}}$ may be calculated as given in Chapter 5 for the n pressure points $\underline{p}$, giving the n+1 deformations $\underline{w}$.

Then

$$\underline{h} = (\underline{\underline{E}} \mid \underline{v}) \; (\underline{p} \mid h_c) + \underline{s} \qquad \text{(A5.2)}$$

where $\underline{v}$ is the vector $(1\ 1\ 1 \ldots\ 1)^T$

$\underline{s}$ is given by $\underline{s}_i = \underline{r}_i^2 \,/\, 2R = \underline{r}_* \underline{r}_* / 2R$

With some extra work, this result may be extended to allow for the horizontal deformation. This is done by realising the elements of $\underline{s}$ should be corrected to account for the fact that the undeformed surface is moved when the pressure is applied. Thence a corrected $\underline{s}$, $\underset{\sim}{\underline{s}}$ where

$$\underset{\sim}{\underline{s}}_i = \frac{(\underline{r}_i - \underline{u}_i)^2}{2R} \qquad \text{(A5.3)}$$

Thus if $\underline{U}$ is calculated, in the same manner as $\underline{\underline{F}}$, then

$$\tilde{\underline{s}} = \underline{s} - \frac{1}{R}\underline{r}^*\underline{\underline{U}}\underline{p} + \frac{1}{2R}(\underline{\underline{U}}\underline{p})^*(\underline{\underline{U}}\underline{p}) \qquad (A5.4)$$

This gives a non-linear system to solve, and is not completely accurate, for the matrix $\underline{\underline{U}}$ was calculated at the points $\underline{r}$, not $\underline{r}-\underline{u}$, where it should be.

If it is assumed that the last term in $\underline{s}$ may be neglected, then a linear set of equations is obtained, giving

$$\underline{h} = ((\underline{\underline{F}} - \frac{1}{R}\underline{r}^*\underline{\underline{U}})|\underline{v})(\underline{p}|h_c) + \underline{s} \qquad (A5.5)$$

Hence

$$(\underline{p}|h_c) = ((\underline{\underline{F}} - \frac{1}{R}\underline{r}^*\underline{\underline{U}})|\underline{v})^{-1}(\underline{h}-\underline{s}) \qquad (A5.6)$$

REFERENCES

AHLBERG, J.H.; NILSON, E.N.; WALSH, J.L. 1967
"The Theory of Splines and their Applications". Academic Press.

ALLEN, C.W.; TOWNSEND, D.P.; ZARETSKY, E.V. 1970
"EHD Lubrication of a Spinning Ball in a Non-conforming Groove." TransASME Series F, Vol. 92, No. 1, pp. 89-96.

BOWYER, A. 1977
Private Communication. To be included in:- Computer Stick Slip Analysis. Ph.D. Thesis, London.

BUTLER, L.H. 1960
"The Hydrodynamic Effect between Approaching Surfaces with Interposed Viscous Fluid Films, and its Influence on Surface Deformations." J. Inst. Petroleum, Vol. 46, No. 435, pp. 63-73, March 1960.

CAMERON, A. 1967
"The Principles of Lubrication." Wiley, New York.

CHENG, H.S. and LEE, K.M. 1971
"The Pressure and Deformation Profile Between Two Colliding Lubricated Cylinders." NASA Contract Report Cr 1944. Nov. 1971

CHRISTENSEN, H. 1960
"The Oil Film in a Closing Gap." Ph.D. Thesis, Leeds.

CHRISTENSEN, H. 1962
"The Oil Film in a Closing Gap." Proc. Roy. Soc. Series A, Vol. 266, pp.312-328.

CHRISTENSEN, H. 1967

"Elastohydrodynamic Theory of Spherical Bodies in Normal Approach Motion." MTI 67TR21, April 1967.

CHRISTENSEN.H. 1970

"Elastohrdrodynamic Theory of Spherical Bodies in Normal Approach." Trans. ASME Series F, Journ. Lub. Tech. Vol. 92, No. 1, pp. 145-54, Jan. 1970.

CONTE, S.D.; DE BOOR, C. 1972

"Elementary Numerical Analysis: An Algorithmic Approach." 2nd Ed. McGraw-Hill, N.Y.

CONWAY, H.D. 1973

"The Rate of Change in Film Thickness in the Elastohydrodynamic Squeeze Film Process." Technical Brief Trans.ASME Series F, Vol. 95, pp.391-393.

CONWAY, H,D. and LEE, H.C. 1975

"Impact of a Lubricated Surface by a Sphere." Paper 75-Lub^{S-1}. ASME.

DOWSON, D. 1962

"A Generalised Reynolds Equation for Fluid-Film Lubrication." Int. J. Mech. Sci. Vol. 4, pp. 159-170.

DOWSON, D. and JONES, D.A. 1967

"Lubricant Entrapment Between Approaching Elastic Solids." Nature Vol. 214, No. 5091, pp. 947-8.

DOWSON. D. and WHITAKER, D.A. 1967

"A Numerical Procedure for the Solution of the EHD Problem of Rolling and Sliding Contacts Lubricated by a Newtonian Fluid." Proc. IME 180 Pt. 3B, pp. 57-71.

DWIGHT, H.B. 1961

"Tables of Integrals and Dther Mathematical Data." 4th Ed. McMillan Co.

EIRICH, F.R. and TABDR, D. 1948

"Collisions Through Liquid Films." Proc. Camb. Phil. Soc. Vol. 44, pp.566-58D.

FDDRD, C. 1968

"Pitting and Film Thickness in Rolling Contact." Ph.D. Thesis, London.

FDWLES, P.E. 197D

"A Simpler Form of the General Reynolds Equation." Trans ASME Series F, Vol. 92, pp. 661-662.

GAMAN, I.D.C.; HIGGINSDN, G.R. and NDRMAN. R. 1974

"Fluid Entrapment by a Soft Surface Layer." Wear. Vol. 28, 1974, pp.345-352

GEAR, C.W. 1971

"Numerical Initial Value Problems in Drdinary Differential Equations." Prentice-Hall Inc. NJ 1971.

GOULD, P. 1971

"High Pressure Spherical Squeeze Films." Jan 1971, Trans ASME Series F, Vol. 93, pp. 207-8.

HERREBURGH, K. 1970

"EHL Squeeze Films Between Two Cylinders in Normal Approach." (69-Lub-13) J. Lub. Tech. ASME Series F, Vol. 92, pp. 292-302.

HINDMARSH, A.C. 1974

"GEAR: Drdinary Differential Equations Solver." UCID 30001 Rev. 3, Dec. 1974

Lawrence-Livermore Lab.

HINDMARSH, A.C. and BYRNE, G.D. 1975

"EPISODE: An Experimental Package for the Integration of Systems of Ordinary Differential Equations." Lawrence Livermore Lab. UCID 30112 May 1975.

HIRST, W. and LEWIS, M.G. 1973

"The Rheology of Oils during Impact." III Elastic Behaviour, 1973. Proc. Roy. Soc. Series A, Vol. 334, pp. 1-18.

MARCUS, M. and MINC. H. 1964

"A Survey of Matrix Theory and Matrix Inequalities." Vol 14, Prindle, Weber and Schmidt, Inc. 1964.

MOORE, D.F. 1965

"Review of Squeeze Films." Wear-Usure-Verschleiss Vol. 8, pp. 245-263, 1965.

NAG 1977

Numerical Algorithm Group. Fortran Library Manual, Mark V Nag 1977

NAKANO, E. and HORI, Y. 1975

Squeeze Films: The Effect of the Elastic Deformation of Parallel Squeeze Film Surfaces. 1975 JSLE/ASLE Lubrication Conference pp. 325-332.

NEEDS, S.J. 1940

"Boundary Film Investigations." Trans ASME (1940) Vol. 62, pp. 331-45.

NORMAN, R. 1971

"The Lubrication of Porous Elastic Solids with Reference to the Functioning of Animal Joints." Ph.D. Thesis, Durham 1971.

PAUL, G.R. 1971

"Optical Determination of the High Pressure Refracture Index and Viscosity of Liquids Entrapped in Point Contacts." Ph.D. Thesis, London 1971.

RANGER, A.P. 1974

"Numerical Solutions to the Elastohydrodynamic Equations." Ph.D. Thesis, London 1974.

RABINOWICZ. E. 1952

"Metal Transfer during Static Loading and Impacting." Proc.Phys. Soc. 1952, B 65, pp. 630-40.

REYNOLDS, O. 1886

"On the Theory of Lubrication and its Application to Mr. Beauchamp Tower's Experiments, including an Experimental Determination of the Viscosity of Olive Oil." Phil. Trans. Roy. Soc. London (1886) pp. 157-234.

ROHOE, S.M. and OH, K.P. 1975

"A Unified Treatment of Thick and Thin Film Elastohydrodynamic Problems Using Higher Order Element Methods." Proc. Roy. Soc. Series A, Vol. 343, May 1975, pp. 315-331.

STEFAN, J. 1874

"Versuche über die schienbare Adhasion." Sitzungsber d.k. Akad. Wissenschaften (Math. u.Natur w. Cla.) Wien (1974) V.69 (abt 2) pp.713-35.

TABOR, D. 1949

"Collisions Through Liquid Layers." Engineering Vol. 167. (1949) pp. 145-7.

TIMONSHENKO, S.P. and GOODIER, J.N. 1970

"Theory of Elasticity". 3rd. Ed. International Student Ed. McGraw-Hill Inc.

VOGELPOHL. G. 1937

"Beitrage zur Kenntis der Gleitlager Reibung." Ver. Deutsch. Ing. (1937) Forschungs Heft. 386

WESTLAKE, F.J. 1970

"An Interferometric Study of Ultra Thin Films." London Ph.D. Thesis, 1970